

Forces at the scale of the cell

K. Vijay Kumar*

International Centre for Theoretical Sciences, Tata Institute of Fundamental Research, Bengaluru North 560089, India.

Mandar M. Inamdar†

Department of Civil Engineering, Indian Institute of Technology, Bombay, Mumbai 400076, India.

Pramod A. Pullarkat‡

Raman Research Institute, Bengaluru 560080, India

Gautam I. Menon§

Trivedi School of Biosciences and Department of Physics, Ashoka University, Sonapat 131029 India

(Dated: December 10, 2025)

The importance of molecular-scale forces in sculpting biological form and function has been acknowledged for more than a century. Accounting for forces in biology is a problem that lies at the intersection of soft condensed matter physics, statistical mechanics, computer simulations and novel experimental methodologies, all adapted to a cellular context. This review surveys how forces arise within the cell. We provide a summary of the relevant background in basic biophysics, of soft-matter systems in and out of thermodynamic equilibrium, and of various force measurement methods in biology. We then show how these ideas can be incorporated into a description of cell-scale processes where forces are involved. Our examples include polymerization forces, motion of molecular motors, the properties of the actomyosin cortex, the mechanics of cell division, and shape changes in tissues. We show how new conceptual frameworks are required for understanding the consequences of cell-scale forces for biological function. We emphasize active matter descriptions, methodological tools that provide ways of incorporating non-equilibrium effects in a systematic manner into conceptual as well as quantitative descriptions. Understanding the functions of cells will necessarily require integrating the role of physical forces with the assimilation and processing of information. This integration is likely to have been a significant driver of evolutionary change.

CONTENTS

I. Introduction	2	A. Stochastic descriptions	10
II. Basic Biology for Biophysics	3	B. Polymer mechanics	12
A. Constituents of life	4	C. Membrane mechanics	12
B. Cells and compartmentalization	5	D. Hydrodynamic descriptions	13
C. Structural framework of cells and tissues	5	1. Simple Fluids	14
D. Non-equilibrium active processes in cells	7	2. Elastic Solids	14
III. Forces and their consequences	7	3. Viscoelastic Materials	15
A. Equilibrium and non-equilibrium forces	9	E. Linear response	15
B. Quantifying forces with dimensional analysis	9	F. Onsager relations and generalized hydrodynamics	17
IV. Living matter is soft-condensed matter	10	G. Orientational order	17
		H. Soft-materials driven out of equilibrium	19
		V. How do cells infer forces?	20
		VI. Measuring mechanical forces	20
		A. Atomic Force Microscopes (AFM)	20
		B. Magnetic tweezers	21
		C. Optical tweezers	21
		D. Single molecule tracking and	

* vijaykumar@icts.res.in

† minamdar@iitb.ac.in

‡ pramod@rri.res.in

§ gautam.menon@ashoka.edu.in

microrheology	22
E. Shear rheology	22
F. Measurement of cell-substrate traction forces	23
G. Measuring membrane mechanical responses	24
H. Other methods	24
VII. Principles of mechanochemical transduction	24
VIII. Polymerization forces	25
A. Force-generation due to polymerization	26
B. Listeria propulsion	27
C. Filopodial extension	28
IX. Molecular motors	28
A. Brownian ratchet models	29
B. Collection of molecular motors	30
1. Muscle contraction	30
2. Cilia and flagella	30
X. Actomyosin cortex	31
A. Myosin patterns	32
B. Cell polarity	33
C. Cell motility	34
D. Coupling to membrane organization	34
XI. Cell division	35
A. Chromosome organization	35
B. Spindle	37
C. Cytokinesis	38
XII. Tissue mechanics	39
A. Planar 2D epithelial monolayers	39
XIII. A few other examples	42
A. Virus assembly and genome packaging	42
B. Swimming	42
C. Plants	43
XIV. Conclusions	43
XV. Glossary	44
Acknowledgments	45
References	45

I. INTRODUCTION

That the cell is the basic structural and functional unit of life, that genes provide the mechanism of heredity, that natural selection provides a mechanisms for evolution, and that chemistry underlies life, are the great ideas of biology. That biological organization has evolved to support the coding, decoding and processing of information in manifold forms is a further insight [1].

Cells are structured in space and time, allowing them to perform the physiological processes required for life [2]. Such structuring requires forces that act at the scale of the cell [3]. At the molecular level, these forces arise through configurational changes in biological macromolecules [4]. Such configurational changes are typically induced by the binding, unbinding and translocation of molecules at specific sites along relevant biological macromolecules. They can also be driven by variations in the local environment, including pH and electrostatics [5, 6]

Sustained force generation is impossible in thermodynamic equilibrium. Since microscopic processes occur in a statistically time-reversible manner, such processes cannot generate a net force without a persistent energy flow to bias them. This necessitates forces originating from energy-consuming processes. What distinguishes biological systems from other systems with a continuous energy throughput is that force generation in biology typically involves the consumption (hydrolysis) of small energy-storing molecules such as adenosine triphosphate (ATP) [2], often referred to as the energy currency of the cell. This localized, nanoscale energy input is called *activity* [7]. The concentration of ATP molecules is maintained out of equilibrium through metabolism, the name given to the biochemical processes involved in converting nutrients into energy [2]. Living matter has evolved to occupy one end of a continuum of systems with energy throughput, employing a nearly universal energy currency in the form of ATP.

This review is premised on the idea that molecular-scale cellular forces, originating in non-equilibrium processes, are a key component of the organization of living systems, a connection that we believe is as fundamental to biology as the great ideas listed above [8]. This idea is broadly reminiscent of descriptions of “dissipative structures” in non-equilibrium thermodynamics [9]. The difference is that it is *active forces* that maintain such structures and underly the functioning of living systems. We would like to accord the subcellular nonequilibrium

forces that sculpt biological form and function their rightful place among the central ideas of biology.

At the purely biophysical level, we can think of a living cell as a complex soft-matter system imbued with activity [10]. Theoretical and experimental models of soft matter systems that incorporate such activity can be shown to share many mechanical features of living systems. The contemporary field of *active matter* emphasizes these connections, although with many applications beyond biology [11].

Active matter ideas were initially developed to describe the emergent behavior of particles capable of autonomous motion [12, 13]. An example is flocking, the phenomenon by which groups of birds, fish, and other organisms locally coordinate their motion, overcoming noise, to establish robust and dynamic collective patterns at scales much larger than the individual. A convenient description is in terms of self-propelled objects, particles that convert energy extracted from an internal depot into work required to sustain motion in a viscous, fluid environment [7]. Connections to *force-free systems*, models for the self-propelled motion of bacteria in fluids, were made early on, and the first major conference devoted to understanding the relationship between driven soft matter and biological systems brought many of these intriguing connections to the fore [14]. While much initial work focused on what we now refer to as orientable active systems, it became obvious that this physics was mirrored in biophysical descriptions of the cellular cytoskeleton, cell surface organization and bacterial motility. These phenomena could also be replicated outside the cell, as in the example of beads that displayed spontaneous motion when coated with polymerizing biological components [15].

This review addresses forces that operate at the scale of a single cell. Such forces are crucial to the generation and maintenance of form, broadly the processes of development, homeostasis, and physiological function in living systems. However, we also provide a few examples of individual force-generating units at the subcellular scale, as well as of the behaviour of aggregates of cells. We emphasize the relationships between key ideas from the physics of non-equilibrium systems and descriptions of diverse biological systems at the cellular level.

Biological form and function, driven by activity, participate in a robust back-and-forth with information processing and storage. Information is, centrally, physical and manipulating information costs energy. Infor-

mation processing in biological systems should be constrained by the means through which localized energy consumption can be turned into forces. Such an expanded view of *mechanobiology* is conceptually central to this review [16].

The understanding of forces at the scale of the cell, requires some knowledge of what a cell actually is and what processes go on within it [2]. We first supply a compact introduction to the relevant biology, aimed at a physics audience. We then summarize those aspects of soft condensed matter physics and non-equilibrium statistical mechanics that are especially relevant to understanding forces in cells. We outline some broad principles of mechanobiology that connect generalized thermodynamic forces to fluxes in biological contexts. We then show how such forces can be experimentally measured, demonstrating how coordinated forces in the cellular cytoskeleton underlie cell division and cell movement. We describe how simple models of tissues can be constructed, bridging the behavior of individual cells with that of cell collectives.

This review is targeted at (a) physicists from disciplines other than biological physics who wish to learn about how forces act at the scale of the cell, (b) biologists who wish to understand the motivation behind the theoretical descriptions, and (c) students potentially interested in entering this field. We assume familiarity with introductory physics and mathematics at the undergraduate level, but little more.

A review that attempts to tie all these diverse strands together must, of necessity, make choices as to what to retain and what to omit. In our concluding section, we detail some of these omissions, providing references and a brief discussion of how they relate to our discussion here. We end by emphasizing the links between the many contexts in which forces are relevant to biological function at the cellular scale, reiterating the need for new tools that bridge function to a general physical description in terms of active matter. A glossary of technical terms that we use in this review is provided at the end.

II. BASIC BIOLOGY FOR BIOPHYSICS

All that is living can be understood in terms of fundamental units called cells. Living organisms can be classified into two broad categories, eukaryotes (such as the cells in our bodies) and prokaryotes (bacteria). Eukaryotes are larger and have enclosed organelles (the nucleus,

mitochondria, endoplasmic reticulum etc.), bound by a membrane. Prokaryotes are small, evolutionarily more ancient and lack complex intracellular structuring [2, 17].

Cells vary in size and shape. They range in size from about $1\ \mu\text{m}$ (e.g., bacteria) to about $100\ \mu\text{m}$ (e.g., human egg cells), although nerve cells (neurons) can be much longer. Eukaryotes contain organelles ranging in size from $\sim 10\ \text{nm}$ to $\sim 1\ \mu\text{m}$. A good approximation for the density of cell constituents is the density of water $\approx 10^3\ \text{kg/m}^3$: a bacterium of about $1\ \mu\text{m}$ in size weighs approximately one pico-gram [18].

Life’s organization involves formation of extended structures from constituent molecules. For example, cellular organelles are typically protected by a thin continuous bilayer membrane of thickness $\approx 4 - 5\ \text{nm}$ [18]. Long polymers, ranging from a few nanometers to microns in scale, constitute another class of cellular structures. Complex folds in membraneous structures (e.g., the Golgi body or mitochondria) provide higher levels of structural organization, as do dense polymers that are crosslinked (e.g., cytoskeleton, cortex) [2]. The development of a complex multicellular organism starting from a single fertilized egg involves shape and size changes at the level of aggregates of cells (tissues). This process is called morphogenesis.

Purely biochemical processes are fast. They occur over time-scales ranging from $10^{-12}\ \text{s}$ to $10^{-9}\ \text{s}$. However, processes at the scale of the cells that are relevant to sustained force generation are typically in the time-range of micro-seconds to seconds or longer [18]. When a mother cell divides into two daughter cells, hereditary information is transferred from the mother to the daughters. The typical interval between cell division ranges from a few minutes to several hours [18]. Some cells do not divide at all (e.g., neurons).

There is a fundamental distinction between the physics of assemblages of biological molecules that are studied outside the cell, and their physics within a living cell. The former, referred to as *in vitro* studies, typically involves a much smaller set of purified components, ignoring their underlying cellular context. In contrast, the latter, or *in vivo*, studies these components as they present themselves in a living cell with its attendant complications of crowding, confinement, and regulation.

A. Constituents of life

About 20 elements suffice to generate all of life’s molecules [19]. The variety of organic molecules derives from the almost infinite ways in which complex molecules are formed through bonding. A convenient measure of energy scales involved with such bonds is $1\ k_B T \approx 4.1\ \text{pN nm} \approx 1/40\ \text{eV}$, corresponding to $T \approx 300\ \text{K} = 37\ \text{°C}$ or the physiological temperature. Covalent bonds are strong, typically taking $10 - 100\ k_B T$ to break. The breaking of a triphosphate bond (e.g., the hydrolysis of adenosine triphosphate – ATP – sometimes referred to as the cell’s energy currency) leads to a release of an energy of about $20\ k_B T$. Hydrogen bonds range in strength between $2 - 12\ k_B T$.

There are four major types of significant biological molecules: proteins, carbohydrates, lipids, and nucleic acids [20]. Protein molecules are specified as a sequence of smaller amino acids, drawing from 20 amino acids known to occur naturally. A natural unit for the measurement of the mass of proteins is the Dalton (Da), defined as $1/12^{\text{th}}$ of the mass of the carbon atom. In these units, the mass of a single amino acid $\sim 100\ \text{Da}$. Proteins can be short or long, incorporating between ~ 10 and $\sim 10^4$ amino acid units. The mass of a typical small protein (a common example is a lysozyme) with 130 amino acids is $14\ \text{kDa}$. Proteins are structurally diverse, ranging from collapsed globular structures to long linear ones [2].

Proteins can function individually, or as protein complexes [19]. For example, the basic unit of the microtubule, a linear polymeric structure typically formed by combining 13 protofilaments together in the form of a hollow cylinder, is a dimer of two types of tubulin, alpha and beta. Macromolecular machines, such as the ribosome (size $\approx 20\ \text{nm}$ and molecular mass $\approx 4\ \text{MDa}$) that synthesizes proteins, are protein complexes. Protein-protein interactions per amino acid involve energies intermediate between that of a covalent bond ($\approx 100k_B T$) and thermal energies ($\approx k_B T$).

Lipids are small amphiphilic molecules with a typical molecular length of about $2\ \text{nm}$ in length [18]. They are made of a hydrophilic (polar and hence “water-loving” as the name implies) head group and one or two hydrophobic (“water-hating”) chains. Lipid molecules are the constituents of cell and nuclear membranes. They are found, in general, wherever any material needs to be encapsulated. The self-assembly of lipid molecules into membrane-like structures can occur even in thermody-

namic equilibrium.

Nucleic acids, both DNA and RNA, are long molecules that embed information required for cell function and replication. DNA structure is conveniently described as a sequence of 4 possible bases on a single strand – adenine (A), thymine (T), guanine (G) and cytosine (C) – with a reactive component along its edge, linked to a sugar molecule (deoxyribose), which pairs with another, ‘complementary’ strand. Bases pair together in specific ways: A with T and G with C with each member of the pair attaching to a sugar-phosphate backbone. These pairs form the rungs of a ladder of two strands wound around in the form of a right-handed double helix. The information contained in the DNA sequence is first transcribed into an mRNA molecule and then translated into a protein sequence [21]. Triplets of nucleic acid (codons) correspond to particular amino acids. Both these processes, of *transcription* and *translation*, require energy [22].

Carbohydrates are a prominent energy storehouse for cells. These are broken down in the body into sugars. Further breakdown of a single glucose molecule under aerobic conditions leads to the production of around 30 ATP molecules [23]. In addition to their role in forming information processing molecules, each nucleotide is associated with high energy phosphate molecules, generally denoted as NTP. N is either of the nucleotides A, T, G, or C. However, most cellular machinery operates by using the energy released by the hydrolysis of predominantly ATP, sometimes GTP. The energy cost per nucleotide of transcribing a typical gene into an RNA or that for translating an RNA molecule into protein is the energy released from the hydrolysis of $\sim 1 - 5$ ATP molecules. It is estimated that the human body turns over an equivalent of half its weight in ATP molecules each day [18].

B. Cells and compartmentalization

The four basic classes of molecules are the building blocks of more complex structures inside living cells. Figure 1(a) shows a simple bacterium of size $\approx 1\mu\text{m}$, with a rotary motor embedded in its cell wall. Eukaryotic cells, shown schematically in Figure 1(b), contain multiple intracellular organelles. These use internal membranes to separate the inside from the outside. These membrane bound compartments include mitochondria, endoplasmic reticulum, Golgi body, and the nucleus itself, in addition to other organelles. A detailed glossary of these struc-

tures is available in Ref. [24].

The most prominent compartment is the cell itself. A typical eukaryotic cell is contained within a *plasma membrane*, an effectively two-dimensional bilayer fluid membrane made of lipid molecules, proteins, and sugars. These are well-described as fluid films, governed by in-plane tension and an out-of-plane bending cost. The membranes of living cells are in a state of constant dynamical flux via processes through which the cells exchange nutrients and signaling molecules with the external environment. The shapes and dynamics of membranous organelles are governed by an interplay between mechanical forces and chemical currents. Ion-channels and ion-pumps are proteins that span the plasma membrane (transmembrane), selectively transferring chemical species from side to the other. These help to maintain potential differences across the cell surface.

Compartments provide niches where specific chemical reactions requiring specialized environments can be carried out. They thus allow for the isolation and maintenance of spatially heterogeneous regions within a cell. Driven by energy flows, thermodynamically unfavorable processes can be carried out in such regions. These regions, e.g., mitochondria, can also act as energy depots that help to drive cellular processes on time-scales much longer than the time-scales for energy production.

Finally, it is possible to achieve compartmentalization without membranes. This can happen through phase separation that can create contiguous regions enriched in specific biochemical components, (e.g., nucleoli and Cajal bodies) [25, 26].

C. Structural framework of cells and tissues

Living systems have evolved cross-linked networks of polymers, collectively called the cytoskeleton, that can generate and transmit mechanical forces. The cellular cytoskeleton is composed of filaments of varying sizes, with the largest of their lengths comparable to the cellular scale of $\approx 1 - 10\mu\text{m}$. The cellular skeleton is distributed across the cell and especially reinforced just below the plasma membrane (cortex).

The cytoskeleton in eukaryotic cells is composed of three types of polymeric filaments (microtubules, actin filaments and intermediate filaments) along with proteins that bind to them [4, 27]. Specific force generating elements, such as molecular motors, interact with the cytoskeleton. These polymeric filaments are formed

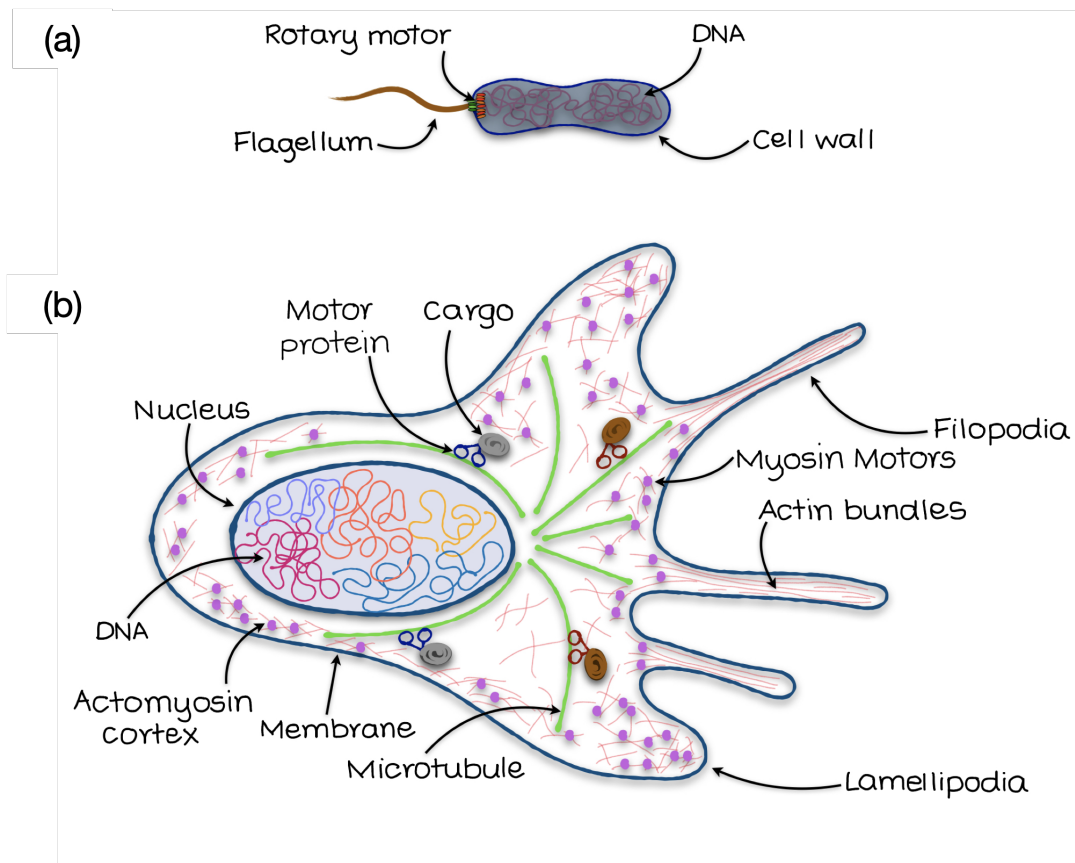


FIG. 1. Schematic representations of a prokaryotic and a eukaryotic cell (not to scale). The figure illustrates some of the well-studied organelles in these cells whose physics we discuss in this review. Typically, prokaryotic cells are small ($\sim 1 - 2 \mu\text{m}$) compared to eukaryotic cells ($\sim 10 - 20 \mu\text{m}$). Genetic information is stored in the form of DNA across most cellular forms of life. A typical prokaryote, such as an *E. coli* cell, lacks intracellular membrane compartments and has its DNA floating around in the bulk of the cell. It uses a rotary motor to turn flagellar filaments which aid in the propulsion of the cell. The internal structure of a eukaryotic cell is dynamically maintained in an organized manner. The DNA is packaged, at several hierarchical levels of organization, into chromosomes. These chromosomes are enclosed inside a double-walled lipid bilayer, reinforced by a supporting polymer mesh (lamins), forming the nucleus. Long polymeric filaments (microtubules) act as tracks on which molecular motors transport cargo across different parts of the cell. A meshwork of actin filaments, myosin motors, and crosslinkers forms the “cortex” found towards the periphery of the cell. Active mechanochemical processes in this actomyosin cortex generates cellular protrusions such as filopodia and lamellopodia that help the cell to anchor on substrates or to move.

through self-assembly. Microtubules and actin filaments, shown in the FIG. 1(b), have structural polarity [2]. These filaments can further organize into higher order structures that provide structural integrity to the cell, facilitate cell division, attach to substrates, propel cells, and also serve as tracks for cargo transport by specialist protein molecules called molecular motors. Intermediate filaments provide tensile strength and mechanical resilience, particularly in epithelial tissues and neurons [2]. However, since they do not directly participate in ATP-driven force generation, we do not discuss them further here.

Cytoskeletal filaments differ in their diameter, struc-

tural and mechanical properties. Of these, microtubules, with diameter $\approx 25 \text{ nm}$, are the stiffest. Microtubules are hollow structures, made up of tubulin dimers. A number of microtubule-associated proteins bind to the microtubule, modulating its properties. Actin filaments are made of two polymer filaments which wind about each other with an a helical pitch of $\approx 72 \text{ nm}$ and an overall diameter of $\approx 8 \text{ nm}$. Bacterial cells possess analogs of tubulin and actin proteins [28].

Modern approaches, developed over the past few decades, account for the presence of active elements such as pumps on the membrane surface and the underlying meshwork of protein filaments, the actomyosin cortex.

This meshwork, ranging from a few tens to hundreds of nanometers in thickness [29], is a dense crosslinked polymer layer with embedded molecular motors that consume ATP and generate active stresses (FIG. 1(b)). The coupling between the cell cortex and the plasma membrane regulates important biophysical properties of the cell membrane [30–33].

D. Non-equilibrium active processes in cells

The notion of a system being in thermodynamic equilibrium depends on the time-scales of observation [34]. Typically, fast processes such as the opening and closing of ion channels ($\sim 1\mu\text{s}$) and the binding-unbinding of small (ligand) molecules ($\sim 1 - 10\mu\text{s}$) can be understood within the framework of equilibrium statistical mechanics [35, 36]. Slower processes such as protein synthesis ($\sim 1 - 10\text{ s}$), cell division/locomotion ($\sim 10^2\text{ s}$), and morphogenesis ($\sim 10^3 - 10^5\text{ s}$) are driven by a throughput of energy. The consumption of energy to drive non-equilibrium processes makes the cell an *active* system.

An exemplar of active processes is the directed transport of material via molecular motor proteins that move unidirectionally on filamentous tracks. Molecular motors use energy derived from the hydrolysis of small ATP molecules, or from the electrochemical potential of proton gradients across cell membranes, to generate such unidirectional motion. These motor proteins must work against the viscous drag forces that dominate the crowded environment of the cell, where the viscosity can be up to ~ 10 times that of water.

ATP-driven linear molecular motors include myosins, kinesins, and dyneins. They are indispensable for cellular activities such as muscle contraction and intracellular vesicle transport. Other linear motors take part in processes such as replication, transcription and genome maintenance (helicases and polymerases). While biochemical experiments have shed light on collective motor motion, as in muscle cells, much of single molecule biophysics work has concentrated on *in vivo* measurements of motor speeds, and measuring the relationship between forces and velocities.

Rotary motors driven by proton-gradients are found in the ATP synthase [37] and the bacterial flagellar motor [38] (shown in FIG. 1(a)). The ATP synthase is a molecular machine, a complex of proteins, in which one part can rotate relatively to the other. In a proton gradient, the unidirectional rotation of the ATP-synthase can

generate ATP from excess ADP molecules. In the reverse process, the energy released from the hydrolysis of ATP is used to rotate the ATP-synthase. It can rotate at speeds of ≈ 4 rotations per second while generating torques of up to 40 pN nm [39].

Molecular motors are an archetypal example of the transduction of chemical energy into mechanical work. Since no net mechanical work can be extracted from systems at thermodynamic equilibrium without changing the state of the system irreversibly, the sustained generation of net force in a cellular system must therefore involve continuous energy throughput. It is thus necessary to go beyond frameworks of thermodynamic equilibrium. The mechanical forces that are generated in such non-equilibrium scenarios drive vital cellular functions. What are the consequences of such forces?

III. FORCES AND THEIR CONSEQUENCES

Force is what force does: forces move, accelerate, deform or rotate the objects they are applied to. FIG. 2 shows, on a logarithmic scale, the range of forces involved in important cellular biophysical processes. One can roughly estimate the scale of forces required to be sensed, as well as exerted at the single molecule level. For a molecule to be able to sense a force, the scale of the force must be suitably larger than the forces arising from spontaneous thermal fluctuations at that scale, i.e., they must be larger than $F \sim k_B T/a$ where $a \sim 1\text{ nm}$ is a characteristic molecular scale, if they are to have an effect. Forces exerted as a consequence of ATP hydrolysis are bounded above by $F \sim 20k_B T/a$ where $20k_B T$ is the approximate value of the energy released through the hydrolysis of a single ATP molecule. This yields force scales in the regime 10 – 100 pN for forces acting at the single molecule scale in biological systems.

At scales relevant to cell biology, all forces operate in a fluid medium. It is often easier to abandon discrete descriptions in favor of continuum ones that can include the effects of the surrounding fluid in a straightforward manner. Newtonian mechanics provides a linear relationship between acceleration and forces, $\ddot{\mathbf{r}} \propto \mathbf{F}$; where an overdot indicates a time-derivative. In a highly overdamped system, however, with friction provided by an ambient fluid medium, the formulation $\dot{\mathbf{r}} \propto \mathbf{F}$ provides a more practical description of the effective dynamics at long times.

Quantum mechanical fluctuations in the dipole moment of neutral, non-polar atoms lead to a character-

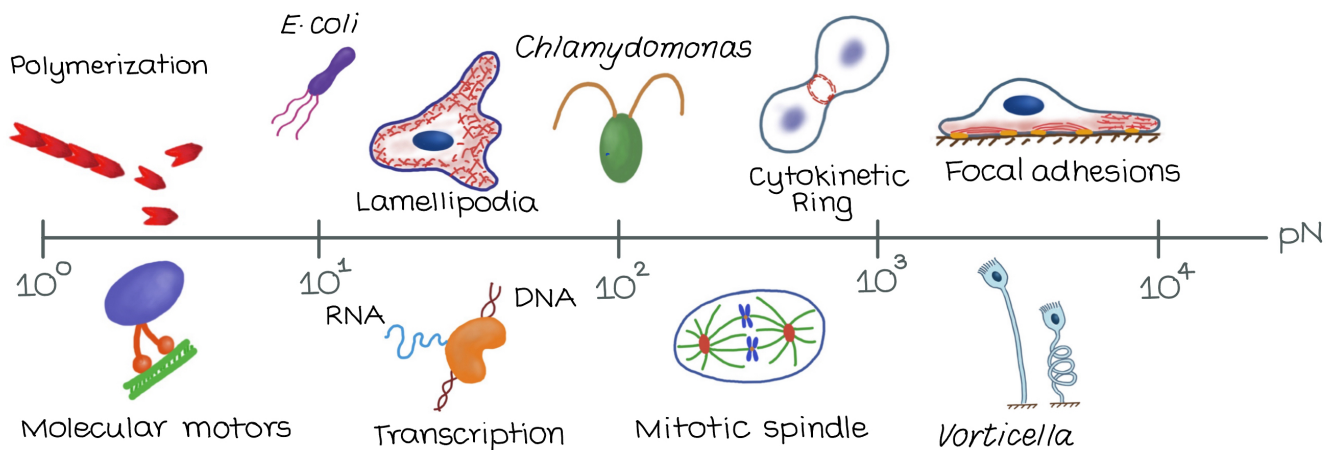


FIG. 2. This figure illustrates the hierarchy of force scales at the level of a single cell and below. The appropriate force scale is the pico-Newton (10^{-12} N). Forces from molecular motor translocation are in the regime 1 – 10 pN while the forces involved in cell adhesion are typically 2 – 3 orders of magnitude larger.

istic van der Waals $1/r^6$ attraction [40]. At shorter scales, electron repulsion and the Pauli principle contribute a repulsive core. This combination can be summarized through the classic Lennard-Jones form involving a characteristic energy scale ϵ and a size σ : $V(r) = 4\epsilon [(\sigma/r)^{12} - (\sigma/r)^6]$ for non-retarded interactions between isotropic, charge-neutral entities of arbitrary shapes [41]. The Lennard-Jones and similar interactions are non-bonding interactions because they do not involve the transfer or sharing of electrons between atoms. Bonds between atoms can be described in terms of the balance between the transfer (ionic) and sharing (covalent) of electrons.

The subtle effects of the medium enter in how non-bonded interactions are modified by a solvent. For a solute particle that is uncharged in vacuum, immersing it in a solvent can leave it with a net charge as surface chemical groups dissociate, releasing mobile counter-ions [40]. In a polar solvent, such as water, a network of hydrogen bonds lends water its anomalous properties, including that of being an exceptional solvent for most biological molecules. For all such mesoscopic objects, the effects of the underlying electromagnetic interactions are modulated to yield effective interactions in which the properties of solute and solvent are both involved.

To illustrate these complexities, consider the interaction between small protein molecules, each uncharged in the vacuum. When placed in water, charged chemical groups on the protein can dissociate, leading to a background charge distributed along the protein and associ-

ated mobile counterions in the solution. Any added salt can also dissociate in the solvent, providing mobile ions that can contribute to charge screening, thus modifying the effective interaction between the proteins. A Debye screening length $\ell_D = \sqrt{\epsilon k_B T / 2e^2 n}$ is related to the distance over which the field due to a test charge decays due to screening, where n is the number density of the ions. For pure water at room temperature $\ell_D \sim 1 \mu\text{m}$ while for the cellular cytoplasm $\ell_D \sim 1 \text{ nm}$ [42]. This separation of scales is due to the highly salty cytoplasm. Interactions mediated by water molecules, deriving from the structuring of the hydrogen bond network around protein surfaces, are called hydrophobic interactions. Conformational changes occurring as a result of forces acting on a protein can alter the specificity of its interactions and functions, forming the basis of mechanosensitivity of protein-protein interactions.

Even in the absence of direct electrostatic interactions, effective interactions arising from entropy maximization can be conceptualized as forces. Such forces are conventionally termed as statistical forces. A well known example of these statistical forces, the *depletion interaction*, is seen in a system with particles of different sizes immersed in a thermal bath. Clumping the larger particles together increases the configurational space for smaller particles, and thus the overall entropy, resulting in an effective entropic attraction between the larger particles [43]. Polymer systems that can explore their configurational space via thermal fluctuations resist the reduction of their entropy when confined. This is the basis of another variety

of effective entropic interaction.

The elastic response of the cytoskeleton is largely entropic and entropy reduction involves a corresponding restoring force. The forces that arise across a semi-permeable membrane with differential concentrations of solute – osmotic forces – are partly entropic in origin [44]. The glycocalyx, a polymer brush of sugar molecules present on the outer surface of cells, is an attractive candidate for entropic interactions [45]. Fluctuation-induced forces can also arise in non-thermal situations [46].

In the following sections, we briefly review some of the theoretical frameworks required to describe forces/stresses and their consequences, both in the equilibrium and non-equilibrium contexts. We also discuss appropriate experimental techniques to measure these forces in the context of living systems.

A. Equilibrium and non-equilibrium forces

A system in thermodynamic equilibrium minimizes an appropriate free energy. No net currents flow between any of its microscopic states. If a system is perturbed slightly away from its equilibrium state, *thermodynamic forces* restore it to equilibrium [47].

Consider now a system which is held in a steady-state but out of equilibrium. It can be maintained in such a state only by a constant flux, typically of energy and matter. For instance, the operation of nano-scale biological machines such as molecular motors and ion-pumps relies on a continuous supply of energy. However, the “forces” involved in these processes, typically, do not have a simple and generic relationship with the free energy or any analog. Much of the cell’s functionalities derive from such “active” force generating processes. Living systems have evolved metabolic pathways to convert energy input from the external surroundings into a global currency of high-energy molecules, for instance NTPs.

At a microscopic scale, it is plainly impossible to describe the dynamics of the approximately $\sim 10^{15}$ molecules that typically constitute a single cell. Clearly, a reduced description in terms of a much smaller set of important variables is appropriate. Choosing such variables is a problem of coarse-graining. Traditionally, such coarse-graining is in terms of *hydrodynamic variables* [48]. These are collective modes of interacting systems such that when perturbed away from their equilibrium values, the relaxation time of these deviations diverges with the wavelength of the perturbation. For

instance, the densities of conserved quantities such as particle number and momenta, order parameter fluctuations at the critical point, or transverse fluctuations of a continuous broken symmetry variable are all hydrodynamic variables. However, given the finite size of the cell and limited time-scale of observation, non-hydrodynamic variables may often be important.

The choice of appropriate coarse-grained variables is as much an art as science. What is often done is to use microscopic computational models that are constructed so as to capture the essential physics in the hydrodynamic limit [41], to perform computations using simplified kinetic models [49], or simply to use general symmetry arguments [48] to pick out all possible lowest order relevant terms that should enter the equations of motion.

B. Quantifying forces with dimensional analysis

Forces can lead to deformations and flows. For fluid flows, an important dimensionless combination of relevant physical quantities is the Reynolds number. For a flow with a characteristic velocity v , a length scale L , shear viscosity η and a density ρ , the Reynolds number is $\text{Re} = \rho Lv/\eta$. This can be interpreted as the ratio of inertial and viscous forces. For example, large scale hydrodynamic flows ($v \approx 10 \mu\text{m}/\text{min}$, $\rho = \rho_{\text{water}} = 10^3 \text{ kg}/\text{m}^3$, $\eta = \eta_{\text{water}} = 10^{-3} \text{ Pa}\cdot\text{s}$, and $L \approx 50 \mu\text{m}$) in the actomyosin cortex of the *C. elegans* embryo correspond to $\text{Re} \approx 10^{-6} - 10^{-5}$ [50]. For bacteria swimming in water ($v \approx 30 \mu\text{m}/\text{s}$ and $L \approx 1 \mu\text{m}$), $\text{Re} \approx 10^{-5} - 10^{-4}$ [51]. Thus, hydrodynamic flows at the cellular level are almost always at low Reynolds number. Inertial forces are negligible at these scales.

Most biological materials are viscoelastic, i.e., they exhibit a combination of fluid-like and solid-like behaviors. Linear viscoelastic fluids resist deformations induced by applied forces up to a certain fluidization time-scale, known as the Maxwell time, beyond which they flow [50, 52].

For biological flows in which diffusion and directed transport compete, the appropriate dimensionless quantity is the Péclet number $\text{Pe} = vL/D$, where v is the typical advection velocity on a scale L , and D is the diffusion coefficient. In the cellular context, the Péclet number ranges from values $\text{Pe} \ll 1$ (e.g., for spatial profiles of signalling molecules established by diffusion), $\text{Pe} \approx 1$ (e.g. the movement of molecular motors, cytoplasmic streaming, cortical flows), to values $\text{Pe} \gg 1$ (e.g., in cell motility

mechanisms such as crawling and swimming, blood flow). The diffusion coefficients referred to here need not be of thermal origin.

IV. LIVING MATTER IS SOFT-CONDENSED MATTER

Soft materials in equilibrium are many-body systems in which typical energies for deformation are comparable to the thermal energy. Because of this, thermal fluctuations cannot be neglected. In general, the fluctuations can also be non-thermal, for instance in active systems. Biological materials are archetypal examples of driven soft matter.

At thermodynamic equilibrium, response coefficients such as susceptibilities, conductivities, etc., are intimately connected to spontaneous fluctuations. These constraints are expressed in the form of fluctuation-dissipation relations. However, for a system far away from thermodynamic equilibrium, there are no such constraints between spontaneous fluctuations and response coefficients. Stochastic fluctuations in active materials generically violate detailed balance conditions, discussed in more detail below, leading to non-trivial consequences for their macroscopic descriptions.

A generic statistical mechanical theory for systems far from thermodynamic equilibrium does not exist, at least as of now. Nevertheless, physical descriptions developed for near-equilibrium systems provide a useful framework, since their predictions can be quantitatively compared to experimental observations. In the next few subsections, we develop a sequence of increasingly coarse-grained descriptions that are valid both at thermodynamic equilibrium and for driven states *close* to thermodynamic equilibrium. After a brief description of various biophysical experimental techniques to measure stochastic fluctuations and response functions, we will use the theoretical formalism developed here to describe several cellular processes.

A. Stochastic descriptions

For systems with discrete states such as, for instance, the number of molecules involved in transcription or translation, an appropriate description for the stochastic dynamics is via a master equation [53]. The probability to find the system in a configuration C evolves in time

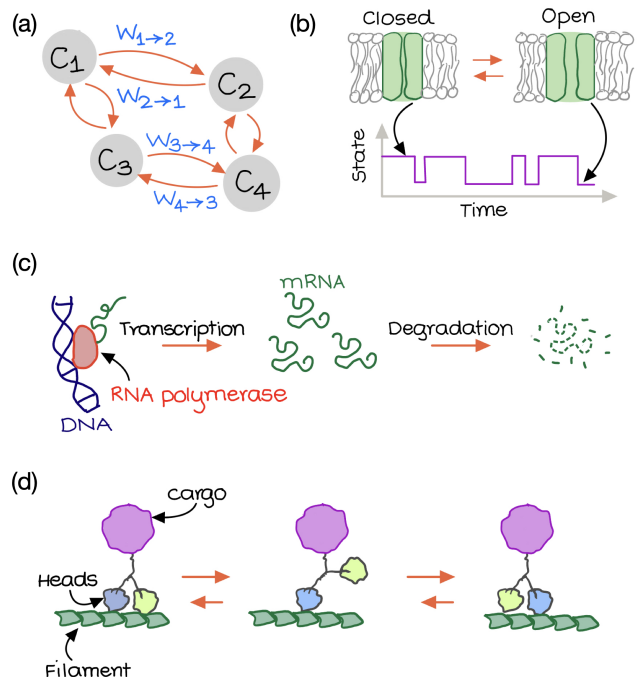


FIG. 3. (a) A schematic of the master equation (1) indicating stochastic transitions between the states C_i with transition rates $W_{i \rightarrow j}$. (b) Ion-channels are proteins embedded in the cell-membrane which transition between “open” and “closed” states in a stochastic manner. (c) The production (by transcription) and degradation of the mRNA molecules can be captured within a master equation approach where $P(n, t)$ represents the probability of finding n mRNA molecules at time t . (d) The translocation of molecular motors transporting cargo on filaments is another example of a stochastic process with discrete states. Here the internal states of the system are the attachment configurations of the two heads of the motor. The coupling between these transitions and directional asymmetries in the filament leads to motion of the motor.

according to the master equation:

$$\frac{dP(C, t)}{dt} = \sum_{C' \neq C} [W_{C' \rightarrow C} P(C', t) - W_{C \rightarrow C'} P(C, t)] \quad (1)$$

where $W_{C \rightarrow C'}$ is the transition rate from a configuration C to C' . We must have $\sum_C P(C, t) = 1$, since probabilities must add to unity, implying that $\frac{d}{dt} \sum_C P(C, t) = 0$. This leads to the constraint $W_{C \rightarrow C} = \sum_{C' \neq C} W_{C \rightarrow C'}$. Figure 3(a) illustrates the discrete configurations and the transitions between them. The opening and closing of an ion-channel, shown in FIG. 3(b), is an example of a two-state stochastic process.

Defining $\mathbf{P} = \{P(C_1), P(C_2), \dots\}$ and the matrix

of transition rates \mathcal{W} , we get the matrix version of the master equation $\dot{\mathbf{P}} = \mathcal{W} \cdot \mathbf{P}$. The master equation description is valid for systems both at equilibrium and those that are out of equilibrium. For equilibrium systems, the detailed balance condition $W_{C' \rightarrow C} P(C', t) = W_{C \rightarrow C'} P(C, t)$ (which ensures that there are no net currents) together with a Boltzmann probability $P_{\text{eqm}}(C, t) \sim \exp(-E_C/(k_B T))$, completely describes the dynamics. Note that the detailed balance condition is a macroscopic remnant of the underlying time-reversal invariance of Hamiltonian dynamics. However, for driven nonequilibrium systems that break time-reversal invariance, there are no such general descriptions. Most cellular processes are driven by energy inputs and, as such, are out of equilibrium.

For instance, in the case of DNA transcription into mRNA, as shown in FIG. 3(c) with P_n describing the probability of finding n molecules, the appropriate master equation is

$$\frac{dP_n}{dt} = \gamma(n+1)P_{n+1} + \kappa P_{n-1} - (\gamma n + \kappa)P_n, \quad (2)$$

where κ is the production rate and γ is the degradation rate. Another example of a stochastic process is the directional stepping of a molecular motor shown in FIG. 3(d).

In certain limits, one can reduce the master equation description of transitions between states to a set of stochastic differential equations (SDE) for continuous variables. The translocation of a motor protein such as kinesin moving on microtubules, although best described microscopically in terms of transitions between discrete molecular configurations, can be modeled at a coarse-grained level by changes in a continuous position coordinate. Brownian motion is an archetypal example of such a SDE where one considers the stochastic dynamics of a few “slow” variables while the effects of the other “fast” variables are represented by effective forces arising from a coupling to the medium.

The effects of the medium on an embedded particle come from two sources. One is a drag force, proportional to the velocity of the particle and the other an instantaneous “noise” term. For a particle of mass m moving under the influence of a potential $U(\mathbf{x})$, the Langevin equation describing the stochastic dynamics is [54]

$$m \frac{d\mathbf{v}}{dt} = -\nabla U(\mathbf{x}) - \int_0^t dt' \Gamma(t-t') \cdot \mathbf{v}(t') + \mathbf{f}(t), \quad (3)$$

where the friction kernel $\Gamma(t)$ represents the drag force and the stochastic term $\mathbf{f}(t)$ represents the noise. The

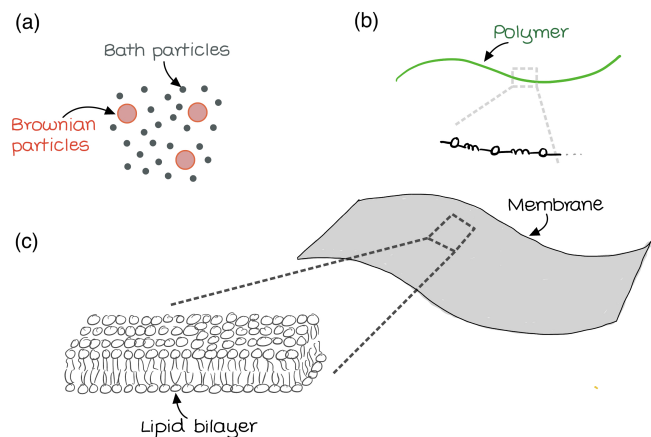


FIG. 4. Collections of interacting particles driven by stochastic forces arising from the thermal environment. (a) shows a few colloidal scale particles (10^{-6} m) immersed in a bath of smaller particles. The interactions of the colloidal particles with the heat bath leads to diffusive dynamics at long time. (b) and (c) show extended structures – one a polymer filament and the other a membrane sheet. The strength of the stochastic forces are comparable to the energies required to cause significant shape change. The extended nature of these structures requires that their energetics be modeled through energy functionals that depend upon shape.

noise term is most often modeled as being drawn from a Gaussian distribution, with zero mean and a characteristic width that is proportional to the temperature. Specifically, for a system at thermodynamic equilibrium, the strength of the fluctuations and the rate of dissipation must be proportional. This leads to the fluctuation-dissipation theorem $\langle f_i(t) f_j(t') \rangle = 2k_B T \Gamma(t-t') \delta_{ij}$, where $\langle \dots \rangle$ denotes an average over stochastic realizations and i, j refer to spatial indices. Typically, $\Gamma(\tau)$ is sharply peaked around $\tau = 0$, is non-zero only in a small region of τ , and can be approximated by $\Gamma(\tau) \approx \gamma \delta(\tau)$. On timescales $t \gg \gamma/m$, one can also neglect the inertial term, leading to a purely overdamped equation of motion. The position vector \mathbf{x} then evolves according to:

$$\frac{d\mathbf{x}}{dt} = -\mu \nabla U(\mathbf{x}) + \boldsymbol{\zeta}(t), \quad (4)$$

where $\mu = 1/\gamma$ is the mobility and $U(\mathbf{x})$ is a confining potential. The stochastic term $\boldsymbol{\zeta}$, representing the effects of the fluctuating environment, is a Gaussian white noise process with zero mean and $\langle \zeta_i(t) \zeta_j(t') \rangle = 2D \delta_{ij} \delta(t-t')$ where the diffusion constant $D = \mu k_B T$ is set by the Einstein relation.

In a continuum description of states, the master equation (1) becomes the Fokker-Planck equation. In sec-

tion IX, we will use the Fokker-Planck description to illustrate how directed motion occurs in models of molecular motors. Physically, the Fokker-Planck equation contains two terms - one representing the tendency of probabilities to “spread out”, via processes connected to diffusion, while the second represents the effects of external forces, typically derivable from a potential. The equation governing the time-evolution of the probability density $P(\mathbf{x}, t)$, of finding the particle at position \mathbf{x} and time t , is governed by the corresponding Fokker-Planck equation (in this context, the Smoluchowski equation):

$$\frac{\partial P(\mathbf{x}, t)}{\partial t} = -\nabla \cdot \mathbf{J}, \quad \mathbf{J} = -\mu \nabla U(\mathbf{x}) P - D \nabla P, \quad (5)$$

where \mathbf{J} is the probability current [55]. At thermodynamic equilibrium, the probability current $\mathbf{J} = 0$. This ensures that the Boltzmann distribution $P_{\text{eqm}} \sim e^{-U(\mathbf{x})/k_B T}$ is the asymptotic solution. The stochastic descriptions discussed above can be generalized to include interactions among particles.

B. Polymer mechanics

Specific cases of interacting particle systems of biological interest include polymers and membranes. We can idealize the polymer as a smooth one-dimensional curve and the membrane as a smooth two-dimensional surface. For an inextensible one-dimensional curve of length L with a unit tangent vector $\hat{\mathbf{t}}$, an appropriate elastic energy functional is

$$E_p = \int_0^L ds \frac{\kappa}{2} K^2, \quad (6)$$

where s is the arc-length parameter along the polymer, the curvature $K = \partial_s \hat{\mathbf{t}}(s)$ measures the rate at which the unit-tangent vector changes along the curve, and κ represents the free-energy cost to bend the polymer – a bending modulus. This description is also known as the worm-like chain model for the polymer [56]. The stiffness of any polymer is related to the correlation between tangent vectors at different points along the curve. The persistence length is defined by the correlation function $\langle \hat{\mathbf{t}}(s) \cdot \hat{\mathbf{t}}(s') \rangle \sim \exp(-|s - s'|/\ell)$ where $\langle \dots \rangle$ denotes equilibrium averages. If the environment is a heat-bath at temperature T , then ℓ is a thermal persistence length $\ell_{k_B T}$. Typical biopolymers have $\ell_{k_B T} \sim 50$ nm for double-stranded DNA, $\ell_{k_B T} \sim 10$ μm for actin and $\ell_{k_B T} \sim 1$ mm for microtubules.

Measurements of the force-extension relationship for DNA/RNA *in vitro* attach a colloidal particle to one end of the DNA molecule which is tethered at the other end, and trap this colloidal particle in a movable optical trap [57–59]. Exerting a calibrated force on the DNA molecule leads to its extension. Such measurements indicate that DNA at large length scales (greater than ~ 150 base-pairs) can best be described as a semi-flexible polymer. A remarkably accurate form for the force-extension relation that only involves the persistence length is [60]

$$\frac{f \ell_B}{k_B T} = \frac{z}{L} + \frac{1}{4(1 - z/L)^2} - \frac{1}{4}, \quad (7)$$

where f is the force required to stretch the polymer of contour length L by an amount z in the direction of the force. The scale of such forces for a 5 – 10% strain (z/L) is of the order of few tens of piconewtons.

In an environment with active fluctuations, such as in a cell, where the probability distributions will be non-Boltzmann, ℓ will be set by the scale of the nonequilibrium fluctuations and could be significantly different from $\ell_{k_B T}$. For example, measurements of bending fluctuations of microtubules in reconstituted actin networks with embedded myosin motors show that $\ell \sim 1$ μm for microtubules [61].

C. Membrane mechanics

For a two-dimensional fluid membrane, one in which the constituent molecules can diffuse past each other, the corresponding coarse-grained energy functional to lowest order is the Canham-Helfrich energy functional

$$E_m = \int dS \left(\sigma_s + \frac{\kappa}{2} (H - H_0)^2 + \bar{\kappa} \mathcal{K} \right). \quad (8)$$

The effective surface tension σ_s (sometimes called the membrane tension), represents the free energy cost to change the area of the membrane by a unit amount. The curvature of the membrane is described by two quantities H and \mathcal{K} , the mean and Gaussian curvatures respectively. The spontaneous mean-curvature H_0 is non-zero only for an when the two leaflets of the membrane are inequivalent. The free energy cost of bending the membrane is given by κ and $\bar{\kappa}$, the appropriate bending rigidities [62]. For closed surfaces with a fixed topology, as in many biological contexts, the integral $\int dS \mathcal{K} = 2\pi\chi$ is a constant.

A measure of planarity for a 2D membrane is the correlation function $\langle \hat{\mathbf{n}}(\mathbf{x}) \cdot \hat{\mathbf{n}}(\mathbf{x}') \rangle$ of the unit normal vector $\hat{\mathbf{n}}$ at two-different points \mathbf{x} and \mathbf{x}' . A careful analysis of

this correlation function shows that the associated persistence length $\ell_{k_{BT}} \sim b \exp(\beta C \kappa)$ where C is a numerical constant, b is a molecular length-scale and κ is the bending rigidity [63].

To find the shape that minimizes the energy E_m , we write the Euler-Lagrange equations for membrane shape with appropriate constraints such as a fixed volume and topology. This then leads to a shape equation [64, 65]

$$\kappa \nabla^2 H + 2\kappa(H^2 - HH_0 - \mathcal{K})(H - H_0) - 2\sigma_s H + \Delta p = 0 \quad (9)$$

where Δp is the pressure difference between the inside and the outside of the surface which acts a Lagrange multiplier to conserve the volume. If the bending rigidity can be neglected, then in the case of a sphere with radius R , a simple balance of forces in equilibrium leads to the Young-Laplace law:

$$2\sigma_s H = \Delta p, \quad (10)$$

where $H = 1/R$. This relation is used to measure the membrane tension experimentally, see e.g., section VI G.

The plasma membrane of a eukaryotic cell controls the movement of material across it. It is inhomogeneous – in addition to being composed of various kinds of lipids, the cell membrane contains many transmembrane proteins. The cell can transport material across the membrane either by fusing lipid vesicles containing internal cargo with the plasma membrane (exocytosis) or by pinching a vesicle from the membrane to encapsulate external cargo (endocytosis). These fusion/fission processes of the membrane are regulated by specialized protein complexes. The forces involved here are $\sim 10 - 100$ pN [66].

Material can also be transported across a membrane due to the activity of pumps and channels. These are proteins embedded in the membrane. Pumps consume chemical energy to drive ions against a concentration gradient. Ion channels, on the other hand, allow passive transport of specific ions across the membrane. Gating of these channels can be sensitive to membrane tension.

Early studies of the shape fluctuations (flicker) in red blood cells observed under a light microscope, assumed that these were purely thermal in nature [67]. However, over the past two decades, evidence has accumulated for a strong active component to such fluctuations [68]. It is possible to write stochastic differential equations at this coarse-grained level using the energy functional (8). These must include terms representing the active forcing of, e.g., membrane pumps through ATP hydrolysis.

For instance, for a nearly flat membrane, the height-field $h(\mathbf{x}, t)$ describing the membrane position above a xy -plane evolves according to

$$\frac{\partial h(\mathbf{x}, t)}{\partial t} = -\mu \frac{\delta E_m[h(\mathbf{x}, t)]}{\delta h(\mathbf{x}, t)} + \zeta(\mathbf{x}, t) + \zeta_{\text{act}}(\mathbf{x}, t), \quad (11)$$

where μ is a kinetic coefficient, $\zeta(\mathbf{x}, t)$ is a thermal noise and the $\zeta_{\text{act}}(\mathbf{x}, t)$ represents active forcing. The active forces can be associated with the density of pumps [69]. Theoretical analysis where (11) is supplemented by equations describing fluid flow in the vicinity of the membrane and pump motion within the membrane provides evidence for a fluctuation spectrum that is athermal, as well as for interesting instabilities arising from curvature-pump density couplings [70]. These have been studied experimentally [71].

The nuclear envelope is a double bilayer membrane supported below the inner bilayer by a dense layer of filamentous proteins. Molecules such as mRNA and proteins shuttle across the nuclear envelope through pore complexes. Energy dependent processes are likely involved in the transport of these molecules within the nucleus and across the nuclear envelope [72, 73]. Moreover, the nuclear envelope also integrates mechanochemical signals, allowing the cell to regulate gene transcription and functionality [74].

D. Hydrodynamic descriptions

The hydrodynamic approach extends the thermodynamic description to include spatiotemporal variations at the longest relevant length- and time-scales [48]. The equations that result from such an approach typically involve several phenomenological coefficients. The hydrodynamic description of an isothermal elastic solid or viscous fluid composed of point particles is written in terms of the mass density $\rho(\mathbf{x}, t) = \langle \sum_{\alpha} m_{\alpha} \delta(\mathbf{x} - \mathbf{x}_{\alpha}) \rangle$ and the momentum density $\mathbf{g}(\mathbf{x}, t) = \langle \sum_{\alpha} m_{\alpha} \mathbf{v}_{\alpha} \delta(\mathbf{x} - \mathbf{x}_{\alpha}) \rangle$ where m_{α} and \mathbf{v}_{α} are the mass and velocity of the α^{th} particle located at \mathbf{x}_{α} . The hydrodynamic equations for the mass and momentum densities are

$$\partial_t \rho = -\nabla \cdot \mathbf{g}, \quad \partial_t \mathbf{g} = -\nabla \cdot \Pi, \quad (12)$$

where the momentum flux tensor $\Pi = \mathbf{g} \otimes \mathbf{v} - \Sigma$ where $\mathbf{v} = \mathbf{g}/\rho$ the hydrodynamic velocity and \otimes is a tensor-product [48]. The generically symmetric second-rank stress-tensor Σ encodes the interactions of the mesoscopic continuum element with its surroundings.

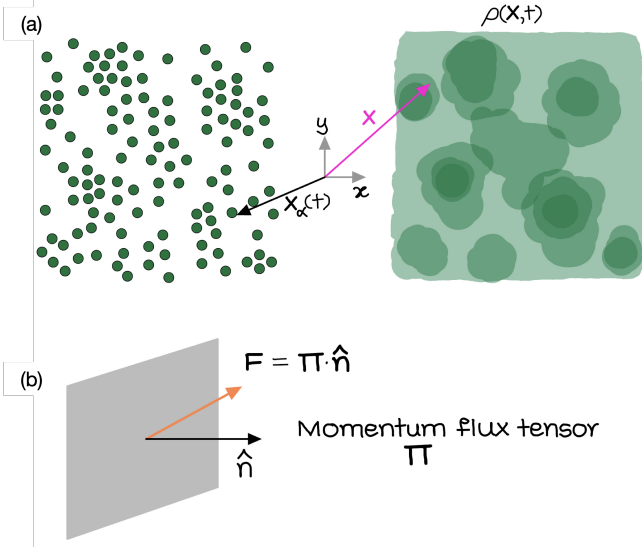


FIG. 5. Coarse-grained descriptions. (a) Shows a varying particle density leads to the construction of a density field $\rho(\mathbf{x}, t)$ as shown. (b) The momentum flux tensor Π measures the flux of momentum through an infinitesimal area element with normal $\hat{\mathbf{n}}$. In particular, the force per unit-area acting on this area element is $\mathbf{F} = \Pi \cdot \hat{\mathbf{n}}$.

1. Simple Fluids

For a simple Newtonian fluid, with a shear-viscosity η and a bulk-viscosity η_b , the stress-tensor is

$$\Sigma_f = -p \mathbb{I} + 2\eta \left[\epsilon - \frac{\text{Tr}(\epsilon)}{d} \mathbb{I} \right] + \eta_b \text{Tr}(\epsilon) \mathbb{I}, \quad (13)$$

where p is the thermodynamic pressure, and

$$\epsilon = \frac{\nabla \mathbf{v} + (\nabla \mathbf{v})^T}{2} \quad (14)$$

is the shear-rate tensor, \mathbb{I} is the identity tensor in d -dimensions and $(\dots)^T$ denotes a transpose. For an incompressible fluid ($\text{Tr}(\epsilon) = \nabla \cdot \mathbf{v} = 0$), this leads to the conventional form of the Navier-Stokes equation for the velocity field

$$\partial_t \mathbf{v} + \mathbf{v} \cdot \nabla \mathbf{v} = -\frac{1}{\rho} \nabla p + \nu \nabla^2 \mathbf{v}, \quad (15)$$

where the kinematic viscosity, $\nu = \eta/\rho$, can be thought of as a diffusion constant for velocity.

At the scale of cells and tissues, we can often ignore nonlinearities associated with the equation of motion of the fluid since the Reynolds number $\text{Re} \ll 1$. A further approximation is to drop the time-derivatives of the velocity field as the accelerations ($\partial_t \mathbf{v} \approx 0$). The velocity can then be assumed to adapt instantly to the applied

force. The governing equations of the velocity field are linear and time-reversible.

This has consequences for swimming at low Reynolds number. The problem of swimming is to understand how cyclic shape changes in the swimmer, coupled to fluid flow, result in net motion of the swimmer. Swimming at low Reynolds number presents rather counterintuitive physics. The absence of net motion in a system with a single degree of freedom that varies cyclically is one consequence – the *scallop theorem* [51]. A swimmer in a fluid is a force-free system. A monopole force field cannot enter its description. To lowest order, such a swimmer must be modeled as a force dipole in a fluid. However, a perfectly symmetric force dipole cannot exhibit net motion by symmetry. A prototypical problem for self-propulsion must thus involve flow generated by an asymmetric force-dipole in a fluid. The scale of the velocity, in the low Reynolds number limit, is proportional to the value of the force divided by the product of the viscosity and the length of the dipole [75].

2. Elastic Solids

An elastic material has a ground state (reference configuration), typically also called as the stress-free state. Deformations relative to this reference state cost energy. When a material point with position vector \mathbf{X} in the reference state is moved to a new point \mathbf{x} in the deformed state, the resulting displacement vector is $\mathbf{u} = \mathbf{x} - \mathbf{X}$. When deformations and rotations in the elastic material are small, i.e., $|\nabla \mathbf{u}| \ll 1$, there is a direct analogy between the velocity \mathbf{v} of the Newtonian fluid and displacement \mathbf{u} of the elastic. Hence, analogous to the strain rate (14), the configurational change in the elastic material is captured by the small deformation strain

$$\epsilon = \frac{\nabla \mathbf{u} + (\nabla \mathbf{u})^T}{2}, \quad (16)$$

Consequently, similar to (13) for a Newtonian fluid, the stress for a linear, isotropic elastic material is given by a generalization of Hooke's law

$$\Sigma_s = 2\mu_s \left[\epsilon - \frac{\text{Tr}(\epsilon)}{d} \mathbb{I} \right] + K_b \text{Tr}(\epsilon) \mathbb{I}, \quad (17)$$

where μ_s and K_b are the shear and bulk moduli, respectively, of the solid. In addition, the equation of motion for the displacement field follows from that for the momentum \mathbf{g} , since $\rho \partial_t \mathbf{u} = \mathbf{g}$.

3. Viscoelastic Materials

The descriptions of the ideal Newtonian fluid and the ideal Hookean solid presented above are extreme limits of the mechanical response seen in real biological materials. In living systems, the microscopic constituents are not point particles but can have internal degrees of freedom with their own complex dynamics. For example, the structural configuration of filamentous structures found in cells can continuously undergo dynamical changes – polymerisation/depolymerisation, sliding, and transient crosslinking. The mechanical responses of such non-Newtonian materials are neither those of an ideal solid nor those of an ideal fluid [76].

An often encountered category of non-Newtonian materials are those that show viscoelastic behavior. Two broad classes of such materials are the linear viscoelastic solid (Kelvin material) and the linear viscoelastic fluid (Maxwell material) – see FIG. 6. A viscoelastic solid flows like a fluid for time-scales $t \ll \tau$, where τ is the stress relaxation time-scale, whereas for $t \gg \tau$, it responds to mechanical perturbations like an elastic solid.

On the other hand, a viscoelastic fluid exhibits a short-time elastic response and flows like a fluid at long time scales. As we did for the Newtonian fluid or the Hookean solid, considering a linear relationship between the hydrodynamic stress and mechanical deformations, a simple constitutive model for a Maxwell-Jeffrey viscoelastic fluid is

$$(1 + \tau \mathcal{D}_t) \Sigma = \Sigma_f, \quad (18)$$

where Σ is the hydrodynamic stress, $\mathcal{D}_t \Sigma \equiv \partial_t \Sigma + \mathbf{v} \cdot \nabla \Sigma + \boldsymbol{\omega} \cdot \Sigma - \Sigma \cdot \boldsymbol{\omega}$, is the co-moving, co-rotating derivative with $\boldsymbol{\omega} = (\nabla \mathbf{v} - \nabla^T \mathbf{v})/2$ being the vorticity tensor, and Σ_f is the hydrodynamic fluid stress defined in (13). The co-moving, co-rotating derivative \mathcal{D}_t , as the name suggests, measures the rate of change of a tensor in a frame-invariant manner. Note that in (18), if $\tau = 0$, then the total stress Σ reduces to the fluid stress Σ (13). Typical viscoelastic materials at the cellular scale include the actomyosin cortex (see section X) and at the larger scale, entire tissues (see section XII). The Maxwell relaxation time for the actomyosin cortex is of the order of a second [50] while that for axons is a few tens of seconds [77].

The response of a macroscopic system to external perturbations provides insights into its structure and stability. When the magnitude of applied perturbations is comparable to the strength of spontaneous fluctuations

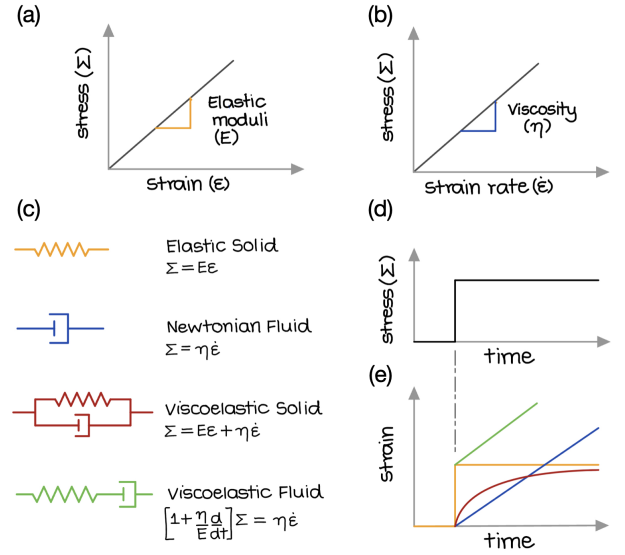


FIG. 6. The response of macroscopic materials to an applied force can be characterized by its stress Σ versus strain ε relationship in equivalent one-dimensional models. (a) For a Hookean elastic solid, the stress is linearly proportional to the strain, with the proportionality constant being the elasticity modulus E . This is represented by a simple spring. (b) For a simple Newtonian fluid, the stress is linearly proportional to the strain-rate, with the proportionality constant being the shear viscosity η as represented by a dashpot. (c) A generic material can display both solid- and liquid-like responses at different timescales. Linear viscoelastic materials can be modeled by serial and parallel arrangements of springs and dashpots. The Kelvin-Voigt viscoelastic solid (red), with the spring and dashpot in parallel, flows like a fluid at short times and is solid-like at long times. The relevant timescale is governed by η/E . On the other hand, the Maxwell-Jeffrey viscoelastic fluid (green), with the spring and dashpot in series, responds as a solid at short times and flows like a fluid at long times. The time-evolution of the strain for the different materials, in response to an imposed step stress (d), are also illustrated in (e).

in the system, linear response theory provides a good approximation to calculate these responses. Remarkably, linear response theory also connects these response functions to correlation functions of spontaneous fluctuations, as we discuss below.

E. Linear response

A fundamental characteristic of many-body systems at (or close to) thermal equilibrium is the relationship between spontaneous fluctuations (as measured by two-

point correlation functions, for instance) and the response of the system to the application of a weak external time-dependent perturbation (as measured by response functions). This connection, called Onsager's regression hypothesis, is codified by linear-response theory and leads to the fluctuation-dissipation theorem [47, 78–80].

One way to characterize the behavior of biological systems is to apply a weak perturbation and study their response. For example, tracking the motion of a small colloidal particle provides insights into the nature of its environment. This can be done in the cytoplasm or the cytoskeleton. For instance, in reconstituted *in-vitro* networks, measuring the deviation between the correlation and response functions provides a characterization of the nonequilibrium nature of the system [81] as shown in FIG. 7.

Empirically, the response of a system to applied perturbations is probed by measuring the (time-dependent) relaxation of a macroscopic quantity A to its equilibrium value A_{eqm} . Consider a generalized force \mathcal{F}_B , that couples to another macroscopic quantity B , applied on the system. Specifically, we assume that the force \mathcal{F}_B enters the microscopic energy in the form $-\mathcal{F}_B \cdot B$, i.e., we assume that \mathcal{F}_B is the thermodynamic variable conjugate to B . If the applied force does not significantly alter the macroscopic thermodynamic equilibrium state of the system, the change $\Delta A(t) \equiv A(t) - A_{\text{eqm}}$ is linearly related to the applied force. If \mathcal{F}_B is switched on adiabatically, i.e, much slower as compared to the molecular relaxation time-scales, from $t = -\infty$, then

$$\Delta A(t) = \int_{-\infty}^t dt' \chi_{AB}(t-t') \mathcal{F}_B(t'), \quad (19)$$

where the response function $\chi_{AB}(t-t')$ captures the coupling between A and B . Note that the response $\Delta A(t)$ is, in general, not in phase with the applied force $\mathcal{F}_B(t)$. Causality implies that $\chi(t-t')$ is non-zero only for $t > t'$.

Spontaneous thermal fluctuations of macroscopic quantities are typically captured via two-point correlation functions. For instance, the statistics of the time-dependent fluctuations of macroscopic quantities A and B around their equilibrium values A_{eqm} and B_{eqm} is captured by the correlation function

$$C_{AB}(t-t') = \langle \Delta A(t) \Delta B(t') \rangle \quad (20)$$

where $\langle \dots \rangle$ denotes an equilibrium average. Linear response theory connects this correlation function with

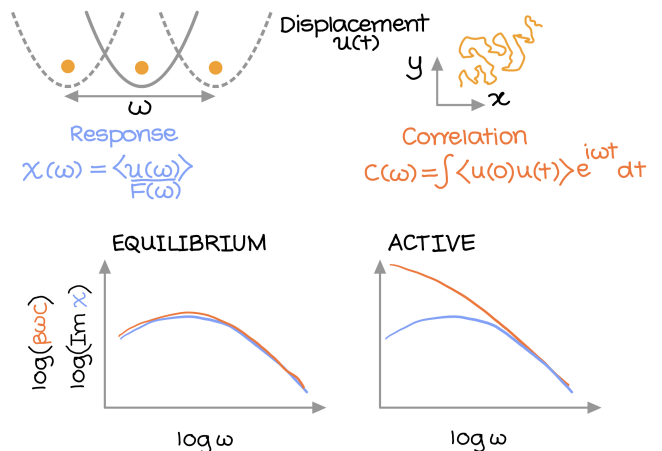


FIG. 7. The reaction of a macroscopic system to an applied infinitesimal force is captured by generalized response functions $R(\omega)$ which depend on the frequency (ω) of the applied force $F(\omega)$. For instance, the response function for a Brownian particle can be measured as the ratio of the average displacement $\langle u(\omega) \rangle$ to the applied force (for instance, in an optical trap). Spontaneous fluctuations of the displacement u , in the absence of external forces, are captured by the Fourier-transform $C(\omega)$ of the two-time correlation function $\langle u(0)u(t) \rangle$. For a system at thermodynamic equilibrium, the fluctuation-dissipation theorem (21) relates the response and correlation functions at all frequencies, a consequence of linear-response theory. For an active system, no such relation exists in general, and the response and correlation functions can be decoupled from each other. However, they typically agree at high frequencies since fast degrees thermalize quickly. Note that, in principle, either or both the response functions and the correlation functions can deviate from their equilibrium behavior in the presence of activity.

the response function $\chi(t-t')$ defined above via the fluctuation-dissipation relation (in Fourier space)

$$\text{Im}[\chi_{AB}(\omega)] = \frac{\omega}{2k_B T} C_{AB}(\omega), \quad (21)$$

where $\text{Im}[\chi_{AB}(\omega)]$ represents the imaginary part. Systems that are driven out-of-equilibrium by external energy inputs violate this fluctuation-dissipation relation (21) [80]. Recent years have seen several attempts to generalize linear response theory to situations where the reference state is a non-equilibrium steady state (NESS) [82, 83].

So far, we have considered the response and correlation functions of spatially homogeneous systems that are close to thermodynamic equilibrium. For a system driven out of equilibrium, we do not, as yet, have a generic framework to discuss its thermodynamics. However, a useful

approximation is that of local thermodynamic equilibrium. In other words, a spatially heterogeneous system at macroscopic length-scales can be thought to be made up of interacting mesoscopic elements each of which are in *local thermodynamic equilibrium*. These mesoscopic regions reach local equilibrium over time-scales that are much smaller compared to the relaxation time of the entire system. An example of this hydrodynamical approach was discussed in the previous section when we considered the macroscopic description of a simple Newtonian fluid. This framework of generalized hydrodynamics, when extended to complex materials, has turned out to be very fruitful in the description of biological systems from cellular to tissue scales [11, 84]. Finally, there is no *a priori* justification for the linear response assumption in far-from-equilibrium steady-states. However, in practice, this assumption appears to provide a reasonable description of many biophysical systems.

F. Onsager relations and generalized hydrodynamics

A systematic way to derive the hydrodynamic equations for the coarse-grained description of a many-body classical system is to develop its linear irreversible thermodynamics. A system at equilibrium is in a state of maximum entropy S . Any perturbations in a *generalized displacement* variable u that takes the system away from this state of maximum entropy are countered by a *generalized force* F which tends to restore the equilibrium state. In the ensuing process, the rate at which entropy is generated is proportional to the product of this generalized force and the flux of the generalized displacement \dot{u} . In the case of several generalized displacements u_i , and the corresponding generalized forces F_i , the rate of entropy production is

$$\frac{d}{dt}\Delta S = \sum_i F_i \dot{u}_i. \quad (22)$$

If the system is close to equilibrium, the generalized force can be expanded in a linear combination of the fluxes, i.e., $F_i = \sum_j L_{ij} \dot{u}_j$, where L_{ij} are called Onsager coefficients.

Time-reversal invariance constrains the symmetry of L_{ij} . For instance, in the case of the simple isotropic fluid discussed earlier, the generalized force is the stress tensor Σ , the generalized flux is the strain rate ϵ , and the viscosities η and η_b are the Onsager coefficients. In the

case of systems with chemical reactions, the differences in chemical potentials are the generalized forces and the rate of chemical reaction are the fluxes. In general, the chemical and mechanical degrees of freedom are coupled to each other leading to mechanochemical effects. Non-equilibrium chemical reactions within cells can generate active stresses (see section VII).

To generalize this approach, we write the conservation laws and generic equations of motion for broken symmetry field variables. We then proceed by identifying the generalized forces and fluxes that enter the entropy production rate. Following Onsager [78, 79] (and similar to the linear-response theory outlined above), we expand the generalized fluxes as a linear combination of the generalized forces, with appropriate considerations for their behavior under time-reversal. These lead to the constitutive equations for the system under consideration. Finally, one identifies those terms that survive in the hydrodynamic limit, i.e., long-times and large-lengths compared to the microscopic degrees of freedom. This leads to a closed set of hydrodynamic equations with several phenomenological coefficients. One can also include stochastic components in the hydrodynamic equations as discussed above in the case of an isotropic simple fluid.

The use of this approach in biological systems is illustrated below.

G. Orientational order

Anisotropic order is often seen in living systems, for example in the cytoskeleton or in cell-ordering in tissues. Understanding the statics and the dynamics of such anisotropic systems requires hydrodynamic descriptions. Orientational order can be of multiple kinds. Fore-aft asymmetric filaments (represented by arrows in FIG. 8) can arrange into an isotropic state or a polar state. Fore-aft symmetric filaments (represented by undirected segments in FIG. 8) can arrange into an isotropic state or a nematic state. Nematic ordering can also arise from a symmetric mixture of polar filaments which are aligned but have no net directionality. A vector order parameter \mathbf{p} is relevant for describing orientation order in a polar system. On the other hand, describing local anisotropy in a nematic system requires a traceless and symmetric second-rank tensor \mathbf{Q} . One can derive the hydrodynamic equations for an anisotropic system with a polar order-parameter \mathbf{p} and/or a nematic order-parameter \mathbf{Q} .

In the case of polar liquid crystals [85], the governing

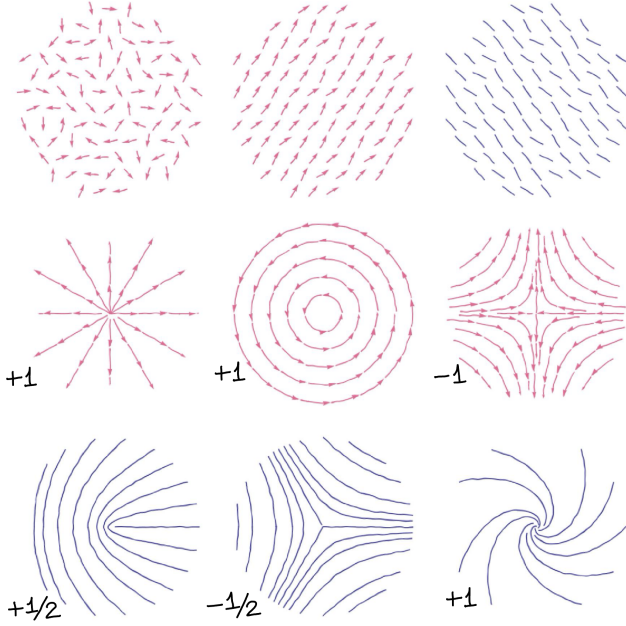


FIG. 8. Orientational degrees of freedom can have either polar (represented by an arrow) or nematic (represented as an undirected segment) symmetry. The top row of figures shows disordered polar, disordered nematic, and ordered polar structures. This order-disorder transition is typically controlled by temperature and/or density. In the ordered phase, topologically stable excitations appear in the form of topological defects in the orientational order. Each such singularity is associated with a topological charge that is obtained by measuring the change in the angle of the order parameter around a loop enclosing the defect. The middle row shows examples of $+1$ and -1 defects. The bottom row shows topological defects peculiar to nematics: $1/2$, $-1/2$ and $+1$.

energy functional is the free energy density

$$\mathcal{F}_p = \int d^d \mathbf{x} \left[\alpha (\mathbf{p} \cdot \mathbf{p}) + \beta (\mathbf{p} \cdot \mathbf{p})^2 + K (\nabla \mathbf{p} : \nabla \mathbf{p}) \right], \quad (23)$$

where α and β govern the physics near the order-disorder transition. The transition from a disordered state $\mathbf{p} = 0$ to an ordered state $\mathbf{p} \neq 0$ occurs at $\alpha = 0$, while stability demands $\beta > 0$ always. The gradient term governs the orientational elasticity of the polar order parameter \mathbf{p} , with K an elastic modulus within the one-constant approximation. The polar order-parameter generates orientational stresses in the system. The stress-tensor therefore has an additional component

$$\Sigma_p = \nu \left[\mathbf{p} \otimes \mathbf{h} + \mathbf{h} \otimes \mathbf{p} - \frac{2}{d} (\mathbf{p} \cdot \mathbf{h}) \mathbb{I} \right] + \bar{\nu} (\mathbf{p} \cdot \mathbf{h}) \mathbb{I}, \quad (24)$$

where the molecular field conjugate to the polarity $\mathbf{h} = -\delta \mathcal{F}_p / \delta \mathbf{p}$, and ν and $\bar{\nu}$ are the alignment parameters. The evolution equation for the order parameter \mathbf{p} is $D_t \mathbf{p} = \mathbf{h} / \bar{\gamma} - \nu \tilde{\epsilon} \cdot \mathbf{p} - \bar{\nu} \text{Tr}(\epsilon) \mathbf{p}$, where $\bar{\gamma}$ is a kinetic coefficient, $\tilde{\epsilon}$ is the traceless part of ϵ and $D_t \mathbf{p} \equiv \partial_t \mathbf{p} + \mathbf{v} \cdot \nabla \mathbf{p} + \boldsymbol{\omega} \cdot \mathbf{p}$ is the co-moving co-rotating derivative with $\boldsymbol{\omega} = (\nabla \mathbf{v} - \nabla^T \mathbf{v}) / 2$ being the vorticity tensor. If the relevant order parameter is a nematic tensor \mathbf{Q} , then the corresponding free energy is

$$\mathcal{F}_n = \int d^d \mathbf{x} \left[\alpha \text{Tr}(\mathbf{Q}^2) + \beta \text{Tr}(\mathbf{Q}^3) + \gamma (\text{Tr}(\mathbf{Q}^2))^2 + \mathcal{K} \nabla \mathbf{Q} : \nabla \mathbf{Q} \right], \quad (25)$$

where α , β , γ govern the physics of the isotropic to nematic phase-transition, the \mathcal{K} is the orientational elasticity modulus, and the corresponding orientational stress is

$$\Sigma_n = \nu \mathbf{H} = -\nu \frac{\delta \mathcal{F}_n}{\delta \mathbf{Q}}, \quad (26)$$

where \mathbf{H} is the conjugate molecular field. The order parameter \mathbf{Q} evolves according to $\mathcal{D}_t \mathbf{Q} = \mathbf{H} / \Gamma - \nu \tilde{\epsilon}$ where Γ is a kinetic coefficient, ν is a flow alignment parameters and the comoving, corotating derivative for a second rank tensor field is defined as $\mathcal{D}_t \mathbf{Q} \equiv \partial_t \mathbf{Q} + \mathbf{v} \cdot \nabla \mathbf{Q} + \boldsymbol{\omega} \cdot \mathbf{Q} - \mathbf{Q} \cdot \boldsymbol{\omega}$.

The total mechanical stress in an isotropic Newtonian fluid is $\Sigma = \Sigma_f$, while for anisotropic fluids $\Sigma = \Sigma_f + \Sigma_p$ or $\Sigma = \Sigma_f + \Sigma_n$ for polar or nematic fluids, respectively. To complete the hydrodynamic description, we need to supplement these equations with appropriate boundary conditions, and, when the time-evolution is of interest, initial conditions as well.

Complex anisotropic fluids typically show a viscoelastic response to applied mechanical perturbations. In other words, depending on the time-scales of observation, the material might show an elastic response or flow like a viscous fluid. The hydrodynamic approach can be extended to describe viscoelastic materials. For instance, in the linear Maxwell-Jeffrey viscoelastic model, the stress evolves according to $(1 + \tau \mathcal{D}_t) (\Sigma - \Sigma_o) = \Sigma_f$, where Σ_o is either Σ_p or Σ_n as appropriate, and the timescale τ governs the transition from an elastic behavior at short times ($t \ll \tau$) to a fluid-like response at long time scales ($t \gg \tau$).

In an ordered medium, such as a group of aligned cytoskeletal filaments, the order parameter measures the local orientation. It is possible for this order parameter to be ill-defined at a finite number of locations. Away from these points, the order parameter must vary smoothly.

This implies the existence of localized topological defects in the ordering associated with these points (FIG. 8). A topological charge, decided by the winding number of smooth curves around the defect, characterizes each such singularity.

For instance, for polar ordering, the topological charges are integer-valued whereas for nematic ordering, they are 1/2–integer valued [86]. The sum of the topological charges in a domain is governed by the topology of the domain, i.e., the connectivity of the domain. Smooth changes of the orientation field or the geometry of the domain (without affecting the topology) does not change the sum of the topological charges. In a system at thermodynamic equilibrium, topological charges of opposite signs have the same dynamics [48].

In an active system, however, the dynamics of defects is influenced by their topological charges. For instance, a +1/2 defect is a polar structure and has a net motility in an active system [87]. Such motile defects have been observed in the large scale orientational order of actin filaments in *in vitro* experiments [88], in developing hydra [89], and also in cell collectives [90]. Recent works have shown that topological defects play an important role in various morphogenetic processes.

H. Soft-materials driven out of equilibrium

In the discussion above, our description has focused on systems that are at thermal equilibrium. For cellular processes, whether an equilibrium description is sufficient depends on the process as well as the time-scales of interest. For instance, most chemical reactions that occur on fast timescales can be understood within an equilibrium formalism [35]. However, on longer timescales, typically, cellular metabolic processes drive energy and material fluxes, thus necessitating a nonequilibrium description.

For systems with discrete states, breaking detailed balance, i.e., $W_{C' \rightarrow C} P(C', t) \neq W_{C \rightarrow C'} P(C, t)$, can lead to nonequilibrium steady-states (when $dP/dt = 0$) with non-zero currents. Note that this is a subtle way to be out of equilibrium compared to the case when there are non-zero external forces, possibly time-dependent, acting on the system that would inject energy into the system. Systems that are force-free can nevertheless be out of equilibrium if the distribution across their internal states does not obey the Boltzmann probability.

A typical way to force a system out of equilibrium is to violate the fluctuation-dissipation theorem, i.e., con-

sider sources of dissipation that are not related to the strength of stochastic fluctuations. At the hydrodynamic level, systems that are macroscopically force- and torque-free can be driven out of equilibrium in multiple ways. A novel class of nonequilibrium systems with an energy throughput, wherein the energy consumption and dissipation occur at the level of the individual units, are “active materials” [84, 91–97]. For such systems, not requiring microscopic time-reversal invariance generically allows additional terms in the hydrodynamic equations. The active stress contributions for polar and nematic systems are

$$\Sigma_{\mathbf{p}}^{\text{active}} = \zeta \Delta\mu \mathbb{I} + \bar{\zeta} \Delta\mu \left[\mathbf{p} \otimes \mathbf{p} - \frac{(\mathbf{p} \cdot \mathbf{p})}{d} \mathbb{I} \right], \quad (27)$$

$$\Sigma_{\mathbf{n}}^{\text{active}} = \zeta \Delta\mu \mathbb{I} + \bar{\zeta} \Delta\mu \mathbf{Q}, \quad (28)$$

where the coefficients $\zeta \Delta\mu$ and $\bar{\zeta} \Delta\mu$ result from active processes. The above expressions are obtained through considerations of symmetry for the stress tensor, while $\Delta\mu$ represents the chemical potential difference for ATP hydrolysis, reflecting the non-equilibrium character of the system. The equilibrium equations of evolution mentioned earlier can be appropriately modified to include all lowest order terms permitted by symmetry (without assuming time-reversal invariance). This yields

$$\begin{aligned} \mathcal{D}_t \mathbf{p} = & \mathbf{h}/\bar{\gamma} - \nu \tilde{\boldsymbol{\epsilon}} \cdot \mathbf{p} - \bar{\nu} \text{Tr}(\boldsymbol{\epsilon}) \mathbf{p} + \lambda_0 \mathbf{p} \\ & - \lambda_1 (\mathbf{p} \cdot \nabla) \mathbf{p} - \lambda_2 (\nabla \cdot \mathbf{p}) \mathbf{p} + \lambda_3 \nabla (\mathbf{p} \cdot \mathbf{p}), \end{aligned} \quad (29)$$

$$\mathcal{D}_t \mathbf{Q} = \Gamma^{-1} \mathbf{H} - \nu \tilde{\boldsymbol{\epsilon}} + \Lambda \mathbf{Q}, \quad (30)$$

where the terms with the coefficients λ_i 's are active terms and must generically vanish at equilibrium. However, if $\lambda_3 = 2\lambda_2$ and $\lambda_1 = 0$, then such terms are permitted even in an equilibrium situation. For instance, in the case of an active polar fluid, equations (12) and (29) together with (13), (24), and (27) complete the hydrodynamic description when supplemented with appropriate initial and boundary conditions.

Variants of these equations were initially written down to represent the physics of self-propelled particles. However, they appear to be more generally applicable even for cellular systems, like in the coarse-grained description of the cytoskeleton [93]. Similar considerations apply in the case of an active nematic material as well.

In the previous sections, we have briefly discussed the particulate and continuum descriptions, both at and away from equilibrium, as relevant to the description of soft materials found in living systems. In particular, we

have focused on how mechanical forces and stresses can alter the statistical dynamics of particles and fields. In the context of living materials, active stresses typically arise in cellular contexts where the activity of molecular motors plays a dominant role. For instance, coarse-grained descriptions of the cellular cytoskeleton or, at larger scales, entire tissues, can be described in the framework of active materials discussed above. We will revisit these specific topics in section XII. However, it is of paramount importance to be able to quantitatively measure these forces and stresses in living systems. With this in mind, we next discuss how cells infer forces and some of the key techniques developed to infer forces in the laboratory setting.

V. HOW DO CELLS INFER FORCES?

The configurations of several cell surface molecules are sensitive to mechanical forces [98]. For instance, the closing and opening of ion channels are influenced by the tension in the membrane. The flux of ions across these channels provides an indirect measure of the forces acting on the cell.

At a larger scale, cilia and flagella can not only generate forces due to internal active processes but can also respond to forces from the external environment. For instance, drag forces from the surrounding fluid affect the manner in which the ciliary structure of the hair cells in the inner ear respond to fluid stress in the cochlea [99]. Here, such forces displace ciliary bundles which control the opening/closing of ion channels. The ensuing ion-currents lead to the sensation of hearing via the activation of specific neurons.

VI. MEASURING MECHANICAL FORCES

Experimental information can be derived either from the living cell itself (*in vivo*), from cytoplasmic material extracted from cells (*cell extracts*), or from purified and reconstituted constituents (*in vitro*). A detailed understanding of the mechanisms of force generation and viscoelastic responses in a cellular context requires quantitative measurements of these processes at different scales, ranging from the single molecule level to cells to tissues.

Mechanical forces at the single molecule level, such as the stepping of single motor protein or elasticity of isolated biopolymer filaments, are intrinsically stochas-

tic in nature. We can only infer a probability distribution of the force from a time-series measurement. At the sub-cellular or single cell level, in addition to stochasticity that can arise from thermal and active processes, spatial heterogeneity can influence mechanical measurements. Several techniques have been developed over the last several decades to overcome these challenges.

Cells infer forces applied on them via mechanochemical pathways by initiating chemical response to forces [100, 101]. For instance, tension sensitive ion channels on the cellular membrane can transduce mechanical effects to chemical events which in turn can modulate active processes such as cell contraction. The activation of myosin-II motor proteins by calcium entry through stretch activated calcium channels is one specific example [102]. More generally, all protein molecules have some force sensing capability since changes in their conformation brought about by applied forces alters their interaction with other molecules via allosteric effects.

Techniques for measuring mechanical forces in living matter can be classified based on whether the experimentally measured quantities are macroscopic averages or fluctuations about them. A further classification of the first type is based on responses that are purely mechanical (for example, flows, displacements, strains) versus those that are mechanochemical (for example, reaction rates, chemical currents, conformation changes). Even where such macroscopic responses vanish on average, it is still possible that non-trivial fluctuations can lead to statistical forces which can have observable consequences (for example, enhanced mean-square displacements and depletion forces). Most experimental techniques have an underlying model that relates the measured response with the applied force.

A full description of these techniques and their many applications is beyond the scope of this article, but details can be found in Refs. [103–106]. Below we provide the basic operational principles of a few commonly used methods which are summarized pictorially in Figures 9–12.

A. Atomic Force Microscopes (AFM)

AFM is a popular technique that uses a calibrated cantilever to measure forces [107] (FIG. 9a). The force experienced by the cantilever is measured by reflecting a laser beam from the tip of the cantilever and measuring its deflection using a quadrant photodiode—a device that

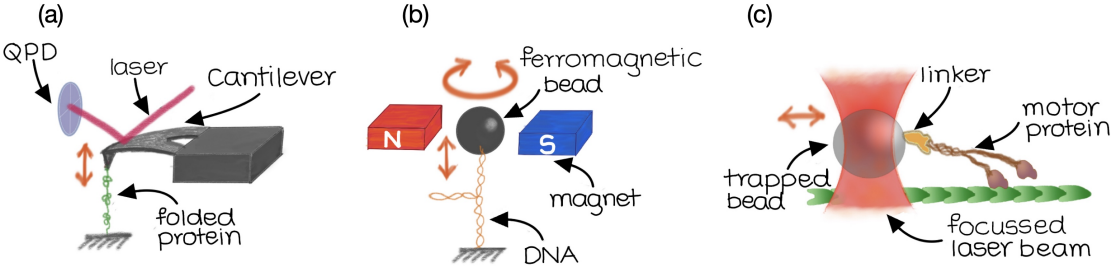


FIG. 9. Schematic diagrams showing some of the popular techniques used for measuring forces at the molecular scale. (a) An Atomic Force Microscope uses a calibrated triangular cantilever having a pointed tip. The cantilever base attached to a piezoelectric translator. The deflection of the cantilever is detected using a laser beam which is reflected from the cantilever tip and a quadrant photodiode (QPD) –a device that can provide position information– as shown. Force-extension curves of proteins like spectrin, for example, can be investigated using this tool. (b) Magnetic Tweezers use a micron-sized ferromagnetic bead to tug or twist molecules like DNA. One end of the DNA strand is attached to a surface and the other is linked to the bead. A permanent magnet can then be used to apply forces by displacing the magnets vertically, or torques by rotating the magnets. The resulting displacements are measured using video microscopy. (c) Optical tweezers use a focused laser beam to trap micron-sized dielectric spheres. The trapped sphere can then be used as a force sensor by calibrating the trapping potential. Several studies of pico-Newton level force generation and nano-meter sized stepping of molecular motors, for example, have been performed using this technique.

can provide position information. A feedback loop allows for control of either force or elongation. AFMs have been used to measure ligand-receptor binding [108], force-extension behaviour of single protein molecules [109], mechanics of reconstituted actin networks [110], cell and tissue mechanics [111, 112]. Typically, in biological systems, AFM can be used to measure forces ranging from $\sim 1 \text{ pN} - 1 \text{ nN}$.

B. Magnetic tweezers

Magnetic tweezers use paramagnetic or ferromagnetic beads/particles, which are $\sim 100 \text{ nm} - 1 \mu\text{m}$ in size. When placed in an external magnetic field gradient, they can be used to apply forces on single molecules or cells [113] (see FIG. 9b). Bead displacements are measured using the methods discussed below (Section VID). When a ferromagnetic bead is used, torques can be applied by rotating the external magnetic field. The use of electromagnets allows for precise control of applied forces and also for their modulation in time.

Forces in the range of $\sim 1 \text{ pN} - 10 \text{ nN}$, a much higher range than provided by optical tweezers, can be achieved by this method. Magnetic tweezers have been used in experiments ranging from measuring the elasticity of DNA strands [114, 115], single protein elasticity [116, 117], and measurements of the local viscoelasticity of the cell cor-

tex [118].

C. Optical tweezers

Forces generated by molecular motors, single filament polymerisation forces, ligand-receptor interaction forces, etc., are of the order of a few pN. They are most conveniently measured using optical tweezers (also known as laser tweezers or optical trap) [119] (see FIG. 9c). This technique uses a tightly focused laser beam to obtain a 3-dimensional trap for micron-sized dielectric beads [120]. The trapping is effected by the momentum transferred to the bead from the light beam as it gets refracted through the bead. The stiffness of the trap is usually measured from the power-spectrum of the trapped bead, which can be approximated as a Brownian particle in a harmonic potential. Any external force acting on the bead is measured by monitoring its displacement from the center of the trap using a quadrant photodiode. One major advantage of this method is that it is non-invasive and can even be used to trap beads/organelles within a cell without mechanically penetrating the cell [121]. Forces in the range of $\sim 0.1 \text{ pN} - 10 \text{ pN}$ can be measured using this method.

D. Single molecule tracking and microrheology

Single molecule tracking is a simple yet powerful technique which relies on the measurement of the trajectory of a microscopic particle (for example, a fluorescent molecule, a microscopic bead or a tiny organelle) (FIG. 10a). Tracking is performed by video time-lapse microscopy and subsequent image analysis [122]. The spatial resolution for tracking an isolated particle is not limited by the resolving power of a light microscope, which is approximately $0.5 \mu\text{m}$, but rather by the accuracy with which the intensity distribution of the particle can be sampled. Spatial resolutions of about 1 nm and temporal resolutions of about 100 Hz can be achieved. For spatially confined particles, like microscopic beads within a cytoskeletal meshwork, tracking at frequencies of the order of a few tens of kHz can be done by scattering a focused laser beam from the particle and imaging the scattered light on to a quadrant photodiode [123]. This allows for the study of frequency dependent responses.

Particle tracking can be used to infer the diffusivity of molecules in membranes by measuring the Mean Square Displacement (MSD) averaged over many realizations [124, 125] (FIG. 10a). For systems at equilibrium, this technique is also used to measure viscoelastic properties of *in vitro* and *in vivo* cytoskeletal gels. While this method is fairly straightforward for systems at equilibrium, data from active structures such as the cytoplasm, the actomyosin cortex or the nucleus has to be interpreted with caution [81]. Tracking two or more beads simultaneously allows for the measurement of correlation functions, providing information on active stress fluctuations within the gel/cortex (Section IV) [126].

The method described in the above paragraph, called passive microrheology, provides information about the spontaneous fluctuations in the medium. In contrast, response properties can be also be inferred by subjecting the probe particle to external forcing, e.g., using optical or magnetic tweezers described above [127, 128](FIG. 10a). For a system close to thermodynamic equilibrium, the fluctuation-dissipation relation connects the response function to the measured correlation function (see FIG. 7 and section IV E). However, for an active system, the correlation of the spontaneous fluctuations need not be connected to the response function. In fact, the deviation between these two quantities is a measure of the non-equilibrium nature of the system [81].

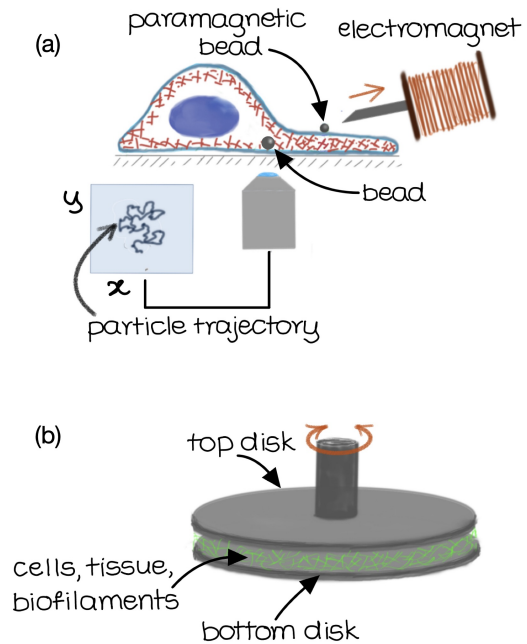


FIG. 10. Schematic diagrams showing the basic principles behind some techniques used for quantifying mechanical responses of cells or tissues at a mesoscopic scale. (a) Local viscoelastic properties can be explored using either a passive particle embedded in the cell or using a magnetic bead pulled using an electromagnet. In passive microrheology, spontaneous fluctuations are monitored using video-microscopy and the data is analysed to extract material properties. In live cells, this technique is sensitive to the active component of the noise, and the analysis should take this into consideration. On the other hand, in active microrheology, a force is applied to a paramagnetic bead attached to the cell using an electromagnet and the resulting response is analysed. (b) Shear rheology is a popular method used to study viscoelastic properties of *in vitro* biopolymer gels.

E. Shear rheology

Shear rheology using rotating disc-shaped plates is a standard technique to probe the viscoelasticity of soft materials and complex fluids [129]. In its simplest configuration, the sample is sandwiched between two circular discs, $\approx 5 \text{ cm}$ in diameter. Shear deformations are applied by the angular displacement (continuous rotation or oscillations) of one of the discs and the resulting shear stress measured (FIG. 10b). A feedback mechanism allows for either shear strain or shear stress controlled measurements. When small amplitude, sinusoidal shear stress (or strain) of frequency ω is applied to a viscoelastic material, the combination of a linear storage (elastic) and

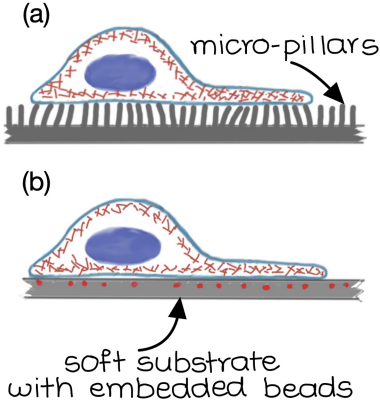


FIG. 11. Schematic diagrams showing the basic principles behind common experimental techniques used for measuring traction forces exerted by cells on a substrate. (a) The micropillar technique uses an array of micro-fabricated pillars which act as cantilevers. These pillars can be calibrated and the spatial distribution of forces can be inferred. (b) In traction force microscopy, cells are allowed to spread on soft elastic substrates which contain dispersed fluorescent beads (red dots). The displacements of the beads due to traction forces exerted by a cell can be mapped using a microscope and the corresponding stress field calculated from this.

a loss (viscous) modulus can be represented as a complex quantity $\chi(\omega) = \text{Re}[\chi(\omega)] + i \text{Im}[\chi(\omega)]$ (see section IV E). The amplitude $|\chi|$ and phase $\tan \delta = \text{Im}[\chi(\omega)]/\text{Re}[\chi(\omega)]$ of the strain (or stress) response are related to the material properties, with $\delta = 0$ for a purely elastic material and $\delta = \pi/2$ for a purely viscous material [130]. Frequency dependent responses, and non-linear responses like shear thickening or shear thinning can also be investigated using this method.

Shear rheology has been used extensively to study reconstituted biopolymer networks [131] with or without associated proteins like crosslinkers or motor proteins [132, 133]. It can also be used to study the rheology of cell monolayers in culture [134] and has been used widely to study tissue mechanics [130].

F. Measurement of cell-substrate traction forces

Traction forces (force per unit area) exerted on a substrate by adherent or crawling single cell, or a group of cells, can be measured using various microscopy techniques [135, 136]. In the *micropillar method* (see FIG. 11a) cells are grown on a micro-patterned substrate consisting of a two-dimensional lattice of cylindrical pil-

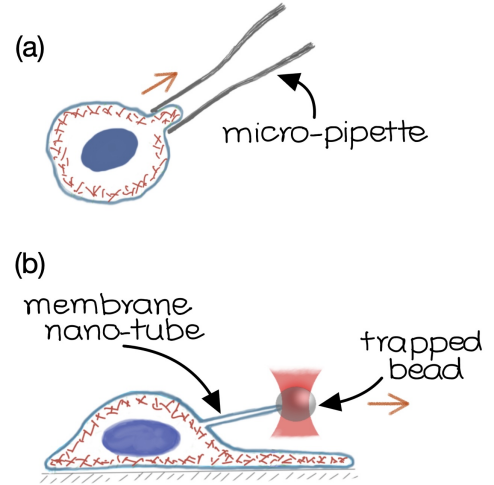


FIG. 12. Schematic diagrams showing the basic principles behind common experimental techniques used for quantifying mechanical responses of cell membranes. (a) In micropipette aspiration, a negative pressure is applied to the pipette to suck in a small portion of the cell. Viscoelastic properties of the interface can be calculated using this method. (b) In optical tweezers measurements, a micron-sized bead attached to the membrane is pulled using an optical trap to extract a membrane nanotube. Relative changes to cell membrane tension and complex dynamical properties of the membrane can be inferred from such force measurements.

lars with each pillar typically being about a micron in thickness and about $10 \mu\text{m}$ in height [137]. The traction force exerted by the cell at each position is measured by measuring the deflection of individual pillars, which are calibrated in advance.

In the *traction force microscopy* method (see FIG. 11b), cells are grown on a sheet of soft elastomer or gel with a layer of sub-micron fluorescent beads embedded into the top surface. Traction forces exerted by the cells on the gel surface cause the gel to deform, resulting in the displacement of the embedded beads, which is mapped out using image analysis. The surface tractions on the gel are estimated from the measured bead displacements given knowledge of the stress-strain constitutive relationship for the gel. This is an inverse boundary value problem in solid mechanics that is numerically solved using techniques such as Fourier transform and finite element analysis [136].

G. Measuring membrane mechanical responses

Cell membrane tension (see section IV) is a major regulator of processes such as endo/exocytosis, the gating of mechano-sensitive ion channels, the formation of protrusive structures like filopodia and a number of other examples. A number of techniques have been developed to quantify membrane tension in cells. A popular method used to investigate the cell membrane, usually along with the membrane associated cortical skeleton, is the *micropipette aspiration technique* [138–140]. In this method (see FIG. 12a), a small part of the cell is aspirated into a glass micropipette whose tip diameter $2R_p$ is small compared to the size of the cell. At steady state, the effective tension γ is calculated from the pressure difference ΔP required to aspirate and the radius of curvature of the end cap of the aspirated portion R_c using the Laplace formula (section IV): $\sigma_s = \Delta P/2(1/R_p - 1/R_c)^{-1}$. Several other applications like measurement of cortical viscoelasticity, mechanics of cell aggregates, cell-cell adhesion have also been developed based on this technique [139, 140].

Another popular method used is the *tether extraction method* (see FIG. 12b) where a membrane nano-tube is pulled out of the cell surface, usually using optical tweezers [141]. This is done by first attaching a micron-size bead to the lipid bilayer without any mechanical linkages to the cytoskeleton. Beyond a threshold force, a cylindrical membrane nano-tube, usually devoid of cytoskeletal elements, ≈ 100 nm in diameter, extends from the cell to the bead. The effective membrane tension σ_s is related to the measured force as $\sigma_s = f^2/(8\pi^2\kappa)$, where $f \sim 10$ pN is the force on the bead and $\kappa \sim 10^{-19}$ Nm is the bending modulus of the membrane [142] (see section IV). In cells, the value of σ_s may also be controlled by adhesion to the cortex and compositional variations in the membrane [143]. If a step-like extension is applied to an existing tether, the force exhibits a multi-timescale relaxation response. This relaxation occurs through various dissipation mechanisms, such as intra-bilayer friction, membrane-cytoskeleton friction, and fluid flow inside the tube [144, 145].

Fluorescent dyes can also be used to gauge in-plane membrane tension or relative changes in tension. In some cases, tension dependent variation of the fluorescence spectrum, caused by changes in the dye micro-environment, is used as the readout [146]. In other cases, changes to fluorescence life time as a function of tension can be used as a read out [147].

H. Other methods

In recent times, genetically encoded molecular level force sensors have been developed as a tool to probe force-induced conformational changes of proteins [148]. This is based on a technique known as Fluorescence Resonance Energy Transfer (FRET) in which a donor fluorescent molecule absorbs a photon, and the energy is non-radiatively transferred to a nearby acceptor molecule which then emits a longer wavelength photon. The efficiency of this energy transfer process depends on the distance between the donor and the acceptor dyes [149].

Laser ablation, a method by which a laser spot is briefly directed at a localized zone, can be used to perturb the mechanical integrity of a cell or tissue. In combination with theoretical models, this method can be used to obtain quantitative estimates of local tensions in bio-filaments, cells, and tissues [52, 150, 151].

In the previous two sections, we have discussed theoretical and experimental methods used to understand mechanical forces. In cells and tissues, mechanical forces and biochemical signals are tightly interconnected. It is, however, unclear what general physical principles underlie such mechanochemically organized structures, a point we turn to in the next section.

VII. PRINCIPLES OF MECHANOCHEMICAL TRANSDUCTION

In a complex many-body system, currents in all macroscopic degrees of freedom vanish identically at thermodynamic equilibrium. However, if such a system is slightly perturbed from equilibrium, at the level of linear response, the generalized thermodynamic forces (F_j) in the various degrees of freedom can drive corresponding currents (J_i) due to cross-couplings (L_{ij}) of the general form [78, 79], i.e.,

$$J_i = \sum_j L_{ij} F_j. \quad (31)$$

For example, electrical currents can generate thermal fluxes (Peltier effect [78]). Of course, left to itself, the system would relax to a state of thermodynamic equilibrium, where all currents vanish ($J_i = 0$). However, if by some mechanism (e.g., metabolism), the thermodynamic flux of one degree of freedom (chemical energy), is maintained at a constant value, not being allowed to vanish, we generically expect non-zero fluxes in the other (translational) degrees of freedom.

A molecular motor is an example of such a system where transitions between different chemical conformations are maintained out of detailed balance by an external supply of a fuel. This biases the chemical reaction in a particular direction [152] (this is true of all metabolic processes). The chemical flux, as a result of the coupling between chemical and mechanical degrees of freedom, can drive material currents. This is the essence of *mechanochemical* coupling.

An intuitive way to visualize such a mechanochemical coupling is shown in FIG. 13. Here, the coordinates shown provide an abstract representation of the chemical and mechanical degrees of freedom of a motor-like molecule. The coupling between these degrees of freedom is depicted by the diagonal lines which represent a generalized non-diagonal mobility tensor. In other words, the diagonal “grooves” in this mechanochemical space are such that a net force in one direction, say, the chemical direction leads to a current in both the directions. This would be the normal operation of motors [152]. The opposite action, wherein chemical currents are generated from mechanical forces, is seen in nanomachines such as the F_0F_1 -ATP synthase present in the membranes of mitochondria [153, 154].

The principles of mechanochemical transduction discussed above are generically applicable in a wide range of cellular processes. In the next few sections, we illustrate these principles by discussing physical models for chromatin organization, force generation by polymerization of biopolymers, stochastic motion of molecular motors on asymmetric tracks, and, at a larger scale, the organization of the cellular cytoskeleton to orchestrate cell polarity, motility, and division.

VIII. POLYMERIZATION FORCES

Microtubules and actin filaments are biopolymers that polymerize and depolymerize in the presence of NTP [2]. Both are polar filaments: the two ends (designated plus and minus) of the filament are chemically distinct. Microtubules are composed of protofilaments surrounding a hollow $25nm$ core, with each individual protofilament formed from dimeric units of tubulin monomers. Typically, filament growth occurs predominantly at the plus-end, with filament shrinkage occurring mainly at the minus-end.

Microtubules remodel via cycles of slow growth and rapid shrinkage (catastrophe) [155]. Actin filaments in

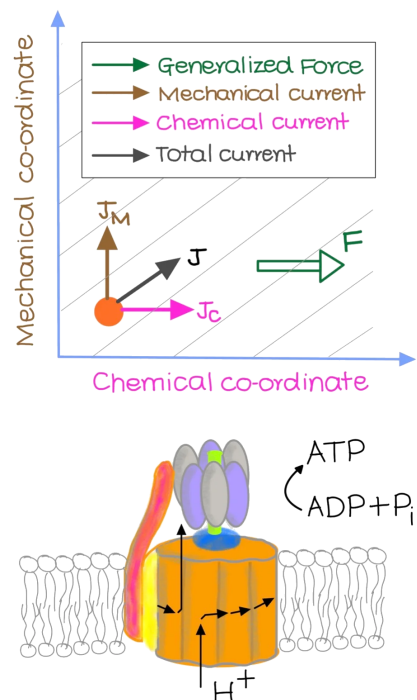


FIG. 13. A schematic representation of the coupling between the chemical (x -axis) and the mechanical (y -axis) degrees of freedom of a mechanochemical entity. In the case of a molecular motor, the horizontal axis represents the chemical state of ATP hydrolysis of the motor while the vertical axis represents its position along a filament. Non-zero off-diagonal mobilities L_{xy}, L_{yx} in this mechanochemical space, as expressed in Eq. (31), are schematically shown by the oblique lines in the figure. In this scenario, a generalized force applied in the chemical (positional) direction leads not only to a chemical (positional) current but also generates a positional (chemical) flux. The tight coupling between these two degrees of freedom implies that the system is constrained to move parallel to the dotted lines.

steady state exhibit “treadmilling”, in which the rate of addition of monomers at the plus end of actin is compensated by the loss of monomers at its minus end. This can be described in terms of an effective advection of the center of mass of the filament.

Composite networks of these two types of biofilaments along with molecular motors are the primary active constituents of the cellular cytoskeleton. Below, we discuss how the dynamics of these filaments contributes emergent phenomena such as positioning cellular organelles, bacterial propulsion, and growth of cellular protrusions.

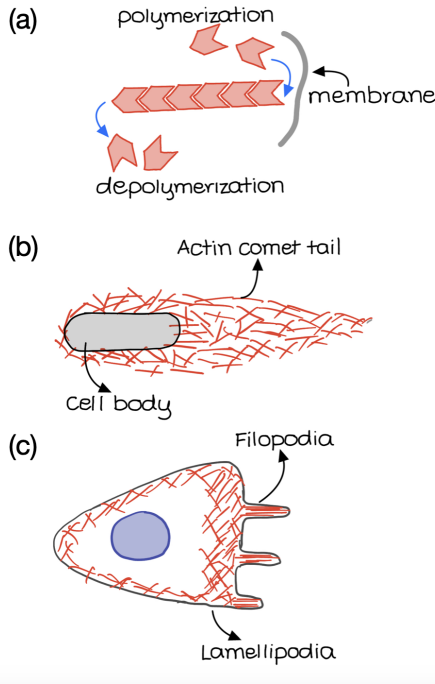


FIG. 14. Some cellular phenomenon wherein forces are generated by polymerization of filaments. (a) Force-generation by the polymerization/depolymerization processes at the level of a single filament pushing against a fluctuating barrier, (b) *Listeria* propulsion using actin polymerization, and (c) Lamellipodial and filopodial protrusions in a cell.

A. Force-generation due to polymerization

Polymerization and depolymerization of biopolymers is an important source of force generation in cells. Polymer growth/shrinkage can generate pushing/pulling forces on mechanical obstacles. These forces are used in process such as cell migration, cell division, etc. It has been demonstrated *in vitro* that polymerizing actin filaments can generate protrusions in membrane vesicles [156], or buckle when they are made to grow against a barrier [157], with typical forces about 1 pN per filament [158].

The simplest model for force generation due to polymerisation is one in which a sub-unit binds to the filament with a rate k_b and unbinds at a different rate k_u . Neglecting the polarity of the filament and assuming that the binding/unbinding rates are identical at the two ends, the master equation governing the probability $P_n(t)$ of finding a polymer with $n > 0$ monomers at time t is

$$\frac{dP_n}{dt} = k_b P_{n-1} - k_b P_n - k_u P_n + k_u P_{n+1}. \quad (32)$$

We assume that a reservoir of actin monomers is avail-

able for polymerization, that a stable nucleating center for polymers is always present, and that we can neglect shape changes of the filament. The calculation is carried out using the reflecting boundary condition $dP_0/dt = -k_b P_0 + k_u P_1$, corresponding to a stable $n = 0$ configuration. With the assumption $k_b < k_u$, the steady-state distribution and the average filament length, respectively, are [159]

$$P_n = \left(1 - \frac{k_b}{k_u}\right) \left(\frac{k_b}{k_u}\right)^n \quad \text{and} \quad \langle n \rangle = \frac{k_b/k_u}{1 - k_b/k_u}. \quad (33)$$

Let the nucleating center be anchored while the freely polymerizing end encounters a barrier (such as the membrane). This process can generate a pushing force when the force-independent rates are such that $k_b^0 > k_u^0$. The reaction force f from the membrane can change the binding-unbinding rates to $k_b = k_b^0 e^{f\alpha/k_B T}$ and $k_u = k_u^0 e^{f(1-\alpha)a/k_B T}$, obtained via a Kramer's approximation, where a is the size of the subunits, and α is a load distribution factor which indicates the differential force dependence of the binding and unbinding rates [160]. If $k_b/k_u = (k_b^0/k_u^0) e^{-fa/k_B T} < 1$, the mean growth velocity v_g of a filament is

$$v_g = [k_b^0 e^{-f\alpha a/k_B T} - k_u^0 e^{f(1-\alpha)a/k_B T}] a. \quad (34)$$

At a critical force f_s , called the stall force, this growth velocity vanishes, i.e., $v_g = 0$. The stall force f_s is

$$f_s = \frac{\Delta\mu}{a}, \quad (35)$$

where $\Delta\mu = k_B T \ln(k_b^0/k_u^0)$ is the free energy of binding of a single monomer – this can also be written in terms of the ratio $c/c_{\text{crit}} = k_b^0/k_u^0$, where c and c_{crit} are the actual and critical concentration of actin monomers at the polymerizing end [158].

In the case of actin polymerization, the free energy gain per added monomer is $\Delta G \approx 3 - 6 k_B T$ (ATP-actin at $40 \mu\text{M}$) with monomer axial spacing $a \approx 2.7 \text{ nm}$. Taking $\Delta\mu = 4 k_B T$, this gives

$$f_s = \frac{\Delta\mu}{a} = \frac{4 k_B T}{2.7 \text{ nm}} \approx \frac{4 \times 4.1 \text{ pN nm}}{2.7 \text{ nm}} \approx 8 \text{ pN}, \quad (36)$$

a number comparable to experimentally reported values of $\approx 1 \text{ pN}$, albeit at much lower ATP-actin concentration. This model can further be extended to incorporate, for example, differential binding/unbinding rates at the two ends of the filaments and explicitly distinguishing the ATP/ADP bound states of the monomers [161].

The above calculation is for the force generated by a single polymerizing filament with one end fixed and pushing against a soft barrier at the other end. A more general situation is the case when there are multiple growing filaments anchored to the nucleating center (FIG. 14). For simplicity, we consider a 1-D geometry and also neglect the interactions between the filaments in the bundle. When the distance between the nucleating center and the barrier is d , the filaments whose lengths $l \sim d$ are the ones that contribute to the pushing force. From (33), the probability of finding a filament with length d is $(1 - k_b/k_u)(k_b/k_u)^{d/a}$, and the force f_s generated from each filament is given in (35). If there are N filaments in the bundle, the repulsive force between the nucleating center and the barrier is then

$$f(d) \sim N \left(1 - \frac{k_b^0}{k_u^0} e^{-\beta f a}\right) \left(\frac{k_b^0}{k_u^0} e^{-\beta f a}\right)^{d/a} \frac{\Delta\mu}{a}. \quad (37)$$

Clearly, $f(d) \rightarrow 0$ as $d \rightarrow \infty$ since $(k_b^0/k_u^0)e^{-\beta f a} < 1$. This is the force that N filaments polymerizing from a fixed nucleating center exert on a soft barrier. Conversely, if the barrier is fixed, the same repulsive force can lead to translocation of the nucleating center. This expression will be used in section XIB to estimate the positioning forces generated by the mitotic spindle during cell division. Pushing forces generated by multiple actin filaments are harnessed by bacteria (like *Listeria*) and also by eukaryotic cells to generate tubular extension such as filopodia.

B. *Listeria* propulsion

A well-investigated example of polymerization forces generated by actin filaments is the propulsion machinery of *Listeria monocytogenes* — a micron-long, cylindrical, pathogenic bacterium that infects mammalian cells, including humans (FIG. 14) [162]. Once inside a host cell, *Listeria* hijacks the actin supply of the eukaryotic cell to become motile and uses this motility to penetrate neighbouring cells [163, 164]. Typical propulsion speeds are of the order of $0.1 - 0.2 \mu\text{m/s}$.

Listeria does this by expressing actin nucleating proteins on its surface. This leads to the formation of a filamentous actin tail which can be tens of microns long [165]. Although polymerization from the bacterial surface requires a loose coupling between the surface and the filament, the bacterium is always attached to the tail due to the large number of filaments. More-

over, crosslinking proteins bind these filaments together as they grow, forming an elastic gel with a finite shear modulus. This tail, made of sub-micron length actin filaments, gradually depolymerizes from the rear, thus giving a motile *Listeria* its characteristic comet-like appearance. Remarkably, motility outside the living cell has been demonstrated using a minimal system consisting of micron size beads coated with an actin nucleating protein [166].

To arrive at an expression for the propulsion speed, we consider a spherical bead on which the actin filaments are polymerizing. An approximate value for the typical thickness of the polymerizing gel can be obtained from the balance of forces resulting from polymerization/depolymerization and the mechanical stresses generated in the elastic medium. Large tangential strains developed in the polymerizing gel lead to a spontaneous symmetry breaking, and hence to the motility of the bead [166].

Consider a spherical bead of radius r covered with an actin nucleating protein, with average spacing ξ , on which actin monomers, of size a , polymerize. The total free energy gained from adding the first layer of actin mesh on the bead surface is $U_\xi = \Delta\mu (4\pi r^2/\xi^2)$, where $\Delta\mu$ is the free energy associated with addition of a single actin monomer to the gel. However, polymerization of subsequent actin layers generates both radial and tangential stresses in the crosslinked actin gel with elastic modulus E . The polymerization is energetically favorable only when the energy reduction U_ξ is lesser than the added work required to polymerize against the radial stress Σ_{rr} . If the thickness of the gel $d \ll r$, then the strain in the gel is $\sim d/r$ and hence, the elastic energy cost is $U_e \sim Ea (d/r)^2 4\pi r^2$. The balance of elastic energy and the free energy gained from polymerization provides an estimate for the thickness of the actin gel $d \approx r \sqrt{\Delta\mu/Ea\xi^2}$ [166]. This estimate assumes that the gel is radially symmetric and is in a steady state at mechanical equilibrium.

For directional motility, the initially uniform actin gel must break symmetry. A simple approximation for this symmetry breaking threshold is to consider tangential strains $d/r \sim 1$. An estimate for the elastic modulus is $E \approx k_B T l_p/\xi_c^4$, where l_p is the persistence length of a single filament and ξ_c is the mean spacing between the crosslinked actin filaments in the gel [62]. Therefore, an estimate for a possible symmetry breaking transition is $(\xi_c^2/\sqrt{l_p a}) \sqrt{\Delta\mu/k_B T} \sim 1$ [166–168]. These expressions

assume that polymerization timescales are much faster compared to the viscoelastic relaxation time of the actin gel.

Once symmetry breaking occurs, a simple way to estimate the motility speed v of the bacterium is to consider the actin tail as an incompressible elastic gel and estimate the resulting flow speed arising from force-balance and volume conservation. This yields the expression [167]

$$\frac{v}{v_p} = 1 - \frac{F_{\text{ext}}}{E S_b}, \quad (38)$$

where v_p is the polymerization rate, F_{ext} is the external force exerted by the medium on the bacterium, and S_b is the cross-sectional area of the bacterium. Incorporating the change in the polymerization rate due to the applied forces, as in (34), does not lead to a qualitative change in the above expression. The external force includes a combination of motile forces arising from actin polymerization and friction forces arising from detachment between *Listeria* and the surrounding actin network. The values of $ES_b \approx 1$ nN [167]. Hence, assuming 100 – 1000 polymerizing actin filaments with stall force of 1 pN each, will give a stall force $F_{\text{ext}} \approx 1$ nN. In summary, we see that force-generation due to actin polymerization induced stresses leads to a spontaneous motility of the *Listeria*.

C. Filopodial extension

Another well known example of actin-based force generation is the growth process of filopodia. These are thin, tubular protrusions, usually seen in motile cells (FIG. 14). Filopodia have a typical diameter of about 100 – 300 nm and consist of ~ 10 to 20 actin filaments organized in a polar bundle. Filopodial growth is driven by actin polymerisation, which generates a pushing force on the membrane as discussed above.

To extend a cylindrical membrane tube of diameter $d_m \sim \sqrt{\kappa/\sigma_s}$, the pushing force must exceed the passive restoring force $F_m \sim \sqrt{\sigma_s \kappa}$ exerted by the membrane, where σ_s is the in-plane tension and κ is the bending rigidity of the membrane – typically, $d_m \sim 100$ nm and $F_m \sim 10$ pN. However, the force exerted by a single polymerizing actin filament ~ 1 pN. The large active forces required for pushing the membrane in a filopodia result from the coordinated polymerization of multiple actin filaments driven by bundling proteins.

Filopodia are highly dynamic structures and play an important role in sensing chemical and mechanical cues

during cell locomotion or axonal growth cone guidance [162]. While the growth of filopodia is reasonably well explained, its mechanosensitivity and filopodial retraction are still not fully explained and multiple mechanisms may be involved [169–171].

This section focused on force-generation due to filament polymerization and neglected the effect of molecular motors that translocate on these filaments using chemical energy. Such motor activity is another route to force-generation in cells and tissues.

IX. MOLECULAR MOTORS

How is directed transport of cargo achieved within the crowded and stochastic environment of a cell? Brownian diffusion is effective for transport in small micron-sized cells (e.g., bacteria). However, for larger cells (e.g., neurons), diffusive transport is highly ineffective. Transport mechanisms that involve specialized protein molecules called molecular motors moving unidirectionally on asymmetric polymeric tracks provide a significantly more efficient and fast way of transporting material within cells.

For an object to move unidirectionally in the absence of external forces in a viscous environment, it must be able to transduce energy internally (be active) as well as derive its sense of direction through the absence of a fore-aft symmetry. This is the essence of the Curie principle [172]. Molecular motors are examples of the operation of the Curie principle at the cellular level.

The molecular motor is a nano-scale entity, fruitfully thought of as having multiple internal states. The motor moves on a one-dimensional and periodic biopolymer track (e.g., microtubules with a periodicity of ~ 8 nm). Due to their small size, these motors function in a highly noisy environment. For a motor to move unidirectionally at a steady mean velocity, work must be performed against a drag force from the ambient medium. This requires the transduction of energy at a local scale. This drives conformational changes in the molecular motor.

The interaction of the molecular motor with the track can be represented by a fore-aft asymmetric and periodic potential representing the polar nature and the structural periodicity of the filament, respectively. The conformational changes of the molecular motor can be interpreted as switching between different local interaction potentials with the track. If the transitions between these different conformations (interaction potentials) do not satisfy de-

tailed balance (due to energy flux from ATP hydrolysis), then coupled with the polar nature of the track, the Curie principle implies that we can expect a non-zero mean velocity of the motor.

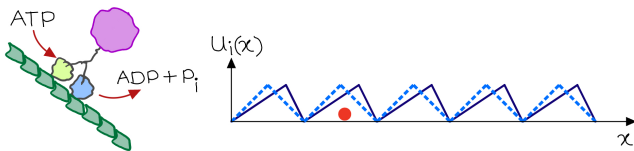


FIG. 15. Directional movement of a typical molecular motor along an asymmetric track. An effective Brownian ratchet model to capture the statistical dynamics of the motor can be visualized as a point particle moving in a spatially periodic but asymmetric potentials shown as $U_i(x)$. Depending on the configurational state of the motor, the potential switches between the profiles represented by the continuous and dashed lines. The transitions between the internal states of the motor is biased by ATP hydrolysis and thus does not satisfy detailed balance. This non-equilibrium energy input, combined with the spatial asymmetry of the track leads to directional transport.

Note that the unidirectional movement of molecular motors is *not* due to spatial temperature gradients since thermal equilibration occurs quickly at the nano-scale and the system can be considered isothermal [152, 173]. On the other hand, the original Feynman-Smoluchowski pawl-and-ratchet model illustrates how irreversible motion might potentially happen in a thermal environment for macroscopic systems [174]. The pawl-and-ratchet model describes a situation where a pawl can move along a ratchet, which is an asymmetric object constructed so that it moves more easily in one direction as opposed to the other. However, thermal fluctuations allow the ratchet to “slip back” so that, on average, there is no net unidirectional motion that can be imparted.

To circumvent this, the advancing and the falling back of the pawl must be induced by the switching of the ratchet potential at rates that do not obey detailed balance. This can be done through the injection of energy, such that the entire system is out of equilibrium. The introduction of a non-equilibrium element destroys the time-reversal symmetry of the original problem, allowing for directed motion.

The force-velocity relation for molecular motors can be obtained by using optical tweezers to measure forces exerted by the motor (see Section VIC). The motion of the motor in an ATP saturating environment can be studied

statistically, leading to the result that the fundamental periodicity of the filament, either microtubules or actin, sets the fundamental step size of the motor. Applying increasing loads finally leads to motor stalling. By mapping this onto a particle moving in an asymmetric potential, the stall force can be related to fundamental aspects of the motor [152, 175].

A. Brownian ratchet models

The thermodynamic ideas underlying the theory of motors, invokes multiple states, in each of which the system rapidly achieves thermal equilibrium. Multiple conformational states of the translocating motor protein have been identified in experiments (up to five or six different states have been identified) [160].

A simple model is the “particle fluctuating between states” model, where one imagines at least two states $i = 1, 2$ with each described phenomenologically by a periodic potential $W_i(x)$. This potential must, of necessity, be fore-aft asymmetric [176]. The non-equilibrium component is added by accounting for transitions between states that occur independently of the energy of that state. This breaks detailed balance.

Let $P_i(x, t)$ be the probability of finding the particle at position x in the state i . The evolution of these probabilities is governed by the Fokker-Planck equations:

$$\partial_t P_1 = -\partial_x J_1 - \omega_{1 \rightarrow 2}(x) P_1 + \omega_{2 \rightarrow 1}(x) P_2, \quad (39)$$

$$\partial_t P_2 = -\partial_x J_2 + \omega_{1 \rightarrow 2}(x) P_1 - \omega_{2 \rightarrow 1}(x) P_2, \quad (40)$$

where $\omega_{i \rightarrow j}(x)$ is the space-dependent transition rate from state i to the state j . The spatial current in each state is of the form

$$J_i = \mu_i (k_B T \partial_x P_i - P_i \partial_x W_i + P_i F_{\text{ext}}), \quad (41)$$

where $\mu_i P_i F_{\text{ext}}$ is the probability current resulting from an applied external force F_{ext} . The total current $J = J_1 + J_2$ can be written in terms of the total probability $P = P_1 + P_2$ as

$$J = J_1 + J_2 = \lambda (k_B T \partial_x P + P \partial_x W_{\text{eff}}(x) + P F_{\text{ext}}), \quad (42)$$

where $\lambda(x) = P_1(x)/P(x)$, $\mu_{\text{eff}}(x) = \mu_1 \lambda + (1 - \lambda) \mu_2$ is the effective mobility, and the effective potential is

$$W_{\text{eff}}(x) - W_{\text{eff}}(0) = \int_0^x dy \left[\frac{\mu_1 \lambda \partial_y W_1 + \mu_2 (1 - \lambda) \partial_y W_2}{\mu_{\text{eff}}(y)} + k_B T [\ln \mu_{\text{eff}}(y)]_0^x \right]. \quad (43)$$

To get directed motion, the effective potential $W_{\text{eff}}(x)$ needs to have a net tilt over the periodicity of the underlying potential. If both the potentials $W_i(x)$ are fore-aft symmetric or if detailed balance is satisfied, then $W_{\text{eff}}(x)$ cannot have a net tilt [152]. The net force generated by the ratchet mechanism described above can be used to tug cargo (e.g., vesicles) effecting intracellular transport. The efficiency of this process, i.e, the work done for every ATP molecule, is quite high compared to that achievable in macroscopic engines. With appropriate modifications, models of the sort that we discussed above can also be used to describe rotary motors as well.

B. Collection of molecular motors

Many biophysical situations involve a collective action of groups of molecular motors. Coupling many processive motors can lead to interesting phenomena, such as collective oscillations and metachronal waves [177, 178]. These responses are associated with important biological processes such as contraction of muscles, cardiomyocyte beating, flagellar motion, and beating of insect wings, etc. Below, we discuss a few cellular processes which are driven by motor generated forces discussed above.

1. Muscle contraction

A prominent example of the collective action of filament-motor systems is muscle contraction. Sarcomeres are the minimum contractile unit of muscle cells. Here actin filaments bundle into parallel arrays with opposing polarity. In a sarcomere, one end of each bundle is anchored onto a protein rich structure called as Z-disk (see FIG. 16). Individual muscle myosin motors are non-processive (a low duty cycle), with only $\approx 4 - 10\%$ attached to actin filaments at any instant. However, in sarcomeres, myosin motors form long chain structures called myosin thick filaments where only a fraction of motor heads are detached at any given time. The coordinated action of such myosin thick filaments pulling on parallel actin bundles generates a net macroscopic contractile force of the order of $30 \text{ nN}/\mu\text{m}^2$ [179, 180]. The regulation of muscle cells contraction is controlled by external signals, such as from neurons. Muscle cells can also show spontaneous oscillations of the contractile force they generate [181, 182]. A recent review can be found in [180].

2. Cilia and flagella

The beating of cilia and flagellae provides another example of emergent phenomena from interacting collections of motors and filaments. These are both filamentous cell protrusions which actively beat repeatedly by consuming ATP. Eukaryotic flagella (not to be confused with bacterial flagella – see Section IID) can be several tens of microns long. They are seen in small numbers (usually < 5) towards the anterior end of swimming organisms like *Chlamydomonas*.

Cilia, on the other hand, are shorter ($< 10 \mu\text{m}$), usually occur as a dense carpet (often $\gg 100$ per cell) and are ubiquitous. In protozoans like *paramecium*, they beat synchronously to generate wave like patterns that propel the cell forward. In filter feeding microorganisms like rotifers, cilia generate fluid flow that drive food particles into the feeding apparatus. In mammals, ciliary carpets line the surface of epithelial tissues, the layers of cells that cover the surface of organs, driving fluid flow. In the respiratory tract, cilia drive mucus towards the nostrils, in the brain cavity, they drive fluid circulation, and within fallopian tubes, they help push the egg cell forward.

Cilia and flagella are structurally almost identical, each being membrane protrusions dense with microtubule bundles (FIG. 16) [183]. Typically, they contain a ring of nine longitudinally aligned microtubule doublets arranged with their plus end away from the cell [184]. Each doublet consists of one complete tubule with about 13 protofilaments attached along its length to a partial tubule with fewer protofilaments. All doublets are anchored at one end. Additionally, a pair of central microtubules is also common. The entire microtubule structure is interlinked by elastic linker proteins. The circularly arranged doublets are coupled to their neighbours by an array of dynein motors such that one doublet acts as a cargo while the heads bind to and push against the adjacent doublet (FIG. 16). Thus this entire structure forms an active elastic bundle. It is known as an axoneme.

It is known that active systems consisting of collection of molecular motors coupled to a viscoelastic solid like medium can generate sustained spontaneous oscillations [185]. The beating of the axoneme may be such an example. It is known that the dynein motors generate longitudinal forces between adjacent microtubule doublets [186]. In the axoneme, these longitudinal forces are exerted with a phase lag across the circumferential ring. The differential stress then translates the longitu-

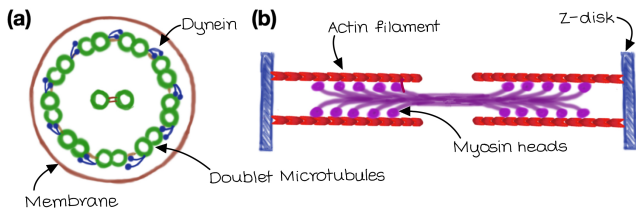


FIG. 16. Molecular motors often operate in a collective manner to generate large forces. Two prominent examples are the beating of cilia and the contraction of muscle cells. (a) Cross section through an axoneme (a $9 + 2$ arrangement of microtubules of overall diameter ~ 100 nm) showing the arrangement of microtubules and the interspersed dynein motors. The microtubules are arranged in doublets and pairs of these filaments can slide past each other via the action of molecular motors. Synchronous forces generated in this manner lead to the large-scale beating of a cilium. (b) The basic unit for contractile force generation in muscle cells are sarcomeres (each unit $\sim 1 \mu\text{m}$). These consist of bundles of antiparallel actin filaments with myosin minifilaments anchored on them. The ATP consuming activity of this collection of motors generates a net contractile force.

dinal force into bending deformations [186]. A study of chiral effects in cilia beating can be found in [187]

Another prominent example of the collective dynamics of filaments and motors occurs in the auditory hair-cells of the inner ear in animals [99, 188]. Here, rows of hair-cells with a staircase-like pattern of kinocilia projecting out of each cell are arranged in an ordered fashion. Each generate active forces that are used to open and close ion channels. Similar mechanisms operate as pressure sensors in the fish lateral line.

X. ACTOMYOSIN CORTEX

Most eukaryotic cells are known to have a membrane associated cortical actin mesh consisting of actin filaments, cross-linkers and myosin motors [2, 32]. This sub-micron thick meshwork [29] is responsible for orchestrating important cellular processes such as division, motility, and polarity. Compared to the scales of a typical eukaryotic cell ($20 \mu\text{m}$), the actomyosin cortex ($\approx 0.5 \mu\text{m}$) can be treated as an effective two-dimensional thin film. Early studies noticed large-scale flows in the layers underneath the cell-membrane that were prominent during cytokinesis [189]. More recent studies have revealed a highly branched and cross-linked meshwork of actin filaments in the actomyosin cortices of moving fibroblast cells [190].

The actomyosin cortex is an active material (see FIG. 17(a-b)). As discussed in Section IX, ATP-fed myosin motors tug on actin filaments. Moreover, the entire actomyosin meshwork is remodelled through the continuous polymerization and de-polymerization of actin filaments with a typical turnover time of several tens of seconds [50]. An appropriate coarse-grained description of the actomyosin cortex would be that of an active viscoelastic gel. The crossover timescale from the short-time elastic to the long-time fluid behavior is typically controlled by the turnover rate of the components of the cortex.

Experimental observations do not reveal significant long-range anisotropic spatial ordering of actin filaments such as found in sarcomeric structures. One would thus expect neither contractile nor extensile stresses, on average. Recent work has shown that the nonlinear elasticity of actin filaments (which can lead to buckling), coupled with the nonequilibrium activity of motors, can break the symmetry between contractile and extensile behavior. This generates a net contraction of the actomyosin networks [191–193]. Further, it appears that the breakdown of detailed balance in the binding-unbinding kinetics of cross-linking proteins is sufficient to generate contractile stresses in polymeric gels without explicit force-generation from the activity of molecular motors [194].

Contractile stresses in the cortex have been measured by compressing rounded fibroblast cells with a flat AFM cantilever or using micropipette aspiration technique (see Section VI), giving a tension of the order of $400 \text{ pN}/\mu\text{m}$. Deactivation of myosin-II motors result in a significant drop in this tension [195].

Active hydrodynamic descriptions have been successful in explaining patterning in actomyosin cortex. We will discuss a couple of them in this section. A simplified one-dimensional model [196, 197] for pattern formation in the actomyosin cortex considers a diffusible molecule with a concentration field $c(x, t)$ which regulates active stresses. In the fluid limit, the total stress Σ generated in the cortex is

$$\Sigma = \eta \partial_x v + \zeta \Delta \mu f(c(x)) \quad (44)$$

where v is the hydrodynamic velocity field in the cortex with a viscosity η . The active stresses are regulated by the function $f[c(x)]$, ζ is an activity coefficient, and $\Delta \mu$ is the chemical potential difference associated with ATP hydrolysis. Low-Reynolds number physics dictates that any fluid element has a force-balance condition imposed on it

at every instant of time. With a simple frictional approximation of the form $F_{\text{ext}} = -\gamma v$ for the traction forces arising from the underlying cytoplasm and the plasma membrane above, the force-balance condition reads

$$\partial_x \Sigma = -F_{\text{ext}} = \gamma v. \quad (45)$$

Using (44) in (45) leads to a flow equation

$$\eta \partial_x^2 v - \gamma v = -\zeta \Delta \mu \partial_x f(c(x)). \quad (46)$$

This equation predicts that gradients in the cortical tension lead to cortical flows. This picture has been experimentally verified by measuring large-scale cortical flows in the zygotes of *C. elegans*, monitored using the spatial profile of myosin as an input [52].

A. Myosin patterns

The flows resulting from contractility gradients, via (46), will advect any molecules present in the cortex. In particular, the elements that are responsible for the generation of active stresses, such as myosin motors, will also be subjected to advective fluxes. The dynamics of the concentration c of the diffusible molecule can be modeled by

$$\partial_t c = -\partial_x j + R(c), \quad j = v c - D \partial_x c, \quad (47)$$

where D is a diffusion coefficient and $R(c)$ represents the changes to the concentration occurring from local chemical reactions, for instance the ever-present turnover of molecules between the cortical surface to the cytoplasmic bulk.

Equations (46) and (47) provide a closed set of autonomous equations for the evolution of the concentration field c and the hydrodynamic velocity field v . A trivial solution is a spatially uniform concentration field c_0 which is a solution of $R(c_0) = 0$ and zero velocity $v = 0$. However, this uniform state can become unstable upon increasing the strength of the active stresses, i.e., the coefficient $\zeta \Delta \mu$.

An intuitive way of understanding this instability is as follows: while diffusive fluxes tend to homogenize concentration fluctuations, advective fluxes generate contractile flows that tend to enhance them. High activity, i.e., large Péclet numbers $P = \zeta \Delta \mu / \gamma D \gg 1$, can destabilize the homogeneous state and lead to a patterned state with an inhomogeneous concentration and flow profile [196].

Specifically, with a choice $R(c) = -k(c - c_0)$, a linear-stability analysis of the above equations shows that concentration fluctuations δc_q at a wavenumber q around the homogeneous state $c = c_0$ have a growth rate λ_q with

$$\lambda_q = -k - D q^2 \left(1 - \frac{P c_0 \partial_c f(c_0)}{1 + q^2 \ell^2} \right) \quad (48)$$

where $\ell = \sqrt{\eta/\gamma}$ and P is the Péclet number defined above [196]. For small $P \ll 1$, we see that these concentration fluctuations are suppressed while for large activities $\gg 1$, these concentration fluctuations grow exponentially until the nonlinear terms suppress their growth. For $k \neq 0$, the growth rate λ_q has a maximum for a non-zero wave number q , which defines the length-scale of the emergent concentration patterns. Figure 17(b) shows such an active mechanochemical pattern in the concentration field of myosin motors in the actomyosin cortex of cells.

It is straightforward to generalize (47) to n species each of which could, in principle, regulate the active stress $\zeta \Delta \mu f(\{c_1, c_2, \dots, c_n\})$. Such extensions lead to active pulsatory patterns [197] and also extend classical Turing patterns for reaction-diffusion systems [198] to mechanochemical patterns.

Generalizing the equations (45)-(47) to a curved shape and coupling them to bulk cytoplasmic flows leads to spontaneous patterns that can either resemble cell-polarity or those corresponding to cell division, depending on the relative values of the cytoplasmic and cortical viscosities [199]. The formation of the cytokinetic ring with enhanced myosin levels in the middle of the cell, the associated orientation patterns of actin filaments and the ensuing contractile flows can thus be accounted for within simplified hydrodynamic models. Furthermore, studies with dynamical shapes can also explain the temporal progression of the cell shape driven by the constriction of the contractile ring towards cytokinesis [200].

Systems with anisotropic order parameters, such as a polarity field \mathbf{p} or a nematic tensor field \mathbf{Q} , have a richer set of pattern forming instabilities [92, 96]. For instance, recognizing that cortical dynamics can influence the dynamics of membrane associated proteins, it has been demonstrated that polar orientational patterns in the actomyosin cytoskeleton regulate the formation of nano-clusters of GPI-anchored proteins. These are involved in various signalling mechanisms. The emerging view is that of an active composite cell surface wherein the composition and dynamics of the cellular periphery is actively regulated by its internal components [201].

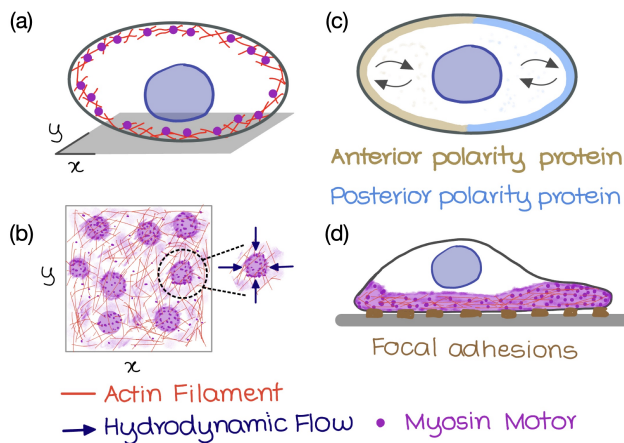


FIG. 17. (a) The actomyosin cortex is a thin meshwork of actin filaments, myosin motors and crosslinkers. Pattern formation in the actomyosin cortex typically results from the competition between surface diffusion, turnover kinetics between the cytoplasm and the cortex, and hydrodynamic flows arising from actomyosin contractility gradients. (b) At high contractility, spontaneous patterns can emerge in both the concentration of active stress regulators and hydrodynamic flows. (c) Such flows can also couple to surface concentrations of cell polarity proteins. The macroscopic segregation of such cell-surface proteins and signaling molecules leads to the establishment of an antero-posterior axis in *C. elegans*. (d) In crawling cells, gradients of acto-myosin contractility between the front and rear end of the cell generate net pushing forces against the substrate via focal adhesions, thus providing motility.

Active anisotropic patterns also explain the orientation pattern of actin filaments in the cytokinetic ring during cell division. The nematic orientation \mathbf{Q} is driven by hydrodynamic flows which are themselves guided by gradients of active stress. Within a simplified two-dimensional theory that is appropriate to a thin-shell description of the cortex, an imposed active stress profile that corresponds to enhanced myosin levels at the cell center generates contractile flows and a corresponding alignment of actin filaments similar to those seen in the cytokinetic ring [202, 203]. Such flow driven orientation patterns during cytokinesis have been experimentally measured. They agree quantitatively with hydrodynamic descriptions [204].

B. Cell polarity

Most cell divisions are symmetric: the two daughter cells are identical in volume, shape, and genetic content. However, some cell divisions, particularly those that occur during cell-fate specification or early embryonic phases, are asymmetric, with the two daughter cells differing in their physical sizes or in the segregation of the cytoplasmic components during cytokinesis. Such asymmetric cell division implies the establishment of a cell polarity which distinguishes the two halves of the dividing cell.

An archetypal example of asymmetric cell division driven by cell-polarity is the first division of the *C. elegans* zygote. Incidentally, this very first division also sets the organismal polarity by defining antero-posterior axis of the organism. Cell polarity here, is established by the asymmetric segregation of PAR (partitioning defective) proteins on the surface of the cell (see FIG. 17(c)). Recent studies have clearly demonstrated that PAR polarity in *C. elegans* zygotes is driven by large-scale hydrodynamical flows generated in the cortex in response to gradients in myosin contractility [205]. The spatiotemporal profiles of the protein concentrations and cortical flows can be quantitatively accounted for using an active gel theory of the actomyosin cortex coupled to reaction-diffusion-advection equations for the concentrations [206].

A typical hydrodynamic model for the establishment of cell polarity takes into account (i) the transport of polarity marker proteins by both passive diffusion and active advection, (ii) biochemical interactions between the components such that spatially homogeneous and patterned profiles coexist within the same parameter regime, and (iii) spatiotemporal cues that trigger the transition of the system from the unpolarized state to the polarized state. Experimental evidence suggests that weak stochastic fluctuations cannot lead to a spontaneous transition of the system from an unpolarized state to a polarized state. This transition is effected when a sufficiently strong upstream signal triggers the system.

Establishing cell polarity is the first step towards selecting a direction for cell movement. In the next subsection, we use the simple model for polarity patterns in the actomyosin cortex developed here to address the motility of crawling cells.

C. Cell motility

Cell migration necessarily requires the development of a front-rear polarity (see FIG. 17(d)). The coupling of this polarity to mechanochemical processes can lead to the emergence of cell motility [162, 207, 208]. As discussed in Section XB on cell polarity, the emergence of a front-rear asymmetry is typically achieved by internal chemical reactions with antagonistic dynamics. Such reactions can lead to bistability between a homogeneous and a polarized distribution in the cell [209]. Such polar patterns in chemical concentrations, when coupled to active stresses in viscous/viscoelastic acto-myosin cortex, can lead to a net velocity for the cell. We now discuss a simple model for cell migration based on this picture [210].

Consider the cell as a one-dimensional, moving viscous active fluid element of length $L(t) = l_+(t) - l_-(t)$, where l_{\pm} are the locations of the front and rear ends. Note that $dl_{\pm}/dt = v(l_{\pm})$, where v is the velocity field. The total stress is of the form $\sigma = \eta \partial_x v + \sigma_a$, where we assume an active stress of the form $\sigma_a = (c/c^*) \zeta \Delta \mu$ is the active stress and c represents the myosin concentration. Using the force balance equation (45) to eliminate the velocity field v , the total stress follows

$$\ell^2 \partial_{xx} \sigma - \sigma = -(c/c^*) \zeta \Delta \mu, \quad (49)$$

where $\ell = \sqrt{\eta/\gamma}$. Following (47), the evolution of c is given by

$$\partial_t c + \gamma^{-1} \partial_x (c \partial_x \sigma) = D \partial_{xx}^2 c. \quad (50)$$

At the moving boundaries, in addition to the kinematic relations

$$dl_{\pm}/dt = \gamma^{-1} \partial_x \sigma|_{x=l_{\pm}}, \quad (51)$$

we assume that c and σ satisfy

$$\partial_x c(l_{\pm}, t) = 0, \quad \sigma(l_{\pm}) = -K (L(t) - L_0)/L_0, \quad (52)$$

where the stress boundary conditions arise from imposing a volume constraint with K being the bulk modulus and L_0 the preferred 1D volume of the cell.

At small values of activity $\zeta \Delta \mu$, the only solution is a uniform profile of $c(x)$ leading to $\sigma(x) = 0$. On the other hand, at high activity, the instability of the homogeneous state can lead to appearance of spontaneous patterns in c and hence in σ . Assuming a steady state patterned solution $c(x)$ and $\sigma(x)$ satisfying (49) and (50)

with $dl_+/dt = dl_-/dt$, i.e., $dL/dt = 0$, the center of mass velocity of the cell is given by

$$V_{\text{cell}} = \frac{\zeta \Delta \mu}{\eta c^*} \int_{-L_s/2}^{L_s/2} \frac{\sinh(z/\ell)}{2 \sinh(L_s/2\ell)} c(z) dz, \quad (53)$$

where z is the spatial coordinate in the center of mass ($z = 0$) frame, and L_s is the steady-state length [207]. Note that if either $\zeta \Delta \mu = 0$ or $c(z)$ is an even function, then $V_{\text{cell}} = 0$. Clearly, it is the odd part of $c(z)$ which breaks the front-rear symmetry, i.e., makes the cell polar. Therefore, for cell motility, we need both non-equilibrium energy input ($\zeta \Delta \mu \neq 0$) and a mechanism to break the fore-aft symmetry ($c(z) \neq c(-z)$) – another illustration of the Curie principle discussed in Section VII.

The mechanism for cell migration discussed above involved the generation of active stresses by the action of molecular motors. However, other mechanisms that can break detailed balance such as treadmilling coupled with spatial symmetry breaking can also lead to cell migration. For instance, in the case of migratory cells known as keratocytes, cell movement is mostly driven by actin treadmilling where polymerization occurs predominantly at the leading edge and depolymerization occurs away from the leading edge [211].

D. Coupling to membrane organization

The integrity of the actomyosin cortex can sometimes be compromised, leading to a rupture of the cortical meshwork from the membrane. The interfacial tension generated in the membrane-cortex composite is balanced by the pressure difference across the cell surface in accordance with Laplace's law. After separation of the cortex from the membrane, the turgor pressure in the cytosol leads to a localized ballooning of the cell membrane – a bleb. The restoration of the cortex allows the bleb to be reabsorbed [212].

Coupling between the actomyosin cortex and the membrane plays an important role in regulating traffic of cargo-laden vesicles into and out of the cell. For instance, actin polymerization can influence the protrusion of the membrane to form vesicles [213].

Over the past few decades, the role of the coupling between the cell cortex and proteins embedded in the plasma membrane has attracted renewed attention. An early hypothesis was that of membrane “rafts”, local fluid-like micro-phase-separated regions on the cell surface which are enriched in specific proteins, signaling

molecules and cholesterol. Such rafts were initially thought to be equilibrium objects, formed through phase separation, consistent with a “fluid mosaic” model for the cell membrane.

Recent work suggests an intriguing alternative closer to available data. The enrichment of nano-domains on living cell membranes is induced by the motion of myosin motors on the cell cortex just below the membrane surface, connected to the relevant integral membrane proteins through appropriate linkers, and modulated by the presence of cholesterol. Motor motion on an actively remodeling cytoskeleton can lead to the formation of star-like structures (asters), with a definite polarity. Motors linked to membrane proteins can drive their cargo to accumulate at points defined by the centres of asters, leading to an enrichment of specific components. The membrane is not the sole arena for phase separation within the membrane, but is aided in this by the underlying active behaviour of the acto-myosin cortex. The complex spatio-temporal organization of myosin motors on reconfiguring actin tracks leads to the formation of spontaneous nano-scale domains that live as long as they are stabilized through protein attachments, after which they dissolve.

Active forces generated in the actomyosin cortex can also lead to large scale fluid flows within cells. Such cytoplasmic flows are implicated in positioning various organelles and even cell motility [214].

XI. CELL DIVISION

A fundamental property of living systems is their ability to replicate. Cell division is achieved in two stages. In the first stage, genetic material in the form of DNA is duplicated, followed by a doubling in cytoplasmic components. In the second stage, the two DNA copies are segregated into opposite sides of the mother cell. Concomitantly, the process of cytokinesis cleaves the mother cell into two daughter cells. Beyond microscopic processes involved during DNA replication, the segregation of chromosomes and cytokinesis must involve cell-scale forces.

The duplication of DNA is achieved by the translocation of helicase motor proteins which unzip the double-stranded DNA, followed by the duplication of the genetic sequence aided by DNA polymerases. Both the translocation of the helicase motor and the action of the DNA polymerase involves mechanical forces. The movement of

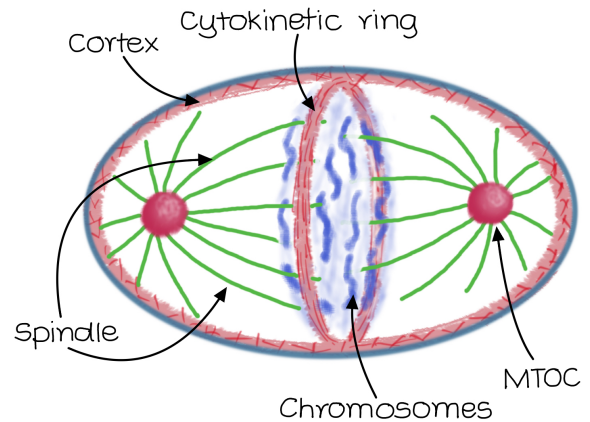


FIG. 18. A dividing cell assembles a highly coordinated complex machinery of the actomyosin and microtubule cytoskeleton to drive segregation of the chromosomes. The mitotic spindle as shown is a structure that facilitates the segregation of the duplicated chromosomes. The spindle involves astral microtubules that emerge from the two microtubule organizing centres (MTOC) and that contact the chromosomes. Large scale cortical flows drive the assembly of the cytokinetic ring on the cellular surface which “pinches” the mother-cell into two daughter cells.

the helicase can be modeled using the Brownian ratchet formalism discussed in Section IX [215].

In eukaryotes, the second stage of cell division involves the formation and positioning of the mitotic spindle and the subsequent scission of the mother cell into two daughter cells. Both these processes involve mechanical forces in an essential manner. Below, we discuss these processes only in the context of eukaryotic cells.

A. Chromosome organization

Chromatin is the term for the organized complex of DNA and proteins that is found in eukaryotic cells. In mammalian cells, DNA is wound around a structure made by dimerizing a complex of four histone proteins to form an octamer. DNA winds around such histone octamers. The combination of DNA and histones is a nucleosome core particle [216].

During various physiological processes, such as packaging into chromosomes, replication, repair, protein binding and transcription, the DNA is subjected to stretching, twisting, and bending. mRNA production, called transcription, is carried out by RNA polymerase (RNAP), a molecular machine that moves on DNA. An upper bound for the force that can be generated by the motor can be

obtained from $F_{\max} = \Delta G/\delta$, where ΔG is the total energy consumed by RNAP from NTP hydrolysis to move a step of size $\delta = 0.34$ nm, corresponding to the size of a typical nucleotide. Because the step-size is small, the maximum force that can be generated for RNAP can be large, up to 30 pN. This is much larger than the forces generated by MT or actin associated motors. The forces generated by RNAP are predominantly spent on untwisting DNA, separating its strands and then moving along the separated strands. This process involves the formation of higher order coiled structures of DNA (supercoils) and requires application of internal torques.

Within the genome, highly compact *heterochromatin* regions, where nucleosome core particles are tightly packed, are typically gene poor and transcribed at low levels, while more loosely bound *euchromatin* regions are gene rich and transcribed more. Fluorescent labelling experiments show that they occupy largely non-overlapping “chromosome territories” within the nuclei of higher eukaryotes (FIG. 19). The location of these territories is not random. Much evidence points to a favored arrangement of chromosomes in which the regions close to the nuclear centre tend to be gene-rich, while gene-poor and more dense regions of chromatin appear more peripherally, towards the nuclear envelope. The creation of such non-trivial spatial patterns requires a coherent movement of large molecules across micron sized regions, arguing for the crucial importance of forces at the nuclear scale.

Current questions regarding force generation at the level of chromatin begin by considering chromosomes as polymers. Some approaches emphasize single polymer properties, such as the statistics of contacts in comparison to the chromosome capture data. Experiments suggest the presence of coherent motions of chromatin across micron size regions over tens of seconds within the nucleus [217]. This dynamics is ATP dependent, suggesting that activity should be a core component of any description of nuclear architecture [218].

A hydrodynamic theory for chromatin can be formulated by incorporating active effects into a coarse-grained stress tensor [219]. However, such approaches are hard to connect to the range of what is actually measurable. A biophysical approach to nuclear architecture emphasizes the connection to active processes by modeling the connections between ATP consuming processes acting on chromosomes with prescribed gene transcription levels. This is done by assuming that the differential transcription levels across 1 megabase (MB) segments

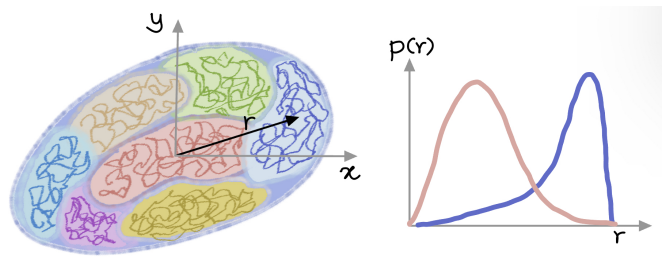


FIG. 19. Chromosomes in higher eukaryotic cells are organized spatially into largely non-overlapping chromosome territories. The spatial arrangement of individual chromosomes is also non-trivial, with more gene-dense chromosomes tending to be found at more interior locations than gene-poor ones. Such non-trivial positioning is apparent in fluorescence in-situ hybridization experiments in which individual chromosomes can be labelled and their distributions across an ensemble of cells quantified.

of the genome correlate to an active temperature [220]. Brownian dynamics simulations of such a model, for human chromosomes, can reproduce the radial organization of chromosomes by gene density, the separation of euchromatin and heterochromatin, the differential positioning of the two X chromosomes in female cells, and chromosome-specific gene density and centre of mass distributions in the nucleus [221]. That differential activity might provide a general explanation for many different properties of large-scale nuclear architecture was suggested in Refs [220, 221]. Other numerical work that studies chromatin and bases itself on an active polymer description includes Refs. [222, 223].

The field of nuclear mechanotransduction studies how local forces might influence transcription programs. There appear to be three mechanisms with which microenvironment regulates gene expression. These are via the control of the nuclear import of different transcription factors, changes in nuclear organization, and spatiotemporal mechanoregulation of co-transcribed genes [224]. All of these can be affected through the dynamics of the cytoskeleton outside the nucleus, itself influenced by the extracellular environment.

Stem cells can also exhibit unusual mechanical properties, such as a negative Poisson’s ratio in a transitional regime [225]. While conventional materials expand in the transverse direction while subjected to a longitudinal compressive force, auxetic materials contract. A theory for such mechanics that incorporates the coupling of nuclear dimensions to chromatin states that arise as a consequence of activity has been proposed in [226].

B. Spindle

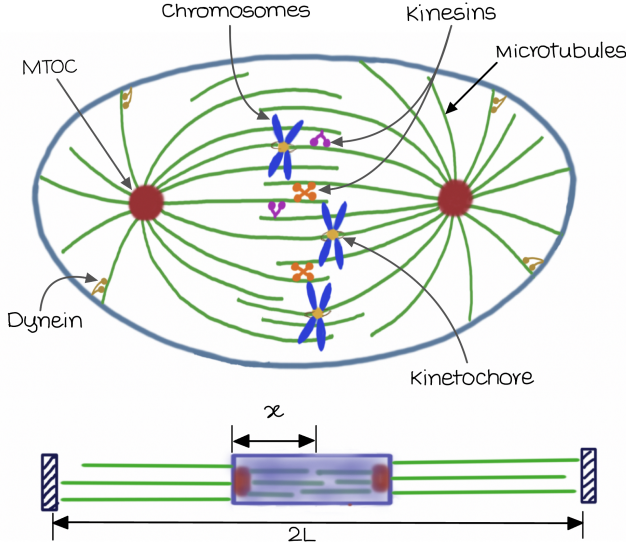


FIG. 20. Top: Schematic showing the typical microtubule arrangement in the mitotic spindle. These microtubules position the condensed chromosome pairs (sister chromatids) along the mid plane of the cell and subsequently help in partitioning them as cell division progresses. Polymerization and depolymerization of microtubules and motor proteins from the kinesin and dynein superfamilies generate forces within this system and at the confining boundary of the cell. Bottom: A simplified one-dimensional model for the positioning of the spindle in which the astral microtubules are a linear bundle of polymerizing and depolymerizing filaments.

One critical processes in eukaryotic cell division is the segregation of chromosomes. The mitotic spindle consists of two microtubule organizing centers (MTOC) from each of which emanate a radial collection of microtubules, forming a bipolar structure (FIG. 20). Through a combination of microtubule polymerization and interaction with the actomyosin cortex, the spindle centers symmetrically within the cell [227]. This process also positions the duplicated chromosomes near the equatorial region of the cell.

Some microtubules emanating from the MTOC attach to condensed chromosome pairs (sister chromatids) via motor proteins and specialized protein complexes known as kinetochores. Subsequent force generation in the spindle microtubules by the action of motor proteins such as kinesins, and depolymerization forces (of the order of 10 pN per chromatid pair), lead to the segregation of sis-

ter chromatids to the opposite ends of the cell [228–230].

In the metaphase stage of cell division, the (astral) microtubules emanating from each of the MTOCs interact with the cell cortex and also with the microtubules emerging from the partner MTOC. These interactions, which include active and passive components, determine the effective mechanical properties and stability of the spindle structure (FIG. 20). A highly simplified picture, in which only polymerization forces acting between the two MTOCs and between MTOCs and the boundary are considered, can provide insight into the mechanisms involved in centering the spindle.

Consider a 1-D toy model of the mitotic spindle with two MTOCs shown in FIG. 20. Assuming that the microtubules growing towards the chromosomes are rigidly coupled, the problem of determining the force on the spindle can be reduced to computing the sum of the repulsive forces generated by each MTOC pushing against the cell barrier. Using arguments similar to those used in section VIII that lead to (37), the net force on the spindle, measuring its displacement x from the mid-point of the cell, is therefore

$$f(x) = \frac{\Delta\mu}{a} \left[N^+ \left(1 - \frac{k_b^+}{k_u^+} \right) \left(\frac{k_b^+}{k_u^+} \right)^{(L-x)/a} - N^- \left(1 - \frac{k_b^-}{k_u^-} \right) \left(\frac{k_b^-}{k_u^-} \right)^{(L+x)/a} \right], \quad (54)$$

where N^\pm , $k_{b,u}^\pm$ are, respectively, the mean-number of polymers and the binding/unbinding rates at the two ends of the cell. Clearly, in the symmetric case, i.e., $N^+ = N^-$, $k_b^+ = k_b^-$, and $k_u^+ = k_u^-$, the equilibrium configuration corresponds to a scenario where the spindle is positioned symmetrically ($x = 0$) with respect to the midpoint of the cell. Experiments using microneedles and magnetic tweezers show that transverse perturbations to the spindle alignment decay within timescales ~ 15 s. This relaxation clearly arises from the interaction of the spindle with the cytoplasm and demonstrates the stability of the positioning and orientation of the spindle.

Forces resulting from the filamentous structures within the spindle and their interaction with the boundary of the cell lead to its positioning. An understanding of the geometrical shape of the spindle should necessarily take into account the cohesive forces between the microtubules, mediated by crosslinkers and motors. The question of the large-scale shape of the spindle is conveniently described within a continuum approach. In this case, the mitotic spindle can be considered as a droplet of active

matter [231]. The action of molecular motors and ATP dependent microtubule dynamics are the sources of activity.

In cell-extracts, giant-number fluctuations observed in the orientational ordering of the spindle microtubules justify an active continuum description [232]. Further this approach allows one to estimate the material parameters of the spindle such as the strength of active stress (≈ 70 Pa), effective spindle surface tension (≈ 140 pN/ μm), and the elastic constant of the orientation elasticity (≈ 400 pN).

Using this continuum approach and the experimentally determined parameters, it is shown that stable spindle shapes can emerge from a competition between bulk active stress due to activity, nematic elasticity of microtubules and surface tension on the boundary. This model can account for the observed shape transitions seen in cell extracts as a function of dynein activity [231]. While active matter theory accounts for the spindle shapes seen in cell extracts, the situation within the cell is, of course, far more complex [233].

C. Cytokinesis

Eukaryotic cells typically divide by the formation and subsequent constriction of actomyosin rings [234] (see Fig 21). In most cell types, polar actin filaments within the ring (of width ≈ 100 nm) organize in a nematic order and also undergo continuous turnover. Constriction of such rings by contractile forces appears to be a general mechanism to “cleave” a volume into two parts, with cytokinetic rings composed of FtsZ filaments achieving a similar effect even in bacterial cells.

All cells maintain an internal clock via cyclic variations in the concentration of cell-cycle associated molecules [235]. At suitable time-points, signals regulated by the cell-cycle enhance the contractility of the actomyosin cortex. Signals from upstream processes can trigger gradients in these active stresses which, in turn, lead to large scale cortical flows. These flows, with speeds $5 - 10$ $\mu\text{m}/\text{min}$, lead to the emergence of spatially non-uniform actomyosin patterns. These eventually form a ring-like structure.

Theoretical studies show that that such ring-like structures can emerge spontaneously from an instability of the uniform state of the actomyosin cortex [199]. The convergent nature of these flows compresses actin filaments and aligns them along the equator of the cell (FIG. 21).

This further enhances the contractile forces within the ring [204, 236] (Sections IV and X). The patterns in the actomyosin cortex and the shape of the cell can thus form a coupled dynamical system for concentration, flow, and stress fields, and geometrical descriptors of the surface. The analyses of such a dynamical system shows that cytokinesis-like patterns in both myosin concentrations and cell shape can arise spontaneously [237].

The nematic order parameter Q for the alignment of actin filaments is non-zero at the equator of the cell (FIG. 21). Specifically, the diagonal component Q of Q evolves according to [238]

$$\partial_t Q = -v \partial_x Q - \frac{\beta}{2} \partial_x v - \frac{1}{\tau} Q + \frac{\ell^2}{\tau \nu} \partial_x^2 Q, \quad (55)$$

where v is the x -component of the cortical velocity (i.e., perpendicular to the actomyosin ring; see FIG. 21), β , τ , and ℓ are material parameters respectively characterizing the flow alignment, the relaxation time of Q , and the hydrodynamic length scale for cortical flows. With an experimentally measured profile $v(x)$ of the active flows, Eq. (55) quantitatively accounts for the steady-state spatial profile of Q , thereby supporting the idea of flow-induced alignment of actin filaments along the cytokinetic ring [204].

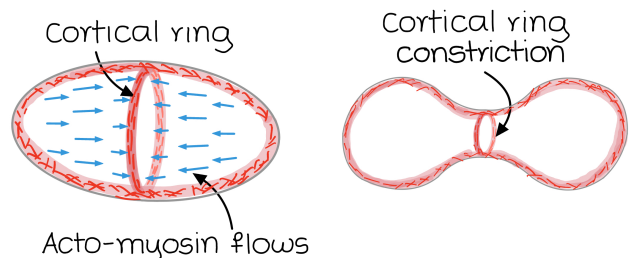


FIG. 21. The cytokinetic ring predominantly results from flow-induced alignment of actin filaments due to large-scale cortical flows. This enhances actomyosin contractile forces at the equatorial region of the cell and leads to constriction eventually culminating in cytokinesis.

Enhanced actomyosin levels generate a pattern of active contractile stresses. While the tangential components of these stress gradients drive in-plane cortical flows, the normal components lead to forces that can deform the cell surface forming a cleavage furrow [239]. These active forces have to overcome the forces arising from the bending elasticity of the cell membrane and external forces (from the cytoplasm and the cell exterior).

In yeast cells, for instance, the circumferential tension generated within the contractile ring has been measured by micropipette aspiration to be ≈ 400 pN [240] which is sufficient to deform and constrict the cell surface. With a given spatiotemporal pattern of these contractile forces, the cellular surface buds in a manner akin to cytokinesis [200]. Constriction seems to proceed at a uniform rate for many cells up to the point where the membranes of the two constricting regions meet [241, 242]. A merger of these membrane surfaces and subsequent scission event completes cytokinesis.

Although there is clear evidence for the presence of myosin in the contractile ring from yeast to mammalian cells, myosin-free contraction of rings have also been observed in some cell types [243]. Additionally, it has theoretically been argued that myosin-free contractile forces can be generated in the ring if the actin filaments undergoing turnover are connected via end-tracking crosslinkers [244].

XII. TISSUE MECHANICS

Tissues are condensed collections of cell and their extra cellular matrix. They integrate form with specific function. In addition to adhesive interactions between neighboring cells, different parts of tissues can also interact with each other via signaling mechanisms. Specific molecules that are secreted by cells and diffuse in extra cellular regions can transmit information between adjacent cells or tissues. Such signaling often leads to local mechanical force generation in a tissue. Tissues are thus conveniently viewed as strongly-correlated many-body collectives of cells.

A. Planar 2D epithelial monolayers

Epithelial monolayers are formed of a single cell thick layer of connected individual cells, called a confluent layer as shown in FIG. 22(a). Cells in the epithelial tissue have an apico-basal polarity, i.e., there is a distinction between the top and the bottom. In many cases, during developmental stages, the epithelial cells develop a polar organization of surface associated proteins known as planar cell polarity (PCP). In addition to the actomyosin cytoskeleton and cortex, and possibly cell-substrate connections, the cell-cell junctions are formed with cadherin molecules. Moreover, the mechanical effect of the actin

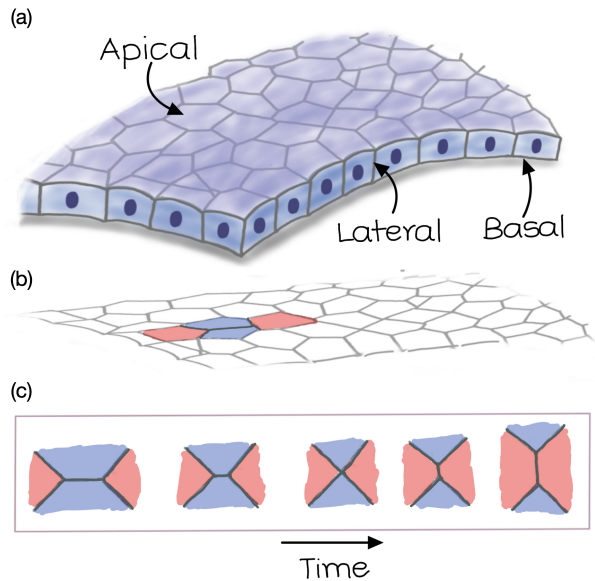


FIG. 22. At scales of many cells (tissues), the interactions between neighbouring cells through junctional elasticity leads to a coarse-grained description of the entire tissue. For epithelial cell layers as shown, which are quasi-two-dimensional structures, deformation of the tissues with time can lead to morphogenetic changes, such as folds and invaginations. (a) A nearly planar quasi two-dimensional tissue. (b) Apical projection of the tissue in (a) leads to the planar vertex model. In addition to junctional elasticity, the vertex model can also incorporate local anisotropy via polarized bond tensions. (c) Active fluctuations in cell edge contractility can result in tissue fluidization via neighbour exchanges.

cytoskeleton, PCP, apico-basal polarity, front-rear polarity and the cell-cell junctions composed of acto-myosin complexes and cadherins can all be individually modulated to give rise to a variety of deformations of the tissues.

Epithelial tissues exhibit wide range of mechanical behavior [245–248]. While they have important biological functions, they are also multifunctional, tunable biomaterials [249]. They can exhibit a large variety of rheological behavior ranging between perfectly elastic and purely viscous over different length and time scales as well as rich mechanics and complex 3D shapes [250–257].

A simple vertex model for an epithelial tissue describes the dynamics of the vertices of cells it contains. A configuration given by a set of vertices $\{\mathbf{r}_i\}$ is associated with

an energy like quantity

$$W = \sum_{\alpha} \frac{K_{\alpha}}{2} (A_{\alpha} - A_{0\alpha})^2 + \sum_{\alpha} \frac{\Gamma_{\alpha}}{2} p_{\alpha}^2 + \sum_{\alpha\beta} \Lambda_{\alpha\beta} l_{\alpha\beta}. \quad (56)$$

Here, for any cell α , K_{α} is the area stiffness, while $A_{0\alpha}$ and A_{α} are the preferred and actual areas, respectively. The second term represents perimeter contractility Γ_{α} that provides a tension of along the cell boundary of the cell with perimeter p_{α} . The final term is an effective edge tension $\Lambda_{\alpha\beta}$ of junction between cells α and β of length $l_{\alpha\beta}$. The edge tension results from a combination of acto-myosin contractility and cell-cell adhesivity. The vertex configuration $\{\mathbf{r}_i\}_{\text{eq}}$ that minimizes the work function corresponds to the mechanical equilibrium of the tissue.

A dynamical way to reach this mechanical equilibrium configuration is via a gradient descent approach, wherein the vertices $\{i\}$ evolve as:

$$\eta \frac{\partial \mathbf{r}_i}{\partial t} = -\frac{\partial W}{\partial \mathbf{r}_i}, \quad (57)$$

where η is the effective friction between the cell vertex and the underlying substrate.

In an epithelial tissue, the cell connectivity does not remain fixed. Cell division and cell death events restructure cell connectivity. Cells can undergo connectivity changes without altering the number of cells via neighbor exchanges (T1 transitions) as shown in FIG. 22(c). Additionally, in non-confluent tissues, merger of isolated cells with a larger collection will also change tissue topology [258]. These topological transitions can be influenced by local cell properties (such as acto-myosin contractility) or by global signalling mechanisms. Collectively, these transitions alter the effective mechanical properties of the tissues. For instance, the most prominently observed T1 transitions fluidize the tissue locally and relax elastic stresses. In the vertex model described above, these topological transitions are an additional input to the vertex dynamics (57).

Consider a homogeneous tissue with $K_{\alpha} = K > 0$, $A_{0\alpha} = A_0$, $\Gamma_{\alpha} = \Gamma > 0$, and $\Lambda_{\alpha\beta} = \Lambda$. When the bond tension $\Lambda < 0$, i.e., cell-cell adhesivity dominates junctional contractility, W in the bulk can be rewritten as

$$W = \sum_{\alpha} \frac{K}{2} (A_{\alpha} - A_0)^2 + \frac{\Gamma}{2} (p_{\alpha} - p_0)^2, \quad (58)$$

where $p_0 = -\Lambda/(2\Gamma)$ becomes the preferred perimeter for the cells in the tissue. An important geometrical quantity characterizing cell shape is $p_0/\sqrt{A_0}$. When $p_0 < 3.8$, the

preferred ground-state of the tissue is an hexagonal array of cells. By tuning Λ/Γ , the tissue undergoes a fluidisation transition from a rigid configuration composed of hexagonal cells to a floppy configuration when $p_0 > 3.82$ (corresponding to regular pentagons). In this case, the tissue contains a mixture of pentagonal, hexagonal, and heptagonal shaped cells. In the floppy configuration, an applied shear stress causes the tissue to flow by an increased in the frequency of T1 transitions [259, 260]. The basic vertex model can be supplemented with additional active components, relating to gene signalling, reaction-diffusion dynamics, angle dependent edge tensions, cell motility, active cell stress, active topological transitions, among many others [254, 256, 261–263].

While the cell-level description within the vertex model is useful in providing insights into various aspects of epithelial morphogenesis, the phase space of parameters is large and difficult to constrain. In the spirit of hydrodynamic descriptions discussed in Section IV, it is natural to ask for coarse-grained continuum descriptions of tissue dynamics. The kinematics of planar tissue deformation during morphogenesis has isotropic and anisotropic components. These are associated with size and shape changes of the tissue, respectively. The isotropic deformations can be associated with individual cell size changes as well as cell division and death. Anisotropic deformations arise from shape changes of individual cells as well as from topological transitions such as neighbour exchanges (T1), division and extrusion (T2). Such contributions can be coarse-grained over space and time and reformulated in the language of continuum mechanics [251, 264, 265]. For example, the mass balance equation takes the following form

$$\frac{\partial \rho}{\partial t} + \nabla \cdot (\rho \mathbf{v}) = k_d(\rho) - k_a(\rho), \quad (59)$$

where k_d and k_a are, respectively, cell birth and death rates. These may have a nonlinear functional dependence on ρ . The tissue velocity \mathbf{v} arises from the force balance condition,

$$\nabla \cdot \Sigma = \gamma \mathbf{v}, \quad (60)$$

where γ is the friction coefficient and the stress tensor $\Sigma = \tilde{\Sigma} - p\mathbb{I}$. Here, the tissue pressure p and the deviatoric stress $\tilde{\Sigma}$ are obtained from

$$p = \mu_a \ln \frac{\rho}{\rho_0}, \quad (61)$$

$$\tilde{\Sigma} = 2\mu_s \mathbf{Q} + \zeta \mathbf{q}. \quad (62)$$

The anisotropies in cell shapes and those arising from chemical polarities are captured by the tensors \mathbf{Q} and \mathbf{q} , respectively. The cell shape anisotropy evolves according to

$$\mathcal{D}_t \mathbf{Q} = \mathbf{R} - \left(\boldsymbol{\epsilon} - \frac{1}{2} \text{Tr}(\boldsymbol{\epsilon}) \mathbb{I} \right), \quad (63)$$

where the strain rate tensor $\boldsymbol{\epsilon}$ is given in (14) and \mathbf{R} represents the contribution from the topological rearrangements of cells. The dynamics of \mathbf{q} is controlled by the manner in which chemical polarities of cells interact with each other as well as with signalling cascades, and tissue mechanics. Typically, \mathbf{q} reaches a steady state profile relatively quickly. In such a scenario, a static spatial profile of \mathbf{q} can be assumed. The shear strain rate resulting from topological transitions evolves according to

$$(1 + \tau_R \mathcal{D}_t) \mathbf{R} = \frac{1}{\tau_Q} \mathbf{Q} + \lambda \mathbf{q}. \quad (64)$$

Here, τ_Q^{-1} is the rate with which cell shape anisotropy \mathbf{Q} . The second term \mathbf{q} on the right-hand captures the role active nematic tensor \mathbf{q} to \mathbf{R} .

To summarize, (59), (60), (63), and (64), govern the evolution of density ρ , cell shape \mathbf{Q} , and topological rearrangements \mathbf{R} , together with the constitutive relations (61) and (62). While our model largely follows [266], there are alternative descriptions [265, 267, 268] for epithelial morphogenesis. We will illustrate the formalism by considering a simple case.

In the simplest scenario, the edge tension $\Lambda_{\alpha\beta}$ is homogeneous across all bonds. However, the presence of morphogen signalling fields can induce both anisotropy and heterogeneity in bond tensions, and lead to tissue deformation and flows. For instance, in the *Drosophila* gonad [269], planar cell polarity (PCP) creates an anisotropic environment.

One way to construct an active vertex model (FIG. 22(b)) is to modify the bond tensions according to [262]

$$\Lambda_{\alpha\beta} = \Lambda_0 + \Lambda_1 \cos 2(\theta_{\alpha\beta} - \theta_0) + \xi(t), \quad (65)$$

where, Λ_0 is the base-level cell-cell bond tension which is amplified or reduced, respectively, by an amount Λ_1 depending on its orientation with respect to a preferred orientation θ_0 , which in turn, is dictated by PCP. The active noise $\xi(t)$ is modelled as an Ornstein-Uhlenbeck process with a correlation time τ , ensuring the persistence of high bond tension fluctuations leading to junctional shrinkage and eventual T1 transitions thereby fluidizing the tissue.

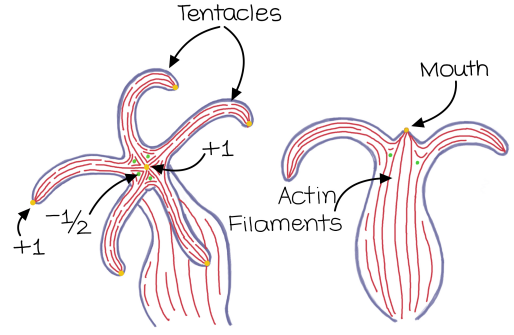


FIG. 23. Topological defects in an active nematic field formed by actin filaments in a developing hydra play an important role during morphogenesis. For example, in hydra, the generation of tentacles is associated with the formation of $+1$ defects (yellow dots) at the future mouth and at the tips of the tentacles, and a pair of $-1/2$ defects (green dots) near the base of each tentacle [89, 270].

At a coarse-grained level, the modification (65) of the bond tensions manifests in the form of the active terms proportional to ζ in (62) and λ in (64). Thus, we effectively have an active, fluidized tissue, with anisotropic bond tensions that result in T1 transitions as well as anisotropic active stresses.

In a tissue confined to a rectangular geometry of size $L_x \times L_y$ with periodic boundary conditions along the x direction, no-slip ($\mathbf{v} = \mathbf{0}$) at the bottom wall ($y = 0$), shear-stress-free ($\sigma_{xy} = 0$) at the top wall ($y = L_y$), and a preferred PCP orientation $\theta_0 = \pi/4$ leads to the emergence of a shear-rate

$$\partial_y v_x = 2 \left(\lambda - \frac{\zeta}{2\mu_s \tau_Q} \right) q_{xy} (1 - e^{-t/\tau_Q}), \quad (66)$$

when we keep $\tau_R = 0$ in (64). This leads to a Couette-flow like steady-state velocity profile

$$v_x(y) = 2y \left(\lambda - \frac{\zeta}{2\mu_s \tau_Q} \right) q_{xy}. \quad (67)$$

Note that this velocity profile, arising spontaneously from the activity, leads to sliding deformation of the tissue. This leads to a steady-state cell elongation of $Q_{xy} = -\zeta/2\mu_s$,

The epithelial tissue, though a monolayer, typically has an apicobasal polarity – it has a well differentiated apical and basal surface and the neighbouring cells are connected to each other via lateral surfaces. In such a tissue, by tuning the absolute and the relative values of the areas of these three surfaces, the tissue can be

rendered into myriad 3D shapes including tissue folding, invaginations and twisting. Although a number of interesting morphogenetic phenomena can be modeled using a planar framework, many important events involve epithelial monolayers undergoing out of plane or 3d deformations [271] either due to buckling (e.g., microvilli formation [272]) or to differential contractilities of the apical and basal surfaces (e.g., cancer morphogenesis of pancreatic ducts [247]).

XIII. A FEW OTHER EXAMPLES

At the molecular level, forces arise when proteins change conformations or when they undergo polymerization. Apart from discussing molecular motors and filament polymerization, we have refrained from discussing in detail the behavior of a number of other important microscopic players. While we have focused on force generation at the cellular level, many exciting questions have to do with how forces are sensed. Mechanisms for force sensing include mechanosensitive ion-channels that are involved in gating ions, and the involvement of molecules involved in cell adhesion, force sensing and motility including talins, vinculin, integrins, cadherins, and others [273]. While controlled *in vitro* studies of the mechanics of these molecules at an individual level are available, much less has been explored concerning their collective role in the *in vivo* context. Similarly, mechanical forces are implicated in the translocation of biopolymers, such as mRNA, through nuclear pores and also through engineered nanochannels under an electric field [274].

Understanding the complexity of force generation in a variety of molecular machines (e.g., helicase, RNA polymerase, ribosome) requires a detailed understanding of their function at the molecular level. Nevertheless, the broad principles we have discussed here, of non-equilibrium ratchets, provide a common set of ideas that generalize across this variety. In particular, transcription process involve a variety of such machines. A few references are [275–282]. In the following subsections, without being exhaustive, we mention a few more relevant systems and processes that are not discussed above, where mechanical forces play a significant role.

A. Virus assembly and genome packaging

Mechanical forces play a significant role in the assembly, compaction, and delivery of DNA/RNA in viruses. For example, in bacteriophages, the DNA is squeezed into the viral capsid by an ATP consuming portal motor that sits at the entrance of the capsid [283]. The portal motor acts against the internal forces that are produced within the capsid due to electrostatic interactions and DNA bending. The pressure arising from the compaction of the nucleic acids into the tight confining space of the capsid must be counterbalanced by the tensile forces on the capsid surface. Atomic force microscopy measurements indicate that the forces involved in deforming these capsids are in the range of a few hundreds of piconewtons. When a virus infects a cell, DNA is injected into the viral host through a processes that relies on the osmotic pressure difference between the viral capsid and the host cell. This osmotic pressure difference is around 10 – 100 atmospheres [284]. See [285, 286] for recent reviews that discuss many physical aspects of virus dynamics.

B. Swimming

Micro-organisms can exhibit diverse modes of swimming. *E. coli* swims (runs) by bundling its flagella together and rotating this bundle counter-clockwise [38]. When the direction of rotation switches from counter-clockwise to clockwise, these flagella fly apart and the bacterium tumbles, then chooses a new direction to run. *C. Reinhardtii* swims by beating its two flagella in a time-asymmetric manner.

Swimming of cells or other structures at low-Reynolds numbers has been studied extensively in the decades since Purcell’s insightful work [51]. The complexities of fluid-structure interaction have been worked out in great detail including swimming in viscoelastic media.

The problem of the swimmer is the coupling of the periodic change in shape to the transfer of momentum to the ambient, thereby effecting a net movement. This problem is particularly non-trivial when the Reynolds number is very small. In this situation, the linearity of the resulting equations for the fluid implies that purely reciprocal shape changes cannot lead to net motion [51]. As such, mechanisms to enact non-reciprocal shape changes are needed to swim at low *Re*. This field has developed extensively over the past several decades. For a recent monograph covering several aspects of cell swimming, see

[287].

C. Plants

Though much of our discussion has focused on animal cells, mechanical forces are vital for many cellular and developmental processes in plants. As in the case of animals, plants too have evolved several mechanisms both for the generation of force and using it for movement over a wide range of timescales. Some of these mechanisms are unique to the plant world and deserve special attention [288]. The control of the movement of water and hence osmotic pressure is central to many biomechanical processes in plants [289–291]. Mechanical stresses driven by cell turgor pressure and coupled with anisotropic mechanical cell-wall properties form the basis of plant morphogenesis [292].

At a cellular level, plants exhibit large-scale fluid movement known as cytoplasmic streaming (similar to those seen in animal cells). This is known to arise from the active self-organization of microfilaments [293]. While the functions of such streaming are not completely known, it is believed that the convective flows that arise provide a more efficient way of mixing nutrients across the cell compared to diffusion.

Plants also exhibit large-scale movement in response to various stimuli such as mechanical, and chemical perturbations [8, 294]. For instance, in response to touch stimuli, plants can generate fast movements driven by changes in osmotic pressure as in the case of leaf-closure in *Mimosa Pudica* [289] or the snapping of the venus-flytrap [295].

At a much longer timescale (\sim hours), plants exhibit movements in response to environmental factors like sunlight, gravity etc. These responses, collectively known as tropisms, typically result from differential growth [296].

XIV. CONCLUSIONS

This review summarizes our current understanding of forces at the scale of the cell. It argues that nanoscale forces originating in non-equilibrium processes at a local level serve to both sculpt physical form as well as to enable biological function, that the contexts in which these forces arise are familiar objects of study in soft condensed matter physics, that soft-matter systems driven out of equilibrium in specific ways provide an appropriate

paradigm in which to assess and study cell-scale forces and, finally, that general tools of statistical physics already exist that can help us address a broad class of questions of relevance to mechanobiology.

Finding a free energy to minimize is of little use in the study of non-equilibrium steady states, since no thermodynamic description can be relied upon. Such states must be described at the level of equations of motion. The fact that biological environments are fluid adds further complexity, since momentum can be transferred via the surrounding aqueous medium whose properties must then also be accounted for. Microscopic atomistic descriptions must then give way to coarse-grained descriptions. There are, currently, no well-established rules for writing down coarse-grained equations of motion for non-equilibrium steady states of any complexity, although it is expected that general hydrodynamic, symmetry-based arguments may be a reasonable starting point.

Steady states of active matter systems are already known to exhibit diverse behaviour, since they are liberated from the constraints of equilibrium physics. These include unusual mechanical properties involving instabilities of initially ordered states, large fluctuations that deviate qualitatively from expectations based on the central limit theorem, and, in some contexts, self-tuning to the vicinity of a dynamical phase transition [7, 11]. How such unusual properties might be reflected in biological function is an active area of research.

Mechanochemical forces arise in the extraction of genetic information encoded in DNA sequences, for example, by the molecular motor RNA polymerase. This was certainly required for the emergence of simple, unicellular life-forms. Since information storage and transmission must finally be implemented at the molecular level, it is quite likely that processes that transduce chemical energy into mechanical forces, controlled by information, may have been favored by natural selection.

Such forces also contribute to enabling the building of large-scale structures, thus supporting the emergence of complex organelles, including the nucleus, the mitotic spindle, and the Golgi complex. The increased cell size required to accommodate these structures raises the question of transporting cargo efficiently across them. Directed transport by molecular motor proteins provides a natural way to solve this problem, as opposed to purely diffusive transport mechanisms. For instance, intracellular transport in neurons, which must happen over distances ranging from millimeters to meters, uses molec-

ular motors.

The involvement of forces in decoding information was already a feature of prokaryotes and could thus have been inherited by eukaryotes. However, the second aspect is a key evolutionary step since it opened up the possibility of the emergence of complex life-forms.

Large-scale force generation mediated by the cellular cytoskeleton would likely have been a key evolutionary event in the ascent of eukaryotic cells. Apart from enabling more complex forms of cellular locomotion, this would have naturally led to collective cellular dynamics, a key feature of multicellular organisms [297–299]. Importantly, innovations in force generation could then enable higher level control of gene expression, cell polarity, multicellular signalling, and developmental organization [224, 300].

In this review, we have attempted to describe the general physical principles that enable cell-scale biological processes involving non-equilibrium force generation. While activity seems to be central to life’s processes, understanding exactly how biological, biochemical and biophysical approaches converge to describe, potentially even recreate, the functionalities of a living cell, remains an exciting as well as a challenging direction for future work. The fundamental question remains the one reflected in the title Schrödinger chose for his influential book “What is Life?” [301].

XV. GLOSSARY

Active process: A physico-chemical process held out of equilibrium through the throughput of energy at the microscopic scale, typically via chemical reactions involving energy storing molecules such as ATP.

Actomyosin cortex: Term applied to the dense layer of actin filaments, myosin motors and actin cross-linkers, along with other regulatory molecules, that lie just below the cell membrane.

Brownian ratchet: A model that has functioned as a paradigm for how processes involving non-equilibrium energy flow can produce biased motion, allowing forces to be exerted.

Chromosome: The term applied to DNA in its cellular context, where it is found bound to many other proteins, including histones, chromatin remodellers and molecular motors such as RNA polymerase.

Comoving corotating derivative: accounts for the kinematical changes in a tensor field as seen in a frame being advected and rotated by a flow field.

Constitutive relation: The relation between stresses and strains (or strain rates) that defines the mechanical response of a material that is being deformed.

Cytokinesis: The cell-scale sequence of processes through which a cell cleaves into two daughter cells.

Cytoskeleton: Term applied to a specific set of polymers (actin, microtubules and intermediate filaments) in the cell, which underlie cell shape, architecture and motility while also provide a scaffolding for several classes of molecular motors.

Detailed balance: The relationship between forward and backward rates of statistical processes that must exist for macroscopic thermodynamic equilibrium states to result from the dynamics.

Epithelial tissue: The layer of cells that form the interface of organs and are exposed directly to fluid flow as well as external perturbations.

Fluctuation-Dissipation theorem: A fundamental relationship between noise strength and damping coefficients that ensures that thermodynamic equilibrium is attained.

Hydrodynamic approach: The procedure of replacing a microscopic description of a large number of momenta and positions with a coarse-grained description where quantities of interest (the density and momentum density) are instead represented by their coarse-grained averages, and a local equation for their evolution, at each point in space and time.

Hydrodynamic stress: Force per unit area acting across surfaces, that arise as a consequence of fluid flow, distortions of an order parameter and gradients in other related quantities.

Linear response theory: The idea that generalized forces (such as a stress or a chemical potential) and generalized fluxes (such as a flow or a chemical reaction rate) must be linearly related.

Markov process: Stochastic process connecting allowed states in which the transition probabilities (or rates) depend only on the current state, not on prior history.

Mechanochemical coupling: The use of chemical reactions to drive mechanical processes and vice-versa, typically shape changes in molecules.

Metabolism: The term applied to biochemical reactions that convert nutrients into high-energy molecules such as ATP.

Mitotic spindle: An ordered, characteristically shaped structure formed from microtubules that separates the duplicated chromosomes.

Molecular motor: A molecular assembly that consumes energy in the form of ATP molecules, changes conformation, and uses this change of conformation to perform mechanical work.

Nematic order: An axially aligned state formed in systems of fore-aft symmetric anisotropic molecules.

Nonequilibrium steady state: Time-independent macroscopic state of a system which is not governed by the thermodynamic equilibrium distribution, and has non-zero fluxes (of energy or matter) and constant entropy production.

Péclet number: A dimensionless number quantifying the balance of directed and diffusive motion.

Polar order: A locally aligned state formed in systems of fore-aft asymmetric anisotropic molecules.

Polymerization force: Forces exerted by molecules that are allowed to polymerize.

Reynolds number: A dimensionless quantity representing the ratio of inertial forces to viscous forces, which effectively measures the balance of advection and dissipation in a fluid.

Rheology: The study of flow and deformation of materials.

Self-organized patterns: Spatiotemporal structures that emerge from the dynamics in non-equilibrium states.

Thermodynamic equilibrium: Macroscopic states with vanishing fluxes (of energy or matter) and no entropy production, wherein the probability of microscopic configurations is governed by the Boltzmann distribution.

Tissue: A collection of cells, and their extracellular matrix, with a specific functionality.

Traction force: Force per unit area applied across a surface.

Transcription: The biochemical process by which DNA sequence is read out into an RNA molecule.

Translation: The biochemical process by which an RNA molecule is converted into a protein.

Vertex model: A, typically two-dimensional, geometrical model for an epithelial tissue in which changes in cell shapes and sizes are accounted by forces at cell-cell junctions, while incorporating dynamical processes that represent their cellular counterparts.

Viscoelastic fluids: Materials which behave as solids on short-time scales and as fluids thereafter.

Viscoelastic solids: Materials which behave as fluids on short-time scales and as solids thereafter.

ACKNOWLEDGMENTS

K.V.K. acknowledges support from the Department of Atomic Energy, Government of India, under Project No. RTI4001, from the Department of Biotechnology, Government of India, through a Ramalingaswami re-entry fellowship, from the Max Planck Society through a Max-Planck-Partner-Group at ICTS-TIFR, and from the John Templeton Foundation. M.M.I. acknowledges financial support from CEFIPRA-CSRP 6704-5. P.A.P. acknowledges support through The Wellcome Trust DBT India Alliance (grant IA/TSG/20/1/600137). G.I.M. acknowledges current support from the Centre for Computational Biology and Bioinformatics at Ashoka University and earlier from the Institute of Mathematical Sciences, Chennai. G.I.M. is grateful to TIFR, Mumbai for an Adjunct Professorship awarded in the initial stages of this work. We thank G. Kumaraswamy, A. Rajput, A. Padmanabhan, R. Parthasarathy and V. Nanjundiah for a careful reading of the manuscript and useful feedback.

-
- [1] P. Nurse, The great ideas of biology, *Clinical medicine* **3**, 560 (2003).
 - [2] B. Alberts, A. Johnson, J. Lewis, D. Morgan, M. Raff, K. Roberts, and P. Walter, *Molecular Biology of the Cell*, 6th ed. (Garland Science, New York, 2014).
 - [3] R. Phillips, J. Kondev, J. Theriot, H. G. Garcia, and N. Orme, *Physical biology of the cell* (Garland Science, 2012).
 - [4] J. Howard, *Mechanics of Motor Proteins and the Cytoskeleton* (Sinauer Associates, 2001).
 - [5] K. Dill and S. Bromberg, *Molecular driving forces: statistical thermodynamics in biology, chemistry, physics, and nanoscience* (Garland Science, 2010).
 - [6] R. Parthasarathy, Resource Letter BP-1: Biological physics, *American Journal of Physics* **89**, 1071 (2021).
 - [7] G. I. Menon, Active matter, in *Rheology of Complex Fluids*, edited by J. M. Krishnan, A. P. Deshpande, and P. B. S. Kumar (Springer, New York, NY, 2010) pp. 193–218.
 - [8] D. W. Thompson, *On Growth and Form: The Complete Revised Edition*, revised ed. (Dover Publications, 1992).
 - [9] D. Kondepudi and I. Prigogine, *Modern thermodynam-*

- ics: from heat engines to dissipative structures* (John Wiley and sons, 2014).
- [10] D. Needleman and Z. Dogic, Active matter at the interface between materials science and cell biology, *Nature Reviews Materials* **2**, 17048 (2017).
- [11] M. Marchetti, J. Joanny, S. Ramaswamy, T. Liverpool, J. Prost, M. Rao, and R. A. Simha, Hydrodynamics of soft active matter, *Rev. Mod. Phys.* **85**, 1143 (2013).
- [12] T. Vicsek, A. Czirok, E. Ben-Jacob, I. Cohen, and O. Shochet, Novel type of phase transition in a system of self-driven particles, *Phys. Rev. Lett.* **75**, 1226 (1995).
- [13] J. Toner, Y. Tu, and S. Ramaswamy, Hydrodynamics and phases of flocks, *Annals of Physics* **318**, 170 (2005).
- [14] G. Menon, J. Prost, S. Ramaswamy, and M. Rao, Workshop on Driven States in Soft and Biological Matter, <https://indico.ictp.it/event/a05198/overview> (2006).
- [15] A. Upadhyaya and A. van Oudenaarden, Biomimetic systems for studying actin-based motility, *Current Biology* **13**, R734 (2003).
- [16] C. T. Lim, A. Bershadsky, and M. P. Sheetz, Mechanobiology, *Journal of The Royal Society Interface* **7**, S291 (2010).
- [17] S. E. Luria, *36 Lectures in Biology* (The MIT Press, 1974).
- [18] R. Milo, P. Jorgensen, U. Moran, G. Weber, and M. Springer, Bionumbers—the database of key numbers in molecular and cell biology, *Nucleic acids research* **38**, D750 (2010).
- [19] D. L. Nelson, A. L. Lehninger, and M. M. Cox, *Lehninger principles of biochemistry* (Macmillan, 2008).
- [20] H. Lodish, A. Berk, C. A. Kaiser, M. Krieger, A. Bretscher, H. Ploegh, K. C. Martin, M. B. Yaffe, and A. Amon, *Molecular Cell Biology*, 9th ed. (Macmillan International Higher Education, New York, 2021).
- [21] J. E. Krebs, B. Lewin, E. S. Goldstein, and S. T. Kilpatrick, *Lewin's essential genes* (Jones and Bartlett Publishers, 2013).
- [22] E. Ortega-Arzola, P. M. Higgins, and C. S. Cockell, The minimum energy required to build a cell, *Scientific Reports* **14**, 5267 (2024).
- [23] R. Milo and R. Phillips, *Cell biology by the numbers* (Garland Science, 2015).
- [24] N. S. Wingreen, A Glossary of Cellular Components, *Physics Today* **59**, 80 (2006).
- [25] A. A. Hyman, C. A. Weber, and F. Jülicher, Liquid-Liquid Phase Separation in Biology, *Annual Review of Cell and Developmental Biology* **30**, 39 (2014).
- [26] J. Berry, C. P. Brangwynne, and M. Haataja, Physical principles of intracellular organization via active and passive phase transitions, *Reports on Progress in Physics* **81**, 046601 (2018).
- [27] T. D. Pollard and R. D. Goldman, eds., *The Cytoskeleton* (Cold Spring Harbor Laboratory Press, Cold Spring Harbor, NY, 2017).
- [28] K. K. Busiek and W. Margolin, Bacterial actin and tubulin homologs in cell growth and division, *Current Biology* **25**, R243 (2015).
- [29] A. G. Clark, K. Dierkes, and E. K. Paluch, Monitoring Actin Cortex Thickness in Live Cells, *Biophysical Journal* **105**, 570 (2013).
- [30] D. Bray, J. Heath, and D. Moss, The Membrane-Associated `Cortex of Animal Cells: Its Structure and Mechanical Properties, *Journal of Cell Science* **1986**, 71 (1986).
- [31] K. J. Chalut and E. K. Paluch, The Actin Cortex A Bridge between Cell Shape and Function, *Developmental Cell* **38**, 571 (2016).
- [32] P. Chugh and E. K. Paluch, The actin cortex at a glance, *Journal of Cell Science* **131**, jcs186254 (2018).
- [33] K. V. Kumar, The Actomyosin Cortex of Cells: A Thin Film of Active Matter, *Journal of the Indian Institute of Science* **101**, 97 (2021).
- [34] S.-K. Ma, *Statistical mechanics* (World Scientific Publishing Company, 1985).
- [35] R. Phillips, Napoleon Is in Equilibrium, *Annual Review of Condensed Matter Physics* **6**, 85 (2015).
- [36] R. Phillips, *The molecular switch: Signaling and Allostery* (Princeton University Press, 2020).
- [37] M. Yoshida, E. Muneyuki, and T. Hisabori, Atp synthase—a marvellous rotary engine of the cell, *Nature reviews Molecular cell biology* **2**, 669 (2001).
- [38] H. C. Berg, *E. coli in Motion* (Springer, 2004).
- [39] H. Noji, R. Yasuda, M. Yoshida, and K. Kinoshita Jr, Direct observation of the rotation of fl-atpase, *Nature* **386**, 299 (1997).
- [40] J. N. Israelachvili, *Intermolecular and surface forces* (Academic press, 2011).
- [41] M. P. Allen and D. J. Tildesley, *Computer simulation of liquids* (Oxford university press, 2017).
- [42] H. Wennerström, E. Vallina Estrada, J. Danielsson, and M. Oliveberg, Colloidal stability of the living cell, *Proceedings of the National Academy of Sciences* **117**, 10113 (2020).
- [43] S. Asakura and F. Oosawa, On interaction between two bodies immersed in a solution of macromolecules, *The Journal of chemical physics* **22**, 1255 (1954).
- [44] M. Doi, *Soft matter physics* (oxford university press, 2013).
- [45] C. R. Shurer, J. C.-H. Kuo, L. M. Roberts, J. G. Gandhi, M. J. Colville, T. A. Enoki, H. Pan, J. Su, J. M. Noble, M. J. Hollander, *et al.*, Physical principles of membrane shape regulation by the glycocalyx, *Cell* **177**, 1757 (2019).
- [46] T. W. Lion and R. J. Allen, Osmosis with active solutes, *Europhysics Letters* **106**, 34003 (2014).

- [47] S. R. De Groot and P. Mazur, *Non-equilibrium thermodynamics* (Courier Corporation, 2013).
- [48] P. M. Chaikin and T. C. Lubensky, *Principles of condensed matter physics* (Foundation Books, 2004).
- [49] S. Succi, *The lattice Boltzmann equation: for fluid dynamics and beyond* (Oxford university press, 2001).
- [50] A. Saha, M. Nishikawa, M. Behrndt, C.-P. Heisenberg, F. Jülicher, and S. W. Grill, Determining physical properties of the cell cortex, *Biophysical journal* **110**, 1421 (2016).
- [51] E. M. Purcell, Life at low reynolds number, *American journal of physics* **45**, 3 (1977).
- [52] M. Mayer, M. Depken, J. S. Bois, F. Jülicher, and S. W. Grill, Anisotropies in cortical tension reveal the physical basis of polarizing cortical flows, *Nature* **467**, 617 (2010).
- [53] N. Van Kampen, *Stochastic Processes in Physics and Chemistry* (North-Holland Publishing Co, 1992).
- [54] R. Zwanzig, *Nonequilibrium statistical mechanics* (Oxford university press, 2001).
- [55] H. Risken, Fokker-planck equation, in *The Fokker-Planck Equation* (Springer, 1996) pp. 63–95.
- [56] M. Doi, S. F. Edwards, and S. F. Edwards, *The theory of polymer dynamics*, Vol. 73 (Oxford university press, 1988).
- [57] S. B. Smith, L. Finzi, and C. Bustamante, Direct mechanical measurements of the elasticity of single DNA molecules by using magnetic beads, *Science* **258**, 1122 (1992).
- [58] S. B. Smith, Y. Cui, and C. Bustamante, Overstretching B-DNA: The Elastic Response of Individual Double-Stranded and Single-Stranded DNA Molecules, *Science* **271**, 795 (1996).
- [59] J. Liphardt, B. Onoa, S. B. Smith, I. Tinoco, and C. Bustamante, Reversible Unfolding of Single RNA Molecules by Mechanical Force, *Science* **292**, 733 (2001).
- [60] C. Bustamante, J. F. Marko, E. D. Siggia, and S. Smith, Entropic Elasticity of λ -Phage DNA, *Science* **265**, 1599 (1994).
- [61] C. Brangwynne, G. Koenderink, F. MacKintosh, and D. Weitz, Nonequilibrium Microtubule Fluctuations in a Model Cytoskeleton, *Physical Review Letters* **100**, 10.1103/PhysRevLett.100.118104 (2008).
- [62] D. Boal and D. H. Boal, *Mechanics of the Cell* (Cambridge University Press, 2012).
- [63] D. Nelson, T. Piran, and S. Weinberg, *Statistical mechanics of membranes and surfaces* (World Scientific, 2004).
- [64] U. Seifert, Configurations of fluid membranes and vesicles, *Advances in Physics* **46**, 13 (1997).
- [65] M. M. Kozlov, Membrane shape equations, *Journal of Physics: Condensed Matter* **18**, S1177 (2006).
- [66] J. Schöneberg, M. R. Pavlin, S. Yan, M. Righini, I.-H. Lee, L.-A. Carlson, A. H. Bahrami, D. H. Goldman, X. Ren, G. Hummer, *et al.*, Atp-dependent force generation and membrane scission by escrt-iii and vps4, *Science* **362**, 1423 (2018).
- [67] F. Brochard and J. Lennon, Frequency spectrum of the flicker phenomenon in erythrocytes, *Journal de Physique* **36**, 1035 (1975).
- [68] H. Turlier, D. A. Fedosov, B. Audoly, T. Auth, N. S. Gov, C. Sykes, J.-F. Joanny, G. Gompper, and T. Betz, Equilibrium physics breakdown reveals the active nature of red blood cell flickering, *Nature physics* **12**, 513 (2016).
- [69] S. Ramaswamy and M. Rao, The physics of active membranes, *Comptes Rendus de l'Académie des Sciences-Series IV-Physics-Astrophysics* **2**, 817 (2001).
- [70] S. Sankararaman, G. I. Menon, and P. S. Kumar, Two-component fluid membranes near repulsive walls: Linearized hydrodynamics of equilibrium and nonequilibrium states, *Physical Review E* **66**, 031914 (2002).
- [71] D. Lacoste and P. Bassereau, An update on active membranes, in *Liposomes, Lipid Bilayers and Model Membranes: From Basic Research to Application*, edited by G. Pabst, N. Kučerka, M.-P. Nieh, and J. Katsaras (CRC Press, Abingdon, UK, 2014) Chap. 14, pp. 271–287.
- [72] Y. Xie and Y. Ren, Mechanisms of nuclear mrna export: A structural perspective, *Traffic* **20**, 829 (2019).
- [73] D. Y. Vargas, A. Raj, S. A. Marras, F. R. Kramer, and S. Tyagi, Mechanism of mrna transport in the nucleus, *Proceedings of the National Academy of Sciences* **102**, 17008 (2005).
- [74] A. Selezneva, A. J. Gibb, and D. Willis, The nuclear envelope as a regulator of immune cell function, *Frontiers in Immunology* **13**, 840069 (2022).
- [75] A. Baskaran and M. C. Marchetti, Statistical mechanics and hydrodynamics of bacterial suspensions., *Proceedings of the National Academy of Sciences of the United States of America* **106**, 15567 (2009).
- [76] P. Oswald, *Rheophysics: The Deformation and Flow of Matter* (Cambridge, 2009).
- [77] R. Bernal, P. A. Pullarkat, and F. Melo, Mechanical properties of axons, *Physical review letters* **99**, 018301 (2007).
- [78] L. Onsager, Reciprocal relations in irreversible processes. II., *Physical Review* **38**, 2265 (1931).
- [79] L. Onsager, Reciprocal Relations in Irreversible Processes. I., *Physical Review* **37**, 405 (1931).
- [80] R. Kubo, M. Toda, and N. Hashitsume, *Statistical physics II: nonequilibrium statistical mechanics*, Vol. 31 (Springer Science and Business Media, 2012).
- [81] D. Mizuno, C. Tardin, C. F. Schmidt, and F. C. MacKintosh, Nonequilibrium Mechanics of Active Cytoskeletal Networks, *Science* **315**, 370 (2007).

- [82] J. Prost, J.-F. Joanny, and J. M. R. Parrondo, Generalized fluctuation-dissipation theorem for steady-state systems, *Phys. Rev. Lett.* **103**, 090601 (2009).
- [83] U. M. B. Marconi, A. Puglisi, L. Rondoni, and A. Vulpiani, Fluctuation–dissipation: response theory in statistical physics, *Physics reports* **461**, 111 (2008).
- [84] F. Jülicher, S. W. Grill, and G. Salbreux, Hydrodynamic theory of active matter, *Reports on Progress in Physics* **81**, 076601 (2018).
- [85] P. G. de Gennes and J. Prost, *The Physics of Liquid Crystals*, 2nd ed. (Clarendon Press, 1993).
- [86] R. Penrose, The topology of ridge systems, *Annals of human genetics* **42**, 435 (1979).
- [87] T. Sanchez, D. T. N. Chen, S. J. DeCamp, M. Heymann, and Z. Dogic, Spontaneous motion in hierarchically assembled active matter, *Nature* **491**, 1 (2012).
- [88] G. Duclos, R. Adkins, D. Banerjee, M. S. E. Peterson, M. Varghese, I. Kolvin, A. Baskaran, R. A. Pelcovits, T. R. Powers, A. Baskaran, F. Toschi, M. F. Hagan, S. J. Streichan, V. Vitelli, D. A. Beller, and Z. Dogic, Topological structure and dynamics of three-dimensional active nematics, *Science* **367**, 1120 (2020).
- [89] Y. Maroudas-Sacks, L. Garion, L. Shani-Zerbib, A. Livshits, E. Braun, and K. Keren, Topological defects in the nematic order of actin fibres as organization centres of Hydra morphogenesis, *Nature Physics* **17**, 251 (2021).
- [90] T. B. Saw, A. Doostmohammadi, V. Nier, L. Kocgozlu, S. Thampi, Y. Toyama, P. Marcq, C. T. Lim, J. M. Yeomans, and B. Ladoux, Topological defects in epithelia govern cell death and extrusion, *Nature* **544**, 212 (2017).
- [91] B. Finlayson and L. Scriven, Convective instability by active stress, *Proceedings of the Royal Society of London. A. Mathematical and Physical Sciences* **310**, 183 (1969).
- [92] F. Jülicher, K. Kruse, J. Prost, and J. F. Joanny, Active behavior of the Cytoskeleton, *Physics Reports* **449**, 3 (2007).
- [93] J. Prost, F. Jülicher, and J.-F. Joanny, Active gel physics, *Nature Physics* **11**, 111 (2015).
- [94] J.-F. Joanny and J. Prost, Active gels as a description of the actin-myosin cytoskeleton, *HFSP Journal* **3**, 94 (2009).
- [95] M. C. Marchetti, J. F. Joanny, S. Ramaswamy, T. B. Liverpool, J. Prost, M. Rao, and R. A. Simha, Hydrodynamics of soft active matter, *Reviews of Modern Physics* **85**, 1143 (2013).
- [96] A. Doostmohammadi, J. Ignés-Mullol, J. M. Yeomans, and F. Sagués, Active nematics, *Nature Communications* **9**, 3246 (2018).
- [97] S. Ramaswamy, Active fluids, *Nature Reviews Physics* **1**, 640 (2019).
- [98] P. Roca-Cusachs, V. Conte, and X. Trepap, Quantifying forces in cell biology, *Nature cell biology* **19**, 742 (2017).
- [99] T. Reichenbach and A. J. Hudspeth, The physics of hearing: Fluid mechanics and the active process of the inner ear, *Reports on Progress in Physics* **77**, 076601 (2014).
- [100] S. Katta, M. Krieg, and M. B. Goodman, Feeling force: physical and physiological principles enabling sensory mechanotransduction, *Annual review of cell and developmental biology* **31**, 347 (2015).
- [101] J. B. Freund, J. G. Goetz, K. L. Hill, and J. Vermot, Fluid flows and forces in development: functions, features and biophysical principles, *Development* **139**, 1229 (2012).
- [102] G. Salbreux, J. F. Joanny, J. Prost, and P. Pullarkat, Shape oscillations of non-adhering fibroblast cells, *Physical Biology* **4**, 268 (2007).
- [103] P. A. Pullarkat, P. A. Fernández, and A. Ott, Rheological properties of the eukaryotic cell cytoskeleton, *Physics Reports* **449**, 29 (2007).
- [104] W. W. Ahmed, É. Fodor, and T. Betz, Active cell mechanics: Measurement and theory, *Biochimica et Biophysica Acta (BBA)-Molecular Cell Research* **1853**, 3083 (2015).
- [105] P.-H. Wu, D. R.-B. Aroush, A. Asnacios, W.-C. Chen, M. E. Dokukin, B. L. Doss, P. Durand-Smet, A. Ekpenyong, J. Guck, N. V. Guz, *et al.*, A comparison of methods to assess cell mechanical properties, *Nature methods* **15**, 491 (2018).
- [106] M. L. Rodriguez, P. J. McGarry, and N. J. Sniddecki, Review on cell mechanics: experimental and modeling approaches, *Applied Mechanics Reviews* **65**, 10.1115/1.4025355 (2013).
- [107] A. Vinckier and G. Semenza, Measuring elasticity of biological materials by atomic force microscopy, *FEBS letters* **430**, 12 (1998).
- [108] G. U. Lee, D. A. Kidwell, and R. J. Colton, Sensing discrete streptavidin-biotin interactions with atomic force microscopy, *Langmuir* **10**, 354 (1994).
- [109] M. S. Kellermayer, S. B. Smith, H. L. Granzier, and C. Bustamante, Folding-unfolding transitions in single titin molecules characterized with laser tweezers, *Science* **276**, 1112 (1997).
- [110] S. H. Parekh, O. Chaudhuri, J. A. Theriot, and D. A. Fletcher, Loading history determines the velocity of actin-network growth, *Nature cell biology* **7**, 1219 (2005).
- [111] A. J. Engler, F. Rehfeldt, S. Sen, and D. E. Discher, Microtissue elasticity: Measurements by atomic force microscopy and its influence on cell differentiation, in *Cell Mechanics*, Methods in Cell Biology, Vol. 83 (Academic Press, 2007) pp. 521–545.
- [112] A. X. Cartagena-Rivera, J. S. Logue, C. M. Waterman, and R. S. Chadwick, Actomyosin cortical mechanical

- properties in nonadherent cells determined by atomic force microscopy, *Biophysical journal* **110**, 2528 (2016).
- [113] P. Kollmannsberger and B. Fabry, Bahigh-force magnetic tweezers with force feedback for biological applications, *Review of Scientific Instruments* **78**, 114301 (2007).
- [114] T. R. Strick, J.-F. Allemand, D. Bensimon, A. Bensimon, and V. Croquette, The elasticity of a single supercoiled dna molecule, *Science* **271**, 1835 (1996).
- [115] R. Sarkar and V. V. Rybenkov, A guide to magnetic tweezers and their applications, *Frontiers in Physics* **4**, 48 (2016).
- [116] S. Chakraborty and S. Haldar, Single-molecule covalent magnetic tweezers, *Trends in Biochemical Sciences* [10.1016/j.tibs.2023.05.002](https://doi.org/10.1016/j.tibs.2023.05.002) (2023).
- [117] E. C. Eckels, S. Haldar, R. Tapia-Rojo, J. A. Rivas-Pardo, and J. M. Fernández, The mechanical power of titin folding, *Cell reports* **27**, 1836 (2019).
- [118] J.-F. Berret, Local viscoelasticity of living cells measured by rotational magnetic spectroscopy, *Nature communications* **7**, 1 (2016).
- [119] C. J. Bustamante, Y. R. Chemla, S. Liu, and M. D. Wang, Optical tweezers in single-molecule biophysics, *Nature Reviews Methods Primers* **1**, 1 (2021).
- [120] K. C. Neuman and S. M. Block, Optical trapping, *Review of scientific instruments* **75**, 2787 (2004).
- [121] V. Soppina, A. K. Rai, A. J. Ramaiya, P. Barak, and R. Mallik, Tug-of-war between dissimilar teams of microtubule motors regulates transport and fission of endosomes, *Proceedings of the National Academy of Sciences* **106**, 19381 (2009).
- [122] W. W. Ahmed, É. Fodor, and T. Betz, Active cell mechanics: Measurement and theory, *Biochimica et Biophysica Acta (BBA) - Molecular Cell Research* **1853**, 3083 (2015), mechanobiology.
- [123] S. Yamada, D. Wirtz, and S. C. Kuo, Mechanics of living cells measured by laser tracking microrheology, *Biophys. J.* **78**, 1736 (2000).
- [124] C. Wilhelm, Out-of-equilibrium microrheology inside living cells, *Physical review letters* **101**, 028101 (2008).
- [125] D. Wirtz *et al.*, Particle-tracking microrheology of living cells: principles and applications, *Annual review of biophysics* **38**, 301 (2009).
- [126] G. Koenderink, M. Atakhorrami, F. MacKintosh, and C. F. Schmidt, High-frequency stress relaxation in semiflexible polymer solutions and networks, *Physical review letters* **96**, 138307 (2006).
- [127] Y. A. Ayala, B. Pontes, D. S. Ether, L. B. Pires, G. R. Araujo, S. Frases, L. F. Rom textasciitilde ao, M. Farina, V. Moura-Neto, N. B. Viana, *et al.*, Rheological properties of cells measured by optical tweezers, *BMC biophysics* **9**, 1 (2016).
- [128] M. Puig-De-Morales, M. Grabulosa, J. Alcaraz, J. Mullol, G. N. Maksym, J. J. Fredberg, and D. Navajas, Measurement of cell microrheology by magnetic twisting cytometry with frequency domain demodulation, *Journal of Applied Physiology* **91**, 1152 (2001).
- [129] C. W. Macosko, Rheology principles, Measurements and Applications [10.1016/b978-1-927885-97-0.50006-3](https://doi.org/10.1016/b978-1-927885-97-0.50006-3) (1994).
- [130] Y.-c. Fung, *Biomechanics: mechanical properties of living tissues* (Springer Science and Business Media, 2013).
- [131] C. Storm, J. J. Pastore, F. C. MacKintosh, T. C. Lubensky, and P. A. Janmey, Nonlinear elasticity in biological gels, *Nature* **435**, 191 (2005).
- [132] D. Humphrey, C. Duggan, D. Saha, D. Smith, and J. Käs, Active fluidization of polymer networks through molecular motors, *Nature* **416**, 413 (2002).
- [133] G. H. Koenderink, Z. Dogic, F. Nakamura, P. M. Bendix, F. C. MacKintosh, J. H. Hartwig, T. P. Stosel, and D. A. Weitz, An active biopolymer network controlled by molecular motors, *Proceedings of the National Academy of Sciences* **106**, 15192 (2009).
- [134] P. Fernández, L. Heymann, A. Ott, N. Aksel, and P. A. Pullarkat, Shear rheology of a cell monolayer, *New Journal of Physics* **9**, 419 (2007).
- [135] M. Dembo and Y.-L. Wang, Stresses at the cell-to-substrate interface during locomotion of fibroblasts, *Biophysical journal* **76**, 2307 (1999).
- [136] U. S. Schwarz and J. R. Soiné, Traction force microscopy on soft elastic substrates: A guide to recent computational advances, *Biochimica et Biophysica Acta (BBA)-Molecular Cell Research* **1853**, 3095 (2015).
- [137] J. L. Tan, J. Tien, D. M. Pirone, D. S. Gray, K. Bhadriraju, and C. S. Chen, Cells lying on a bed of microneedles: an approach to isolate mechanical force, *Proceedings of the National Academy of Sciences* **100**, 1484 (2003).
- [138] R. M. Hochmuth, Micropipette aspiration of living cells, *Journal of biomechanics* **33**, 15 (2000).
- [139] K. Guevorkian and J.-L. Maître, Micropipette aspiration: A unique tool for exploring cell and tissue mechanics in vivo, in *Methods in cell biology*, Vol. 139 (Elsevier, 2017) pp. 187–201.
- [140] B. González-Bermúdez, G. V. Guinea, and G. R. Plaza, Advances in micropipette aspiration: applications in cell biomechanics, models, and extended studies, *Biophysical Journal* **116**, 587 (2019).
- [141] E. Evans, New membrane concept applied to the analysis of fluid shear-and micropipette-deformed red blood cells, *Biophysical journal* **13**, 941 (1973).
- [142] I. Derényi, F. Jülicher, and J. Prost, Formation and interaction of membrane tubes, *Physical review letters* **88**, 238101 (2002).
- [143] F. Hochmuth, J.-Y. Shao, J. Dai, and M. P. Sheetz, Deformation and flow of membrane into tethers extracted

- from neuronal growth cones, *Biophysical journal* **70**, 358 (1996).
- [144] A. Datar, T. Bornschlöggl, P. Bassereau, J. Prost, and P. A. Pullarkat, Dynamics of membrane tethers reveal novel aspects of cytoskeleton-membrane interactions in axons, *Biophysical journal* **108**, 489 (2015).
- [145] Z. Shi, Z. T. Graber, T. Baumgart, H. A. Stone, and A. E. Cohen, Cell membranes resist flow, *Cell* **175**, 1769 (2018).
- [146] Y.-L. Zhang, J. A. Frangos, and M. Chachisvilis, Laurdan fluorescence senses mechanical strain in the lipid bilayer membrane, *Biochemical and biophysical research communications* **347**, 838 (2006).
- [147] A. Colom, E. Derivery, S. Soleimanpour, C. Tomba, M. D. Molin, N. Sakai, M. González-Gaitán, S. Matile, and A. Roux, A fluorescent membrane tension probe, *Nature chemistry* **10**, 1118 (2018).
- [148] A. S. LaCroix, K. E. Rothenberg, M. E. Berginski, A. N. Urs, and B. D. Hoffman, Construction, imaging, and analysis of fret-based tension sensors in living cells, in *Methods in cell biology*, Vol. 125 (Elsevier, 2015) pp. 161–186.
- [149] C. Grashoff, B. D. Hoffman, M. D. Brenner, R. Zhou, M. Parsons, M. T. Yang, M. A. McLean, S. G. Sligar, C. S. Chen, T. Ha, *et al.*, Measuring mechanical tension across vinculin reveals regulation of focal adhesion dynamics, *Nature* **466**, 263 (2010).
- [150] J. Wu, R. B. Dickinson, and T. P. Lele, Investigation of in vivo microtubule and stress fiber mechanics with laser ablation, *Integrative Biology* **4**, 471 (2012).
- [151] P. C. Shivakumar and P.-F. Lenne, Laser ablation to probe the epithelial mechanics in drosophila, *Drosophila*, **241** (2016).
- [152] F. Jülicher, A. Ajdari, and J. Prost, Modeling molecular motors, *Reviews of Modern Physics* **69**, 1269 (1997).
- [153] P. D. Boyer, The atp synthase – a splendid molecular machine, *Annual Review of Biochemistry* **66**, 717 (1997).
- [154] K. Hayashi, H. Ueno, R. Iino, and H. Noji, Fluctuation Theorem Applied to F 1-ATPase, *Physical Review Letters* **104**, 218103 (2010).
- [155] T. Mitchison and M. Kirschner, Dynamic instability of microtubule growth, *nature* **312**, 237 (1984).
- [156] H. Miyata, S. Nishiyama, K.-i. Akashi, and K. Kinoshita Jr, Protrusive growth from giant liposomes driven by actin polymerization, *Proceedings of the National Academy of Sciences* **96**, 2048 (1999).
- [157] D. R. Kovar and T. D. Pollard, Insertional assembly of actin filament barbed ends in association with formins produces piconewton forces, *Proceedings of the National Academy of Sciences* **101**, 14725 (2004).
- [158] M. J. Footer, J. W. J. Kerssemakers, J. A. Theriot, and M. Dogterom, Direct measurement of force generation by actin filament polymerization using an optical trap, *Proceedings of the National Academy of Sciences* **104**, 2181 (2007).
- [159] P. C. Bressloff, *Stochastic processes in cell biology, Vol-1*, 2nd ed. (Springer, 2021).
- [160] A. B. Kolomeisky, *Motor Proteins and Molecular Motors* (CRC Press, 2015).
- [161] P. Ranjith, D. Lacoste, K. Mallick, and J.-F. Joanny, Nonequilibrium self-assembly of a filament coupled to atp/gtp hydrolysis, *Biophysical journal* **96**, 2146 (2009).
- [162] D. Bray, *Cell movements: from molecules to motility* (Garland Science, 2000).
- [163] L. G. Tilney and D. A. Portnoy, Actin filaments and the growth, movement, and spread of the intracellular bacterial parasite, listeria monocytogenes., *The Journal of cell biology* **109**, 1597 (1989).
- [164] J. A. Theriot, T. J. Mitchison, L. G. Tilney, and D. A. Portnoy, The rate of actin-based motility of intracellular listeria monocytogenes equals the rate of actin polymerization, *Nature* **357**, 257 (1992).
- [165] C. H. Contag, P. R. Contag, J. I. Mullins, S. D. Spilman, D. K. Stevenson, and D. A. Benaron, Photonic detection of bacterial pathogens in living hosts, *Molecular microbiology* **18**, 593 (1995).
- [166] V. Noireaux, R. Golsteyn, E. Friederich, J. Prost, C. Antony, D. Louvard, and C. Sykes, Growing an actin gel on spherical surfaces, *Biophysical journal* **78**, 1643 (2000).
- [167] F. Gerbal, V. Noireaux, C. Sykes, F. Jülicher, P. Chaikin, A. Ott, J. Prost, R. Golsteyn, E. Friederich, D. Louvard, *et al.*, On the ‘listeria’ propulsion mechanism, *Pramana* **53**, 155 (1999).
- [168] F. Gerbal, P. Chaikin, Y. Rabin, and J. Prost, An Elastic Analysis of Listeria monocytogenes Propulsion, *Biophysical Journal* **79**, 2259 (2000).
- [169] C. E. Chan and D. J. Odde, Traction Dynamics of Filopodia on Compliant Substrates, *Science* **322**, 1687 (2008).
- [170] N. Leijnse, Y. F. Barooji, M. R. Arastoo, S. L. Sønder, B. Verhagen, L. Wullkopf, J. T. Erler, S. Semsey, J. Nylandsted, L. B. Oddershede, *et al.*, Filopodia rotate and coil by actively generating twist in their actin shaft, *Nature communications* **13**, 1636 (2022).
- [171] T. Bornschlöggl, S. Romero, C. L. Vestergaard, J.-F. Joanny, G. T. Van Nhieu, and P. Bassereau, Filopodial retraction force is generated by cortical actin dynamics and controlled by reversible tethering at the tip, *Proceedings of the National Academy of Sciences* **110**, 18928 (2013).
- [172] P. Curie, Sur la symétrie dans les phénomènes physiques, symétrie d’un champ électrique et d’un champ magnétique, *Journal de physique théorique et appliquée* **3**, 393 (1894).

- [173] M. L. Mugnai, C. Hyeon, M. Hinczewski, and D. Thirumalai, Theoretical perspectives on biological machines, *Reviews of Modern Physics* **92**, 025001 (2020).
- [174] R. Feynmann, R. Leighton, and M. Sands, *The feynmann lectures on physics, volume volumes i-ii-ii* (1963).
- [175] P. Reimann, Brownian motors: Noisy transport far from equilibrium, *Physics Reports* **361**, 57 (2002).
- [176] M. O. Magnasco, Forced thermal ratchets, *Physical Review Letters* **71**, 1477 (1993).
- [177] T. Guérin, J. Prost, P. Martin, and J.-F. Joanny, Coordination and collective properties of molecular motors: theory, *Current opinion in cell biology* **22**, 14 (2010).
- [178] W. Gilpin, M. S. Bull, and M. Prakash, The multiscale physics of cilia and flagella, *Nature Reviews Physics* **2**, 74 (2020).
- [179] F. C. Minozzo, B. M. Baroni, J. A. Correa, M. A. Vaz, and D. E. Rassier, Force produced after stretch in sarcomeres and half-sarcomeres isolated from skeletal muscles, *Scientific reports* **3**, 1 (2013).
- [180] M. Caruel and L. Truskinovsky, Physics of muscle contraction, *Reports on Progress in Physics* **81**, 036602 (2018).
- [181] S. Ishiwata, N. Okamura, H. Shimizu, T. Anazawa, and K. Yasuda, Spontaneous oscillatory contraction (spoc) of sarcomeres in skeletal muscle., *Advances in biophysics* **27**, 227 (1991).
- [182] S. Ishiwata, Y. Shimamoto, and M. Suzuki, Molecular motors as an auto-oscillator, *HFSP journal* **4**, 100 (2010).
- [183] R. W. Linck, H. Chemes, and D. F. Albertini, The axoneme: the propulsive engine of spermatozoa and cilia and associated ciliopathies leading to infertility, *Journal of assisted reproduction and genetics* **33**, 141 (2016).
- [184] U. Euteneuer and J. R. McIntosh, Polarity of some motility-related microtubules., *Proceedings of the National Academy of Sciences* **78**, 372 (1981).
- [185] K. Kruse and F. Jülicher, Oscillations in cell biology, *Current opinion in cell biology* **17**, 20 (2005).
- [186] K. Ishibashi, H. Sakakibara, and K. Oiwa, Force-generating mechanism of axonemal dynein in solo and ensemble, *International Journal of Molecular Sciences* **21**, 2843 (2020).
- [187] A. Hilfinger and F. Jülicher, The chirality of ciliary beats, *Physical Biology* **5**, 016003 (2008).
- [188] A. J. Hudspeth, Integrating the active process of hair cells with cochlear function, *Nature Reviews Neuroscience* **15**, 600 (2014).
- [189] D. Bray and J. White, Cortical flow in animal cells, *Science* **239**, 883 (1988).
- [190] T. M. Svitkina, A. B. Verkhovsky, K. M. McQuade, and G. G. Borisy, Analysis of the Actin–Myosin II System in Fish Epidermal Keratocytes: Mechanism of Cell Body Translocation, *Journal of Cell Biology* **139**, 397 (1997).
- [191] M. Lenz, T. Thoresen, M. L. Gardel, and A. R. Dinner, Contractile Units in Disordered Actomyosin Bundles Arise from F-Actin Buckling, *Physical Review Letters* **108**, 238107 (2012).
- [192] M. Lenz, M. L. Gardel, and A. R. Dinner, Requirements for contractility in disordered cytoskeletal bundles, *New Journal of Physics* **14**, 033037 (2012).
- [193] M. P. Murrell and M. L. Gardel, F-actin buckling coordinates contractility and severing in a biomimetic actomyosin cortex, *Proceedings of the National Academy of Sciences* **109**, 20820 (2012).
- [194] S. Chen, T. Markovich, and F. C. MacKintosh, Motor-Free Contractility in Active Gels, *Physical Review Letters* **125**, 208101 (2020).
- [195] J.-Y. Tinevez, U. Schulze, G. Salbreux, J. Roensch, J.-F. Joanny, and E. Paluch, Role of cortical tension in bleb growth, *Proceedings of the National Academy of Sciences* **106**, 18581 (2009).
- [196] J. S. Bois, F. Jülicher, and S. Grill, Pattern Formation in Active Fluids, *Physical Review Letters* **106**, 1 (2011).
- [197] K. V. Kumar, J. S. Bois, F. Jülicher, and S. W. Grill, Pulsatory Patterns in Active Fluids, *Physical Review Letters* **112**, 208101 (2014).
- [198] A. M. Turing, The Chemical Basis of Morphogenesis, *Philosophical Transactions of the Royal Society B: Biological Sciences* **237**, 37 (1952).
- [199] A. Mietke, V. Jemseena, K. V. Kumar, I. F. Sbalzarini, and F. Jülicher, Minimal Model of Cellular Symmetry Breaking, *Physical Review Letters* **123**, 188101 (2019).
- [200] H. Turlier, B. Audoly, J. Prost, and J.-F. Joanny, Furrow Constriction in Animal Cell Cytokinesis, *Biophysical Journal* **106**, 114 (2014).
- [201] K. Gowrishankar, S. Ghosh, S. Saha, R. C., S. Mayor, and M. Rao, Active Remodeling of Cortical Actin Regulates Spatiotemporal Organization of Cell Surface Molecules, *Cell* **149**, 1353 (2012).
- [202] A. Zumdieck, M. C. Lagomarsino, C. Tanase, K. Kruse, B. Mulder, M. Dogterom, and F. Jülicher, Continuum Description of the Cytoskeleton: Ring Formation in the Cell Cortex, *Physical Review Letters* **95**, 258103 (2005).
- [203] G. Salbreux, J. Prost, and J. F. Joanny, Hydrodynamics of Cellular Cortical Flows and the Formation of Contractile Rings, *Physical Review Letters* **103**, 058102 (2009).
- [204] A.-C. Reymann, F. Staniscia, A. Erzberger, G. Salbreux, and S. W. Grill, Cortical flow aligns actin filaments to form a furrow, *eLife* **5**, e17807 (2016).
- [205] N. W. Goehring, P. K. Trong, J. S. Bois, D. Chowdhury, E. M. Nicola, A. a Hyman, and S. W. Grill, Polarization of PAR proteins by advective triggering of a pattern-forming system., *Science* **334**, 1137 (2011).
- [206] P. Gross, K. V. Kumar, N. W. Goehring, J. S. Bois, C. Hoege, F. Jülicher, and S. W. Grill, Guiding self-

- organized pattern formation in cell polarity establishment, *Nature Physics* **15**, 293 (2019).
- [207] A. E. Carlsson, Mechanisms of cell propulsion by active stresses, *New Journal of Physics* **13**, 073009 (2011).
- [208] P. Recho, T. Putelat, and L. Truskinovsky, Mechanics of motility initiation and motility arrest in crawling cells, *Journal of the Mechanics and Physics of Solids* **84**, 469 (2015).
- [209] Y. Mori, A. Jilkine, and L. Edelstein-Keshet, Wave-pinning and cell polarity from a bistable reaction-diffusion system, *Biophysical Journal* **94**, 3684 (2008).
- [210] P. Recho and L. Truskinovsky, *Physical Models of Cell Motility*, edited by I. S. Aranson, Biological and Medical Physics, Biomedical Engineering (Springer International Publishing, Cham, 2016) Chap. 4.
- [211] A. Mogilner, E. L. Barnhart, and K. Keren, Experiment, theory, and the keratocyte: An ode to a simple model for cell motility, in *Seminars in cell and developmental biology*, Vol. 100 (Elsevier, 2020) pp. 143–151.
- [212] G. Charras and E. Paluch, Blebs lead the way: how to migrate without lamellipodia, *Nature reviews Molecular cell biology* **9**, 730 (2008).
- [213] T. Zhang, R. Sknepnek, M. J. Bowick, and J. M. Schwarz, On the Modeling of Endocytosis in Yeast, *Biophysical Journal* **108**, 508 (2015).
- [214] A. Mogilner and A. Manhart, Intracellular Fluid Mechanics: Coupling Cytoplasmic Flow with Active Cytoskeletal Gel, *Annual Review of Fluid Mechanics* **50**, 347 (2018).
- [215] D. R. Burnham, H. B. Kose, R. B. Hoyle, and H. Yardimci, The mechanism of dna unwinding by the eukaryotic replicative helicase, *Nature communications* **10**, 2159 (2019).
- [216] T. Cremer and M. Cremer, Chromosome territories, *Cold Spring Harbor perspectives in biology* **2**, a003889 (2010).
- [217] A. Zidovska, D. A. Weitz, and T. J. Mitchison, Micron-scale coherence in interphase chromatin dynamics, *Proceedings of the National Academy of Sciences* **110**, 15555 (2013).
- [218] S. C. Weber, A. J. Spakowitz, and J. A. Theriot, Non-thermal atp-dependent fluctuations contribute to the in vivo motion of chromosomal loci, *Proceedings of the National Academy of Sciences* **109**, 7338 (2012).
- [219] R. Bruinsma, A. Y. Grosberg, Y. Rabin, and A. Zidovska, Chromatin Hydrodynamics, *Biophysical Journal* **106**, 1871 (2014).
- [220] N. Ganai, S. Sengupta, and G. I. Menon, Chromosome positioning from activity-based segregation, *Nucleic acids research* **42**, 4145 (2014).
- [221] A. Agrawal, N. Ganai, S. Sengupta, and G. I. Menon, Nonequilibrium biophysical processes influence the large-scale architecture of the cell nucleus, *Biophysical Journal* **118**, 2229 (2020).
- [222] A. Mahajan, W. Yan, A. Zidovska, D. Saintillan, and M. J. Shelley, Euchromatin activity enhances segregation and compaction of heterochromatin in the cell nucleus, *Physical Review X* **12**, 041033 (2022).
- [223] S. A. Rautu, A. Zidovska, D. Saintillan, and M. J. Shelley, *Active hydrodynamic theory of euchromatin and heterochromatin* (2025), arXiv:2503.20964 [cond-mat.soft].
- [224] C. Uhler and G. V. Shivashankar, Regulation of genome organization and gene expression by nuclear mechanotransduction, *Nature Reviews Molecular Cell Biology* **10.1038/nrm.2017.101** (2017).
- [225] S. Pagliara, K. Franze, C. R. McClain, G. Wylde, C. L. Fisher, R. J. Franklin, A. J. Kabla, U. F. Keyser, and K. J. Chalut, Transition from pluripotency in embryonic stem cells distinguished by an auxetic nucleus, *Nature materials* **13**, 638 (2014).
- [226] K. Tripathi and G. I. Menon, Chromatin Compaction, Auxeticity, and the Epigenetic Landscape of Stem Cells, *Physical Review X* **9**, 041020 (2019).
- [227] S. W. Grill, J. Howard, E. Schäffer, E. H. K. Stelzer, and A. A. Hyman, The Distribution of Active Force Generators Controls Mitotic Spindle Position, *Science* **301**, 518 (2003).
- [228] R. B. Nicklas, Measurements of the force produced by the mitotic spindle in anaphase., *The Journal of cell biology* **97**, 542 (1983).
- [229] A. P. Joglekar, K. S. Bloom, and E. Salmon, Mechanisms of force generation by end-on kinetochore-microtubule attachments, *Current opinion in cell biology* **22**, 57 (2010).
- [230] B. Akiyoshi, K. K. Sarangapani, A. F. Powers, C. R. Nelson, S. L. Reichow, H. Arellano-Santoyo, T. Gonen, J. A. Ranish, C. L. Asbury, and S. Biggins, Tension directly stabilizes reconstituted kinetochore-microtubule attachments, *Nature* **468**, 576 (2010).
- [231] D. Oriola, F. Jülicher, and J. Brugués, Active forces shape the metaphase spindle through a mechanical instability, *Proceedings of the National Academy of Sciences* **117**, 16154 (2020).
- [232] J. Brugués and D. Needleman, Physical basis of spindle self-organization, *Proceedings of the National Academy of Sciences* , 201409404 (2014).
- [233] A. Schaeffer, M. Gazzola, M. Gelin, B. Vianay, C. de Pascalis, L. Blanchoin, and M. Théry, Centrosome positioning independently of microtubule-based forces, bioRxiv **10.1101/2024.06.11.598451** (2024).
- [234] T. H. Cheffings, N. J. Burroughs, and M. K. Balasubramanian, Actomyosin ring formation and tension generation in eukaryotic cytokinesis, *Current Biology* **26**, R719 (2016).
- [235] D. O. Morgan, *The cell cycle: principles of control* (New

- science press, 2007).
- [236] J. G. White and G. G. Borisy, On the mechanisms of cytokinesis in animal cells, *Journal of Theoretical Biology* **101**, 289 (1983).
- [237] A. S. Rajput, K. Kumar, M. Nishikawa, and K. V. Kumar, Active geometrodynamics predicts the emergence of cytokinesis, *bioRxiv* [10.1101/2025.11.07.683232](https://doi.org/10.1101/2025.11.07.683232) (2025).
- [238] G. Salbreux, J. Prost, and J.-F. Joanny, Hydrodynamics of cellular cortical flows and the formation of contractile rings, *Physical review letters* **103**, 058102 (2009).
- [239] G. Salbreux, G. Charras, and E. Paluch, Actin cortex mechanics and cellular morphogenesis, *Trends in cell biology* **22**, 536 (2012).
- [240] M. R. Stachowiak, C. Laplante, H. F. Chin, B. Guirao, E. Karatekin, T. D. Pollard, and B. O’Shaughnessy, Mechanism of cytokinetic contractile ring constriction in fission yeast, *Developmental cell* **29**, 547 (2014).
- [241] I. Mabuchi, Cleavage furrow: Timing of emergence of contractile ring actin filaments and establishment of the contractile ring by filament bundling in sea urchin eggs, *Journal of Cell Science* **107**, 1853 (1994).
- [242] R. N. Khaliullin, R. A. Green, L. Z. Shi, J. S. Gomez-Cavazos, M. W. Berns, A. Desai, and K. Oegema, A positive-feedback-based mechanism for constriction rate acceleration during cytokinesis in *Caenorhabditis elegans*, *eLife* **7**, e36073 (2018).
- [243] G. Gerisch and I. Weber, Cytokinesis without myosin ii, *Current opinion in cell biology* **12**, 126 (2000).
- [244] A. Zumdick, K. Kruse, H. Bringmann, A. A. Hyman, and F. Jülicher, Stress generation and filament turnover during actin ring constriction, *PloS one* **2**, e696 (2007).
- [245] C. Pérez-González, R. Alert, C. Blanch-Mercader, M. Gómez-González, T. Kolodziej, E. Bazellieres, J. Casademunt, and X. Trepat, Active wetting of epithelial tissues, *Nature Physics* **15**, 79 (2019).
- [246] E. Latorre, S. Kale, L. Casares, M. Gómez-González, M. Uroz, L. Valon, R. V. Nair, E. Garreta, N. Montserrat, A. del Campo, *et al.*, Active superelasticity in three-dimensional epithelia of controlled shape, *Nature* **563**, 203 (2018).
- [247] H. A. Messal, S. Alt, R. M. Ferreira, C. Gribben, V. M.-Y. Wang, C. G. Cotoi, G. Salbreux, and A. Behrens, Tissue curvature and apicobasal mechanical tension imbalance instruct cancer morphogenesis, *Nature* **566**, 126 (2019).
- [248] M. Merkel, K. Baumgarten, B. P. Tighe, and M. L. Manning, A minimal-length approach unifies rigidity in underconstrained materials, *Proceedings of the National Academy of Sciences* **116**, 6560 (2019).
- [249] W. Xi, T. B. Saw, D. Delacour, C. T. Lim, and B. Ladoux, Material approaches to active tissue mechanics, *Nature Reviews Materials* **4**, 23 (2019).
- [250] R. Etournay, M. Merkel, M. Popović, H. Brandl, N. A. Dye, B. Aigouy, G. Salbreux, S. Eaton, and F. Jülicher, Tissueminer: a multiscale analysis toolkit to quantify how cellular processes create tissue dynamics, *eLife* **5**, e14334 (2016).
- [251] J. Ranft, M. Basan, J. Elgeti, J.-F. Joanny, J. Prost, and F. Jülicher, Fluidization of tissues by cell division and apoptosis, *Proc. Natl. Acad. Sci. USA* **107**, 20863 (2010).
- [252] M. Popović, A. Nandi, M. Merkel, R. Etournay, S. Eaton, F. Jülicher, and G. Salbreux, Active dynamics of tissue shear flow, *New Journal of Physics* **19**, 033006 (2017).
- [253] S. Curran, C. Strandkvist, J. Bathmann, M. de Gennes, A. Kabla, G. Salbreux, and B. Baum, Myosin ii controls junction fluctuations to guide epithelial tissue ordering, *Developmental cell* **43**, 480 (2017).
- [254] M. Krajnc, S. Dasgupta, P. Zihlerl, and J. Prost, Fluidization of epithelial sheets by active cell rearrangements, *Physical Review E* **98**, 022409 (2018).
- [255] M. Merkel, R. Etournay, M. Popović, G. Salbreux, S. Eaton, and F. Jülicher, Triangles bridge the scales: Quantifying cellular contributions to tissue deformation, *Physical Review E* **95**, 032401 (2017).
- [256] J. Comelles, S. Soumya, S. Anvitha, G. Salbreux, F. Jülicher, M. M. Inamdar, and D. Riveline, Elongations of epithelial colony in vitro: symmetry breaking through collective effects, *BioRxiv* , 755181 (2019).
- [257] A. J. Hughes, H. Miyazaki, M. C. Coyle, J. Zhang, M. T. Laurie, D. Chu, Z. Vavrušová, R. A. Schneider, O. D. Klein, and Z. J. Gartner, Engineered tissue folding by mechanical compaction of the mesenchyme, *Developmental cell* **44**, 165 (2018).
- [258] A. G. Fletcher, M. Osterfield, R. E. Baker, and S. Y. Shvartsman, Vertex models of epithelial morphogenesis, *Biophys. J.* **106**, 2291 (2014).
- [259] D. Staple, R. Farhadifar, J.-C. Röper, B. Aigouy, S. Eaton, and F. Jülicher, Mechanics and remodelling of cell packings in epithelia, *Eur. Phys. J. E Soft Matter* **33**, 117 (2010).
- [260] D. Bi, J. Lopez, J. Schwarz, and M. L. Manning, A density-independent glass transition in biological tissues, *Nature Physics* **11**, 1074 (2015).
- [261] N. Noll, M. Mani, I. Heemskerk, S. J. Streichan, and B. I. Shraiman, Active tension network model suggests an exotic mechanical state realized in epithelial tissues, *Nature physics* **13**, 1221 (2017).
- [262] K. Sato, T. Hiraiwa, and T. Shibata, Cell chirality induces collective cell migration in epithelial sheets, *Phys. Rev. Lett* **115**, 188102 (2015).
- [263] S. Okuda, T. Miura, Y. Inoue, T. Adachi, and M. Eiraku, Combining turing and 3d vertex models reproduces autonomous multicellular morphogenesis with

- undulation, tubulation, and branching, [Scientific reports](#) **8**, 2386 (2018).
- [264] R. Etournay, M. Popović, M. Merkel, A. Nandi, C. Blasse, B. Aigouy, H. Brandl, G. Myers, G. Salbreux, F. Jülicher, *et al.*, Interplay of cell dynamics and epithelial tension during morphogenesis of the drosophila pupal wing, [eLife](#) **4**, e07090 (2015).
- [265] B. Guirao, S. U. Rigaud, F. Bosveld, A. Bailles, J. Lopez-Gay, S. Ishihara, K. Sugimura, F. Graner, and Y. Bellaïche, Unified quantitative characterization of epithelial tissue development, [eLife](#) **4**, e08519 (2015).
- [266] M. Popović, A. Nandi, M. Merkel, R. Etournay, S. Eaton, F. Jülicher, and G. Salbreux, Active dynamics of tissue shear flow, [New Journal of Physics](#) **19**, 033006 (2017).
- [267] S. Ishihara, P. Marcq, and K. Sugimura, From cells to tissue: A continuum model of epithelial mechanics, [Phys. Rev. E](#) **96**, 022418 (2017).
- [268] D. Grossman and J.-F. Joanny, Instabilities and geometry of growing tissues, [Physical Review Letters](#) **129**, 048102 (2022).
- [269] K. Sato, T. Hiraiwa, E. Maekawa, A. Isomura, T. Shibata, and E. Kuranaga, Left-right asymmetric cell intercalation drives directional collective cell movement in epithelial morphogenesis, [Nat. Commun.](#) **6**, 10074 (2015).
- [270] D. Singh, S. Ramaswamy, M. K. Jolly, and M. S. Rizvi, Emergence of planar cell polarity from the interplay of local interactions and global gradients, [eLife](#) **13**, e84053 (2024).
- [271] E. Hannezo, J. Prost, and J.-F. Joanny, Theory of epithelial sheet morphology in three dimensions, [Proc Nat Acad Sci USA](#) **111**, 27 (2014).
- [272] E. Hannezo, J. Prost, and J.-F. Joanny, Instabilities of monolayered epithelia: shape and structure of villi and crypts, [Physical Review Letters](#) **107**, 078104 (2011).
- [273] U. S. Schwarz and S. A. Safran, Physics of adherent cells, [Rev. Mod. Phys.](#) **85**, 1327 (2013).
- [274] S. M. Simon, C. S. Peskin, and G. F. Oster, What drives the translocation of proteins?, [Proceedings of the National Academy of Sciences](#) **89**, 3770 (1992).
- [275] T. Quail, S. Golfier, M. Elsner, K. Ishihara, V. Murugesan, R. Renger, F. Jülicher, and J. Brugués, Force generation by protein–DNA co-condensation, [Nature Physics](#) **17**, 1007 (2021).
- [276] A. Lisica, C. Engel, M. Jahnel, É. Roldán, E. A. Galburt, P. Cramer, and S. W. Grill, Mechanisms of backtrack recovery by RNA polymerases I and II, [Proceedings of the National Academy of Sciences](#) **113**, 2946 (2016).
- [277] C. Bustamante, W. Cheng, and Y. X. Mejia, Revisiting the Central Dogma One Molecule at a Time, [Cell](#) **144**, 480 (2011).
- [278] M. D. Wang, M. J. Schnitzer, H. Yin, R. Landick, J. Gelles, and S. M. Block, Force and Velocity Measured for Single Molecules of RNA Polymerase, [Science](#) **282**, 902 (1998).
- [279] C. Lavelle, Pack, unpack, bend, twist, pull, push: The physical side of gene expression, [Current Opinion in Genetics and Development Genome Architecture and Expression](#), **25**, 74 (2014).
- [280] S. A. Sevier and H. Levine, Mechanical Properties of Transcription, [Physical Review Letters](#) **118**, 268101 (2017).
- [281] B. W. Hoogenboom, L. E. Hough, E. A. Lemke, R. Y. H. Lim, P. R. Onck, and A. Zilman, Physics of the nuclear pore complex: Theory, modeling and experiment, [Physics Reports](#) **921**, 1 (2021).
- [282] E. Infante, A. Stannard, S. J. Board, P. Rico-Lastres, E. Rostkova, A. E. M. Beedle, A. Lezamiz, Y. J. Wang, S. G. Breen, F. Panagaki, V. S. Rajan, C. Shanahan, P. Roca-Cusachs, and S. Garcia-Manyes, The mechanical stability of proteins regulates their translocation rate into the cell nucleus, [Nature Physics](#) , 1 (2019).
- [283] J. P. Rickgauer, D. N. Fuller, S. Grimes, P. J. Jardine, D. L. Anderson, and D. E. Smith, Portal motor velocity and internal force resisting viral dna packaging in bacteriophage $\phi 29$, [Biophysical journal](#) **94**, 159 (2008).
- [284] A. Brandariz-Nu textasciitilde nez, T. Liu, T. Du, and A. Evilevitch, Pressure-driven release of viral genome into a host nucleus is a mechanism leading to herpes infection, [Elife](#) **8**, e47212 (2019).
- [285] R. Zandi, B. Dragnea, A. Travesset, and R. Podgornik, On virus growth and form, [Physics Reports On Virus Growth and Form](#), **847**, 1 (2020).
- [286] R. F. Bruinsma, G. J. L. Wuite, and W. H. Roos, Physics of viral dynamics, [Nature Reviews Physics](#) **3**, 76 (2021).
- [287] E. Lauga, *The Fluid Dynamics of Cell Motility* (Cambridge University Press, 2020).
- [288] K. J. Niklas and H.-C. Spatz, *Plant Physics* (Chicago University Press, 2012).
- [289] B. S. Hill and G. P. Findlay, The power of movement in plants: The role of osmotic machines, [Quarterly Reviews of Biophysics](#) **14**, 173 (1981).
- [290] J. Dumais and Y. Forterre, “Vegetable Dynamicks”: The Role of Water in Plant Movements, [Annual Review of Fluid Mechanics](#) **44**, 453 (2012).
- [291] Y. Forterre, Slow, fast and furious: Understanding the physics of plant movements, [Journal of Experimental Botany](#) **64**, 4745 (2013).
- [292] E. Coen and D. J. Cosgrove, The mechanics of plant morphogenesis, [Science](#) **379**, eade8055 (2023).
- [293] F. G. Woodhouse and R. E. Goldstein, Cytoplasmic streaming in plant cells emerges naturally by micro-

- filament self-organization, [Proceedings of the National Academy of Sciences](#) **110**, 14132 (2013).
- [294] C. Darwin and F. E. Darwin, *The power of movement in plants* (John Murray, 1888).
- [295] Y. Forterre, J. M. Skotheim, J. Dumais, and L. Mahadevan, How the Venus flytrap snaps, [Nature](#) **433**, 421 (2005).
- [296] D. E. Moulton, H. Oliveri, and A. Goriely, Multiscale integration of environmental stimuli in plant tropism produces complex behaviors, [Proceedings of the National Academy of Sciences](#) **117**, 32226 (2020).
- [297] R. Zaidel-Bar, G. Zhenhuan, and C. Luxenburg, The contractome—a systems view of actomyosin contractility in non-muscle cells, [Journal of cell science](#) **128**, 2209 (2015).
- [298] M. Thattai, How contraction has shaped evolution, [Elife](#) **8**, e52805 (2019).
- [299] T. Brunet, Cell contractility in early animal evolution, [Current Biology](#) **33**, R966 (2023).
- [300] A. Engler, L. Bacakova, C. Newman, A. Hategan, M. Griffin, and D. Discher, Substrate compliance versus ligand density in cell on gel responses, [Biophys. J.](#) **86**, 617 (2004).
- [301] E. Schrodinger, *What is life? The physical aspect of the living cell* (Cambridge University Press, 1948).